

Advanced High-Lift Leading-Edge (AHLLE) Technologies for Laminar Wings

Final Technical Report

Dr. Michelle M. Bright, Steve Komadina, Andrea Korntheuer, Alan Arslan, Susan Bieck, Kian Tehrani, Thomas Goethe, John Tapee, Nicholas Caldwell, Peter Keding

Northrop Grumman Systems Corporation, Aerospace Systems, El Segundo, California

Dated: April 30, 2012

NASA Langley Research Center
9B Langley Blvd., Bldg. 1195B
M/S 126
Hampton, VA 23681-2199

Prepared for Langley Research Center
Under Contract NNL10AA07B
Task Order NNL11AB27T

September 2020

NASA STI Program . . . in Profile

Since its founding, NASA has been dedicated to the advancement of aeronautics and space science. The NASA scientific and technical information (STI) program plays a key part in helping NASA maintain this important role.

The NASA STI program operates under the auspices of the Agency Chief Information Officer. It collects, organizes, provides for archiving, and disseminates NASA's STI. The NASA STI program provides access to the NTRS Registered and its public interface, the NASA Technical Reports Server, thus providing one of the largest collections of aeronautical and space science STI in the world. Results are published in both non-NASA channels and by NASA in the NASA STI Report Series, which incl
udes the following report types:

- TECHNICAL PUBLICATION. Reports of completed research or a major significant phase of research that present the results of NASA Programs and include extensive data or theoretical analysis. Includes compilations of significant scientific and technical data and information deemed to be of continuing reference value. NASA counter-part of peer-reviewed formal professional papers but has less stringent limitations on manuscript length and extent of graphic presentations.

- TECHNICAL MEMORANDUM. Scientific and technical findings that are preliminary or of specialized interest, e.g., quick release reports, working papers, and bibliographies that contain minimal annotation. Does not contain extensive analysis.

- CONTRACTOR REPORT. Scientific and technical findings by NASA-sponsored contractors and grantees.

- CONFERENCE PUBLICATION. Collected papers from scientific and technical conferences, symposia, seminars, or other meetings sponsored or co-sponsored by NASA.

- SPECIAL PUBLICATION. Scientific, technical, or historical information from NASA programs, projects, and missions, often concerned with subjects having substantial public interest.

- TECHNICAL TRANSLATION. English-language translations of foreign scientific and technical material pertinent to NASA's mission.

Specialized services also include organizing and publishing research results, distributing specialized research announcements and feeds, providing information desk and personal search support, and enabling data exchange services.

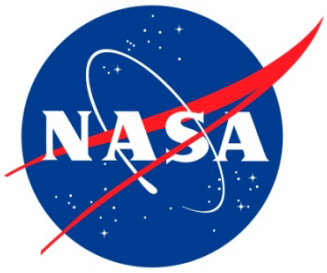
For more information about the NASA STI program, see the following:

- Access the NASA STI program home page at *http://www.sti.nasa.gov*

- E-mail your question to help@sti.nasa.gov

- Phone the NASA STI Information Desk at 757-864-9658

- Write to:
  NASA STI Information Desk
  Mail Stop 148
  NASA Langley Research Center
  Hampton, VA 23681-2199



Advanced High-Lift Leading-Edge (AHLLE) Technologies for Laminar Wings

Final Technical Report

Dr. Michelle M. Bright, Steve Komadina, Andrea Korntheuer, Alan Arslan, Susan Bieck, Kian Tehrani, Thomas Goethe, John Tapee, Nicholas Caldwell, Peter Keding

Northrop Grumman Systems Corporation, Aerospace Systems, El Segundo, California

Dated: April 30, 2012

NASA Langley Research Center
9B Langley Blvd., Bldg. 1195B
M/S 126
Hampton, VA 23681-2199

Prepared for Langley Research Center
Under Contract NNL10AA07B
Task Order NNL11AB27T

September 2020

Foreword

This report documents work completed on the Advanced High-Lift Leading-Edge Technologies for Wings, abbreviated AHLLE program, task order NNL11AB27T. The NASA Langley Research Center was the contract issuing office; under the Structures, Materials, Aerodynamics, Aerothermodynamics, and Acoustics Research and Technology (contract number NNL10AA07B) contract vehicle. The work was performed by Northrop Grumman's Aerospace Systems (NGAS), El Segundo, CA. Dr. John Lin, NASA Langley, was the NASA contracting officer's technical representative. Mr. Steve Komadina was Program Manager for NGAS. A complete list of team members is given below.

- Steve Komadina — Program Manager (Steve.komadina@ngc.com)
- Dr. Michelle M. Bright — Principal Investigator (michelle.bright@ngc.com)
- Andrea Korntheuer — Aerodynamic Analysis and Responsible Test Engineer (andrea.korntheuer@ngc.com)
- Alan Arslan — CFD Aerodynamic Analysis (alan.arslan@ngc.com)
- Susan Bieck — Wind Tunnel Model Design (susan.bieck@ngc.com)
- Kian Tehrani — Wind Tunnel Test Engineer (kian.tehrani@ngc.com)
- Thomas Goethe — Model Manufacturing and Fabrication Manager (Thomas.goethe@ngc.com)
- John Tapee — CFD Aerodynamic Analysis (john.tapee@ngc.com)
- Nicholas Caldwell — Propulsion Engineer (Nicholas.caldwell@ngc.com)
- Peter Keding — Configuration Engineer (peter.keding@ngc.com)
- Steve Bowen — Wind Tunnel Instrumentation Engineer/Data Acquisition (steve.bowen@ngc.com)
- James Ayers — Wind Tunnel Model Technician/Support
- Richard Diaz — Wind Tunnel Model Technician/Support
- Jeff Pate — Wind Tunnel Operations/Instrumentation
- Ron McCool — Wind Tunnel Facility Operations
- Kristen August — Contracting Officer (Kristen.august@ngc.com)

Table of Contents

Foreword ii
Abstract vi
1. Introduction and Overview 1
2. Conceptual Design 4
2.1 Conceptual Design Configurations 5
3. Model Downselect 14
3.1. Configuration Analysis 14
3.2. QFD Down Selection 14
4. Wind Tunnel Test Plan 27
5. Aerodynamic Analysis 31
5.1. Validation of Model Sizing 32
5.2. Static Tap Placement 37
5.3. Pretest CFD Predictions 38
5.4. Trip Dot Sizing 39
6. Wind Tunnel Model Design 39
6.1. Model Design Parameters 40
7. Wind Tunnel Model Installation 52
7.1. High-Pressure Air System Installation 52
7.2. Wind Tunnel Test Plan Execution 55
8. Data Analysis 58
9. Summary 84
10. References 10

Table of Figures

FIGURE 1-1. AHLLE PROGRAM SCHEDULE. 1
FIGURE 1-2. LAMINAR COMPATIBLE LEADING-EDGE CONCEPTS. 2
FIGURE 1-3. PROGRAM AND TEAM ORGANIZATIONAL STRUCTURE. 3
FIGURE 1-4. BASELINE AIRFOIL AND PREDICTION OF LIFT LEADING-EDGE CONFIGURATIONS. 3
FIGURE 2-1. LEADING-EDGE CONCEPTUAL DESIGNS EXAMINED. 4
FIGURE 2-2. BLOWING COEFFICIENT DEFINITION. 4
FIGURE 2-3. LEADING-EDGE CONFIGURATION DOWNSELECTION MATRIX. 5
FIGURE 2-4. FLOW VISUALIZATION OF LAVLET CONFIGURATION. 6
FIGURE 2-5. PREDICTED LIFT CURVES FOR BLOWN SLOT CONFIGURATION. 6
FIGURE 2-6. MORPHED LEADING-EDGE CONFIGURATIONS STUDIED. 7
FIGURE 2-7. FLOW VISUALIZATION FOR MOLEC CONFIGURATION AT 100% DROOP AND ALPHA = 0 DEGREES. 8
FIGURE 2-8. FLOW VISUALIZATION RESULT FOR 100% DROOP CASE AT ALPHA NEAR STALL. 8
FIGURE 2-9. FLOW VISUALIZATION FOR 75% DROOP CASE. 9
FIGURE 2-10. FLOW VISUALIZATION RESULT FOR 50% DROOP CASE. 9
FIGURE 2-11. FLOW VISUALIZATION RESULTS FOR SHOULDER SUCTION 10
FIGURE 2-12. BLOWN SHOULDER CFD RESULTS. 11
FIGURE 2-13. TRAILING-EDGE BLOWING RESULTS ON THE MOLEC CONFIGURATION. 12
FIGURE 2-14. SUMMARY OF MOLEC CONCEPTUAL DESIGN RESULTS. 13
FIGURE 2-15. SUMMARY OF CONCEPTUAL DESIGN STUDY. 13
FIGURE 3-1. QFD ANALYSIS PROCESS. 14
FIGURE 3-2. RELATIVE RANKINGS AND WEIGHTING ASSESSMENT FACTORS FOR QFD 15
FIGURE 3-3. CANDIDATE HIGH-LIFT LEADING-EDGE TECHNOLOGIES. 16
FIGURE 3-4. RESULTS OF THE QFD ANALYSIS. 17
FIGURE 3-5. LAMINAR FLOW COMPATIBILITY SCORES. 18
FIGURE 3-6. REPRESENTATIVE LIFT PERFORMANCE FOR TECHNOLOGIES 19
FIGURE 3-7. POWER REQUIREMENT QFD SCORING. 20
FIGURE 3-8. RELATIVE QFD SCORES DUE TO WEIGHT. 21
FIGURE 3-9. RELATIVE WEIGHTINGS DUE TO NOISE. 22
FIGURE 3-10. RELATIVE WEIGHTINGS DUE TO RELIABILITY. 23
FIGURE 3-11. RELATIVE WEIGHTINGS DUE TO MAINTAINABILITY. 24
FIGURE 3-12. RELATIVE WEIGHTINGS DUE TO COMPLEXITY. 25
FIGURE 3-13. TECHNOLOGY READINESS LEVEL (TRL) ASSESSMENT. 26
FIGURE 3-14. AFFORDABILITY QFD ASSESSMENT. 27
FIGURE 4-1. DESIGN CONSIDERATIONS. 29
FIGURE 4-2 NORTHROP GRUMMAN LSWT. 30
FIGURE 4-3. MODEL CONFIGURATIONS IDENTIFIED FOR THE TEST 30
FIGURE 5-1. WIND TUNNEL MODEL GRID. 32
FIGURE 5-2. MODEL SIZING RESULTS OF 3D CFD. 33
FIGURE 5-3. VALIDATION OF MODEL SIZING FROM 3D ANALYSIS. 34
FIGURE 5-4. COMPARISON OF 2D AND 3D PREDICTED LIFT RESULTS. 35
FIGURE 5-5. PREDICTED EFFECTS WALL EFFECTS ON CP DISTRIBUTIONS 36
FIGURE 5-6. STATIC TAP PLACEMENT ON MODEL. 37
FIGURE 5-7. PRETEST CFD PREDICTIONS. 38
FIGURE 6-1. WIND TUNNEL MODEL DESIGN APPROACH 41
FIGURE 6-2. ALUMINUM CENTER BODY DESIGN. 42
FIGURE 6-3. BASELINE MODEL CONFIGURATION. 43
FIGURE 6-4. LAVLET AND MOLEC CONFIGURATIONS. 44
FIGURE 6-5. PLENUM LAYOUT AND SIDEVIEW OF MODEL. 45
FIGURE 6-6. INSTRUMENTATION ON THE MODEL OML. 46
FIGURE 6-7. INTERNAL MODEL INSTRUMENTATION. 47
FIGURE 6-8. STRESS ANALYSIS REPORT. 48

FIGURE 6-9. MODEL FABRICATION. 49
FIGURE 6-10. MODEL FABRICATION PICTURES. 50
FIGURE 6-11. MODEL INSPECTION CRITERIA AND TOLERANCE REPORTS. 51
FIGURE 7-7-1. INSTALLATION OF THE HIGH-PRESSURE AIR SYSTEM. 52
FIGURE 7-2. MODEL INSTALLATION IN THE 7×10 TUNNEL. 53
FIGURE 7-3. FAILURE OF HIGH-PRESSURE SUPPLY LINES. 54
FIGURE 7-4. NEW METALLIC SUPPLY LINE INSTALLATION. 55
FIGURE 7-5. EXECUTION OF THE WIND TUNNEL TEST PLAN. 56
FIGURE 7-6. MODEL UNINSTALL AND TEST SUMMARY. 57
FIGURE 8-1. BASELINE AHLLE CONFIGURATION. 58
FIGURE 8-2. AHLLE CHOKE PLATE CALIBRATION. 59
FIGURE 8-3. HANDHELD PROBE SURVEYS. 60
FIGURE 8-4. SLOT SURVEY DATA RESULTS. 61
FIGURE 8-5. DATA QUALITY RESULTS. 62
FIGURE 8-6. DATA RESULTS FOR HYSTERESIS SWEEPS. 63
FIGURE 8-7. DATA QUALITY: CMU HYSTERESIS RESULTS. 64
FIGURE 8-8. DATA QUALITY: DATA REPEATABILITY. 65
FIGURE 8-9. EFFECT OF FREESTREAM DYNAMIC PRESSURE. 66
FIGURE 8-10. EFFECT OF FLAP DEFLECTION. 67
FIGURE 8-11. CFD CORRELATION WITH TEST DATA. 68
FIGURE 8-12. CP DISTRIBUTION COMPARISON WITH CFD PREDICTION. 69
FIGURE 8-13. EFFECT OF FLAP BLOWING. 70
FIGURE 8-14. EFFECT OF 1% CHORD SLOT BLOWING ON LAVLET. 72
FIGURE 8-15. EFFECT OF EQUAL SLOT BLOWING ON FORWARD SLOTS. 73
FIGURE 8-16. EFFECT OF DIFFERENTIAL BLOWING ON FORWARD SLOTS. 74
FIGURE 8-17. WIND TUNNEL TEST DATA TO CFD COMPARISONS. 75
FIGURE 8-18. CP COMPARISON OF WIND TUNNEL DATA TO CFD. 76
FIGURE 8-19. MOLEC CONFIGURATION RESULTS. 77
FIGURE 8-20. EFFECT OF Q ON MOLEC CONFIGURATION. 78
FIGURE 8-21. COMPARISON OF WIND TUNNEL TEST DATA TO CFD. 79
FIGURE 8-22. CP DISTRIBUTION COMPARISONS. 80
FIGURE 8-23. BOUNDARY LAYER RAKE DATA. 81
FIGURE 8-24. HIGH-LIFT RESULTS FOR ALL AHLLE CONFIGURATIONS. 82
FIGURE 8-25. CP DISTRIBUTIONS FOR ALL AHLLE CONFIGURATIONS. 83
FIGURE 9-1. LIFT SUMMARY OF AHLLE CONFIGURATIONS. 85
FIGURE 9-2. THE AHLLE TEAM. 87

Abstract

This is the Northrop Grumman final report for the Advanced High-Lift Leading-Edge Technologies for Laminar Wings conceptual design and demonstration program performed for the National Aeronautics and Space Administration Langley Research Center. Northrop Grumman conducted conceptual aerodynamic CFD and QFD analysis to downselect two leading-edge concepts for high lift. The effort included aerodynamic analysis to examine instrumentation placement and propulsion analysis to design internal cavity geometry of the high-pressure blown slot configurations. A wind tunnel model design created a 7-foot span model of the complex configuration. A wind tunnel test plan, which included baseline, deflected trailing-edge, blown deflected trailing-edge, blown leading-edge, morphed leading-edge, and blown/morphed leading-edge airfoil configurations was developed. As a result of this program approach, a successful demonstration of high-lift leading-edge technology was reached, and the target goals for improved lift were exceeded by 30% with a maximum section lift coefficient (Cl) of 5.2. Incremental lift coefficient (ΔCl) of 3.5 and 3.1 was achieved on the two laminar compatible airfoil configurations (at cruise). Our high-lift design yielded a massive 94% lift improvement over conventional high-lift Krueger flap configurations while providing laminar flow capability on the cruise configuration.

1. Introduction and Overview

Northrop Grumman Corporation (NGC) has leveraged its extensive history of laminar flow research and experimentation to explore various methods of achieving high lift with leading-edge methods on a wing section compatible with laminar flow. Gains in maximum lift coefficient could potentially reduce wetted area and parasitic drag and therefore fuel consumption. Without resizing the wing, introducing high-lift capabilities into the wing would allow for the use of additional regional airports to reduce delay times in the National Aerospace System (NAS) to meet aggressive fuel, emission, and noise reduction goals currently set by the customer. Current mechanized leading-edge devices result in unavoidable steps and gaps that cause boundary-layer transition when stowed, making them incompatible with laminar flow at cruise. The Advanced High-Lift Leading-Edge (AHLLE) program, which was executed with the program schedule shown in figure 1-1, achieved exactly this goal of high lift on a laminar 2D airfoil section through wind tunnel testing at representative takeoff/landing Mach and Reynolds numbers.

The development and demonstrations outlined in this program are based on a foundation of progress in the aerospace industry over the last 20 years regarding laminar flow control research and flow control technology. Several Northrop Grumman research programs have advanced the technology readiness through design (MOLEC [1], LAVLET [2]), fabrication and testing for high-lift mobility configurations (IPLC [3,4]), and the advancement of laminar flow technology (HiLDA [5]).

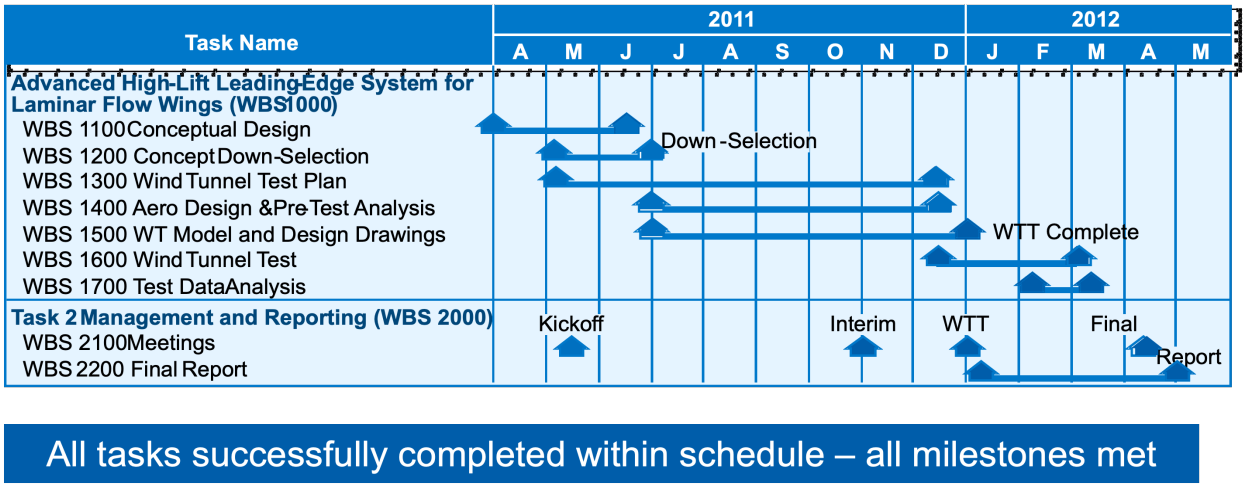


Figure 1-1. AHLLE program schedule.

Our approach to the maturation of high-lift technology incorporates lessons learned from these previous programs into a building block plan that focuses on computational fluid dynamics (CFD) aerodynamic analysis, propulsion design to achieve the desired blown effectiveness, detailed model design to integrate the challenging design strategy, and ground testing for validation. Several new and innovative approaches were developed by Northrop Grumman to deal with the challenges faced by coupling high-lift technology compatible with laminar flow. This program included brief analytical investigations to identify and quickly assess these technologies best suited for reconciling high-lift and laminar-flow wing design. The program also identified two potential methods for achieving high lift with a wing in the absence of a leading-edge slat.

The program emphasis for AHLLE was wind tunnel investigation of downselected, laminar compatible, high-lift leading-edge concepts, summarized in figure 1-2. These configurations are discussed in greater detail in section 2 of this final report. The program examined a baseline laminar flow 2D airfoil section for reference and the trailing edge was then deflected 45 degrees. The trailing-edge slot located at 80% chord was then blown to achieve a reference configuration. The leading-edge configurations included blown slots at 1% and 10% chord, a morphed leading-edge configuration, and a blown slot located at 12% chord with the leading edge morphed.

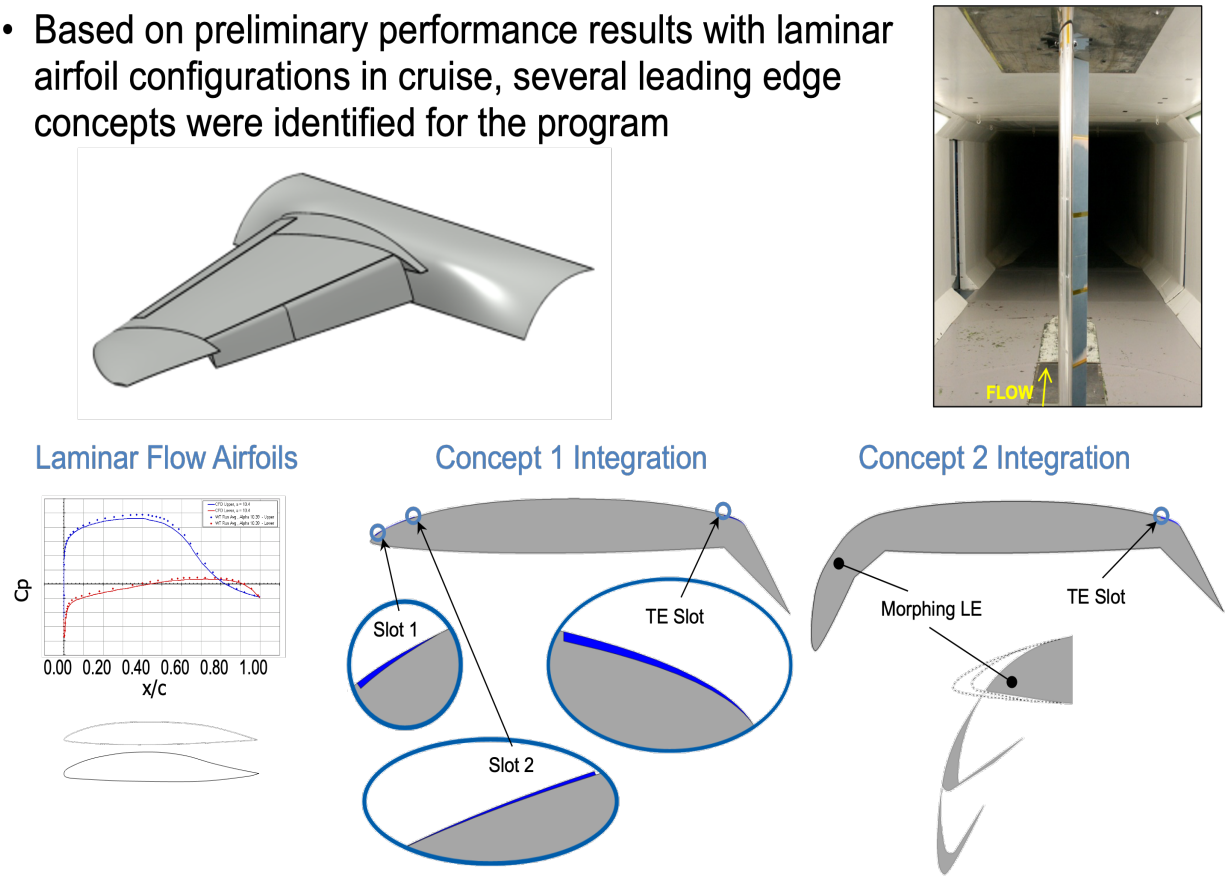


Figure 1-2. Laminar compatible leading-edge concepts.

To accomplish the program, the NGC team was identified with experience in high-lift conceptual design and flow control, aerodynamic analysis, structural and configuration design, wind tunnel analysis, model design, fabrication, and support. The AHLLE team organization is shown in figure 1-3. Predicted high-lift behavior from the NGC flow control toolbox as shown in figure 1-4 anticipated 3D lift on a full-scale wing to achieve a section lift coefficient (Cl) 2.8 for the laminar airfoil virtual leading-edge technology (LAVLET) configuration.

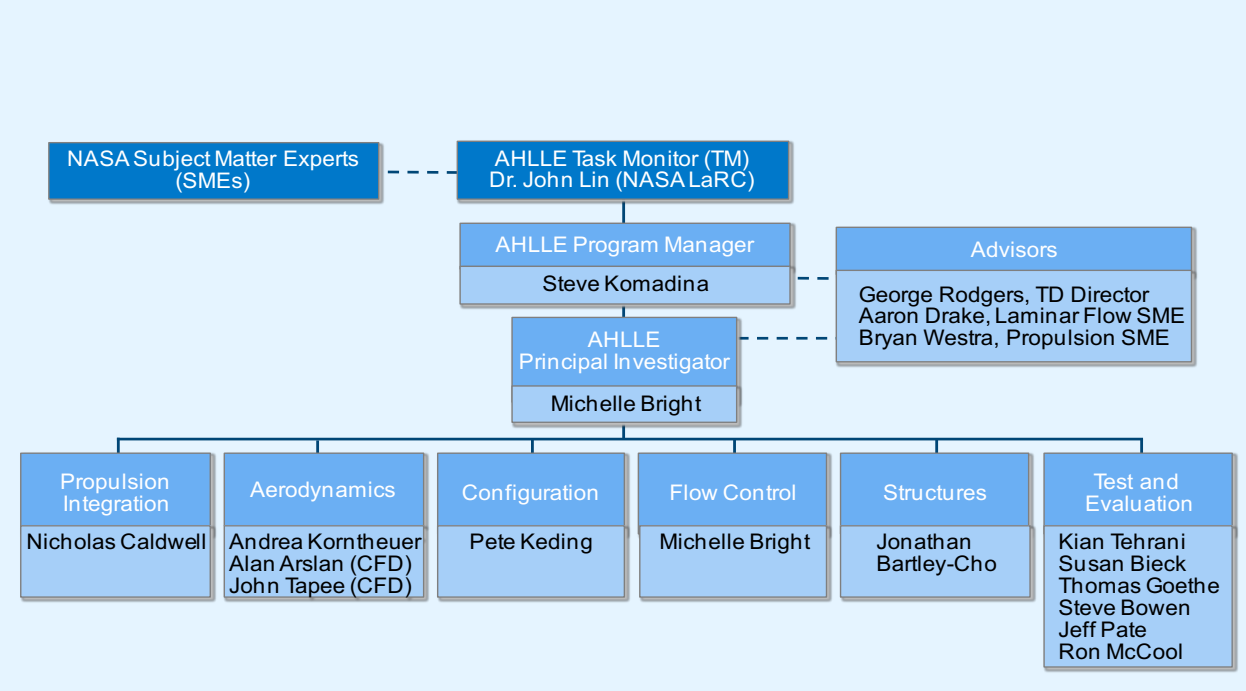


Figure 1-3. Program and team organizational structure.

- Baseline laminar airfoil chosen for AHLLE wind tunnel study
- Predicted behavior of high lift configurations on a laminar airfoil

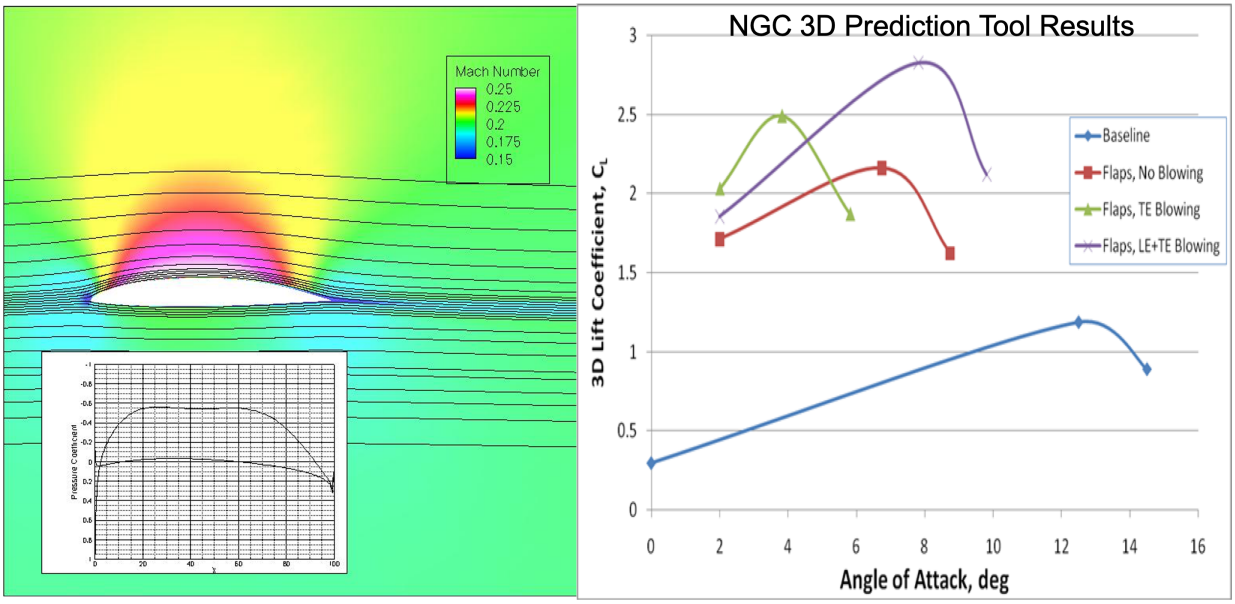


Figure 1-4. Baseline airfoil and prediction of lift leading-edge configurations.

2. Conceptual Design

During Task 1 of the program, several conceptual designs were investigated to achieve high lift and quickly focused on three primary deliverables. As shown in figure 2-1, they include (1) a drooped leading-edge design with two degrees of freedom and articulation at 15% chord, cruise airfoil deflection of 40%, a cruise airfoil extension of 12% chord, a tip deflection of 25 degrees and a tip extension at 8% chord; (2) a blown leading edge with spanwise slots located at 1% and 10% chord; and (3) unsteady leading-edge blowing. The task included Northrop Grumman generalized compressible Navier Stokes (GCNS) solutions for the morphed leading-edge concept (with and without blowing at the shoulder), the steady blown leading-edge concept, and CFD++ examination of unsteady pulsation on the leading edge. All lift results were compared to a traditional leading-edge configuration (Krueger Flap). Figure 2-2 details the definitions used throughout the study.

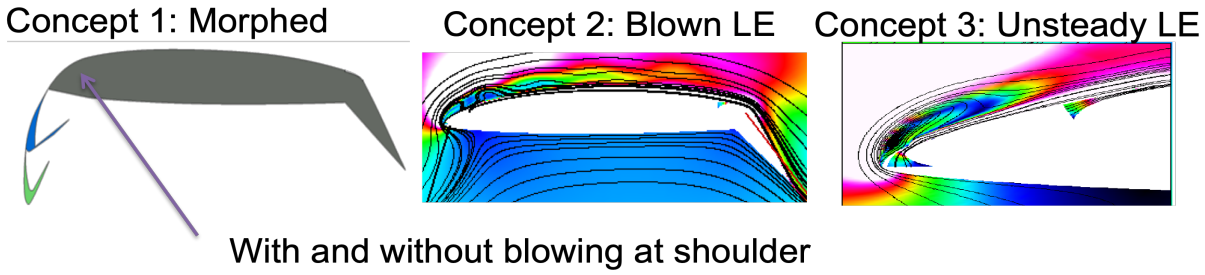


Figure 2-1. Leading-edge conceptual designs examined.

- Definition of Cμ

$$C_\mu = \frac{\dot{m}V_{jet}}{q_\infty S} = \frac{\dot{m}V_{jet}}{\frac{1}{2}\gamma p_\infty M_\infty^2 S}$$

  - Where,
    - Vjet matches an exit Mach number of 1 at plenum nozzle (also referred to Vjet_ideal; 1249.624 ft/s)
    - S is the equivalent reference area of the wind tunnel model (*e.g.* 2' chord x 6' span = 12 ft² = S)

$$C_\mu = \frac{\dot{m}V_{jet,ideal}}{qS}$$

$$M_{jet,ideal} = \sqrt{\frac{2}{\gamma - 1}\left[\left(\frac{P_t}{P_{s0}}\right)^{\frac{\gamma-1}{\gamma}} - 1\right]}$$

$$T_{s,ideal} = \frac{T_t}{\left(1 + \frac{(\gamma-1)}{2} M_{jet,ideal}^2\right)}$$

$$a = \sqrt{\gamma R T_{s,ideal}}$$

$$V_{jet,ideal} = aM_{jet,ideal}$$

Figure 2-2. Blowing coefficient definition.

2.1 Conceptual Design Configurations

As part of Task 1, a conceptual design study was performed to analytically demonstrate high lift with steady blowing and pulsed blowing through CFD analysis. This activity included conceptual design of 10 configurations shown in figure 2-3. A brief first principles examination of steady and pulsed blowing concepts on structural design and configuration integration impacts was also performed during this phase of the program. The configuration drawings determined the maximum cavity sizes, location of structural spars, material thicknesses, and rough geometry considerations that would impact co-location of blowing and mechanization of the leading-edge concepts. Results for the ten configurations are shown in the table of figure 2-3 with predicted section lift and stall angle.

Configuration	Definition	LE1 loc/h/Cmu	LE2 loc/h/Cmu	TE loc/h/Cmu	Full Scale Clmax / Alpha_stall (deg)	WT Scale Clmax / Alpha_stall (deg)
1	Clean Airfoil	-	-	-	1.3 / 11	1.225 / 10
2	Simple TE @ 45 degrees	-	-	80% / 0 / 0	1.65 / 5.5	1.87 / 6.0
3	Blown Simple TE flap (45°)	-	-	80% / 0.2" / 0.035	3.108 / -4.0	3.0 / -4.0
4	2D Blown LE Optimal Configuration	1% / 0.02" / 0.0355	10% / 0.02" / 0.033	80% / 0.2" / 0.035	4.1 / 6	3.85 / 6.0
5	100 % Droop (2D1b)	-	-	80% / 0.2" / 0.035	4.6 / 13	4.17 / 11.0
6	75 % Droop	-	-	80% / 0.2" / 0.035	4.6 / 13	4.65 / 12.0
7	50% Droop	-	-	80% / 0.2" / 0.035	4.2 / 8	4.2 / 8.0
8	25 % Droop	-	-	80% / 0.2" / 0.035	3.75 / 4	3.6 / 2.0
9	Pulsed LE	1% / 0.02"	10% / 0.02"/0.033	80% / 0.2" / 0.035	4.1/6	3.85/6.0
10	50% Droop Bleed at Shoulder		15%/0.4/0.1	80%/0.2"/ 0.035	5.0/13	

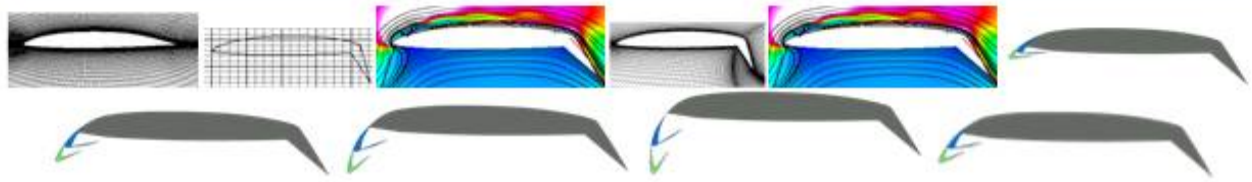


Figure 2-3. Leading-edge configuration downselection matrix.

Figure 2-4 shows the flow visualization result for the best location of leading-edge blown slots on the laminar baseline airfoil. The configuration has leading-edge slots at 1% and 10% chord and a trailing-edge slot at 80% chord over a blown simple flap that is deflected 45 degrees. In this configuration, the LAVLET configuration achieves a section lift $c_l = 4.1$ and a stall angle of

approximately 6 degrees. The resultant lift curves for the blown slot configurations are shown in figure 2-5.

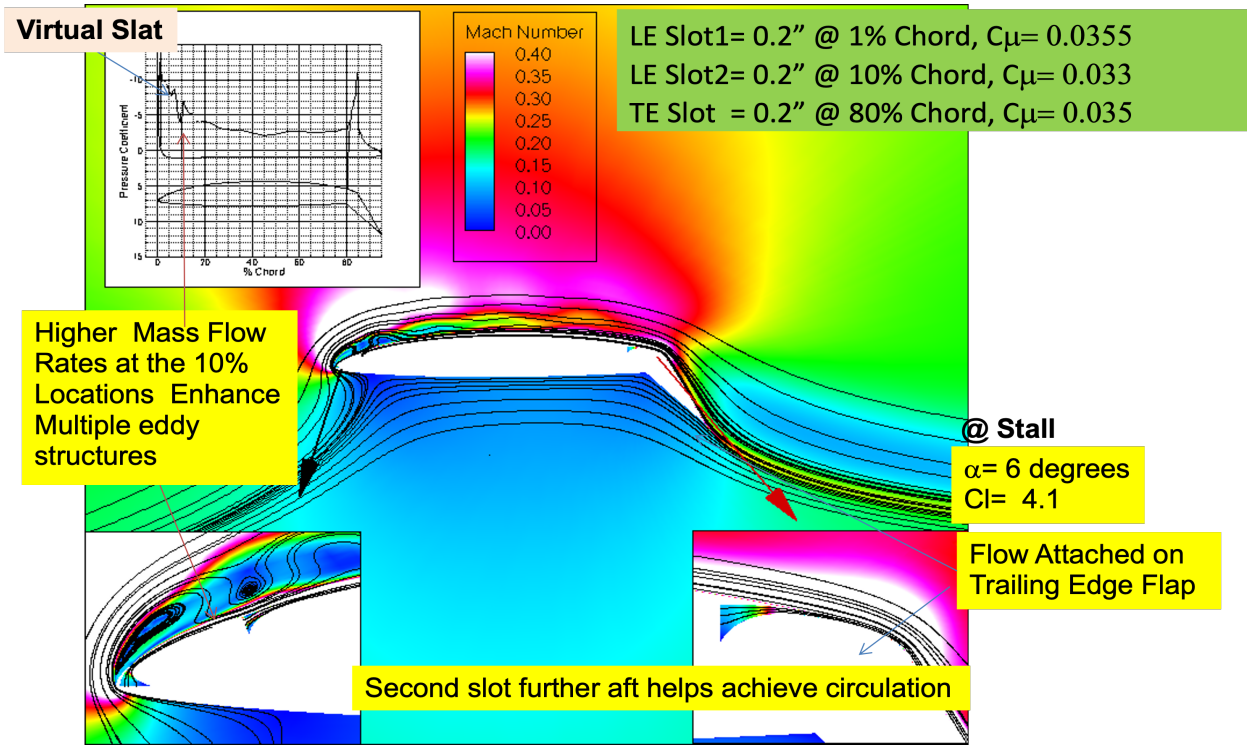


Figure 2-4. Flow visualization of LAVLET configuration.

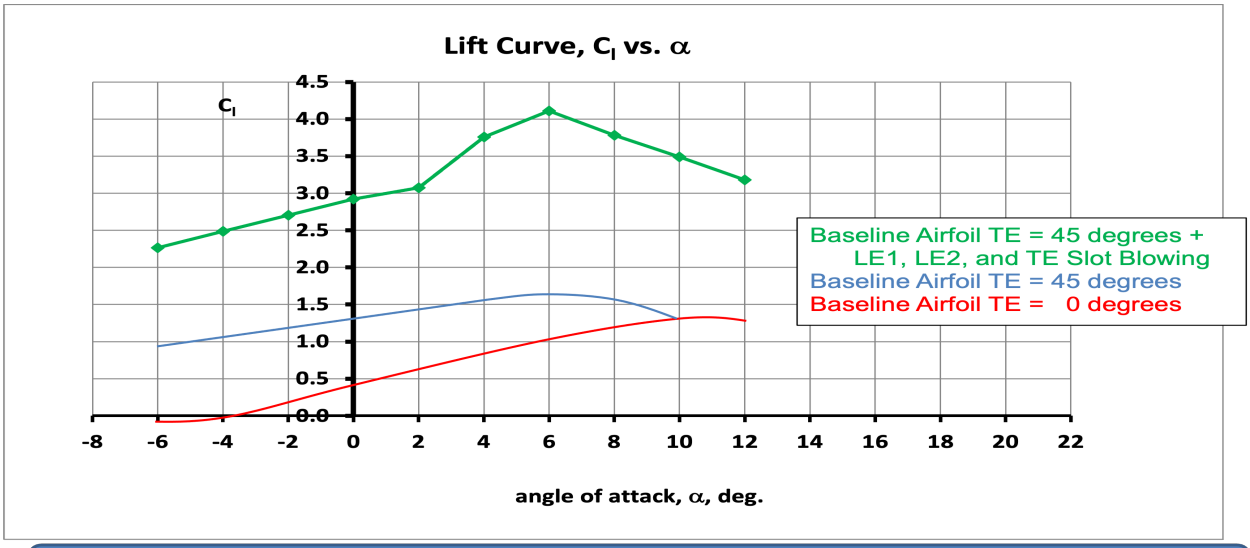


Figure 2-5. Predicted lift curves for blown slot configuration.

The next step in task 1 was to analyze through CFD and structural design the multiobjective leading-edge concepts (MOLEC) configurations shown in figure 2-6. This concept will also be referred to as the "morphed" leading edge. All the deployment strategies shown in figure 2-6 were examined in CFD along with a blown slot at 12% chord, a blown slot at 15%, and with

suction at 15% chord. The resulting flow visualization graphics are represented in figure 2-7 figure 2-11.

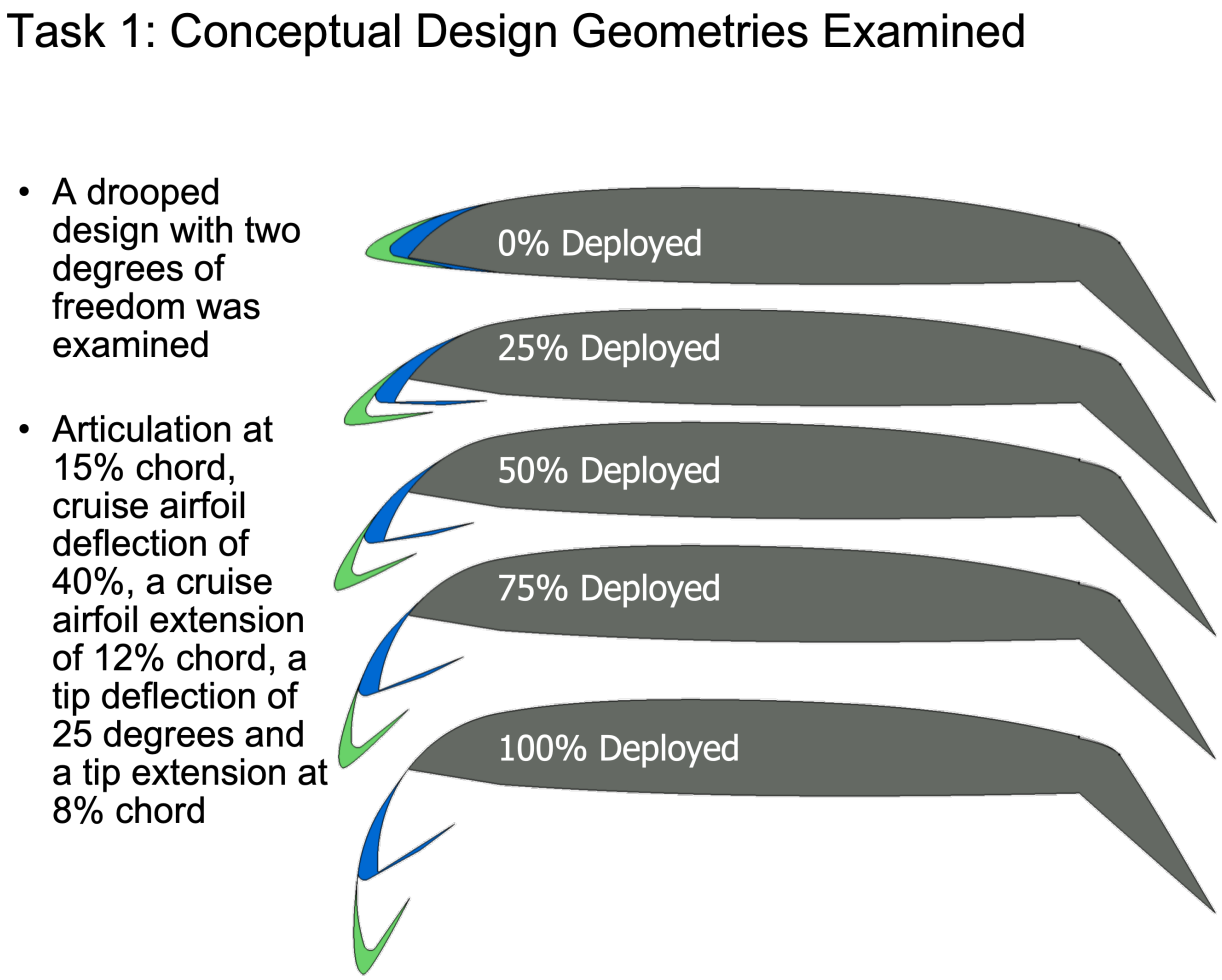


Figure 2-6. Morphed leading-edge configurations studied.

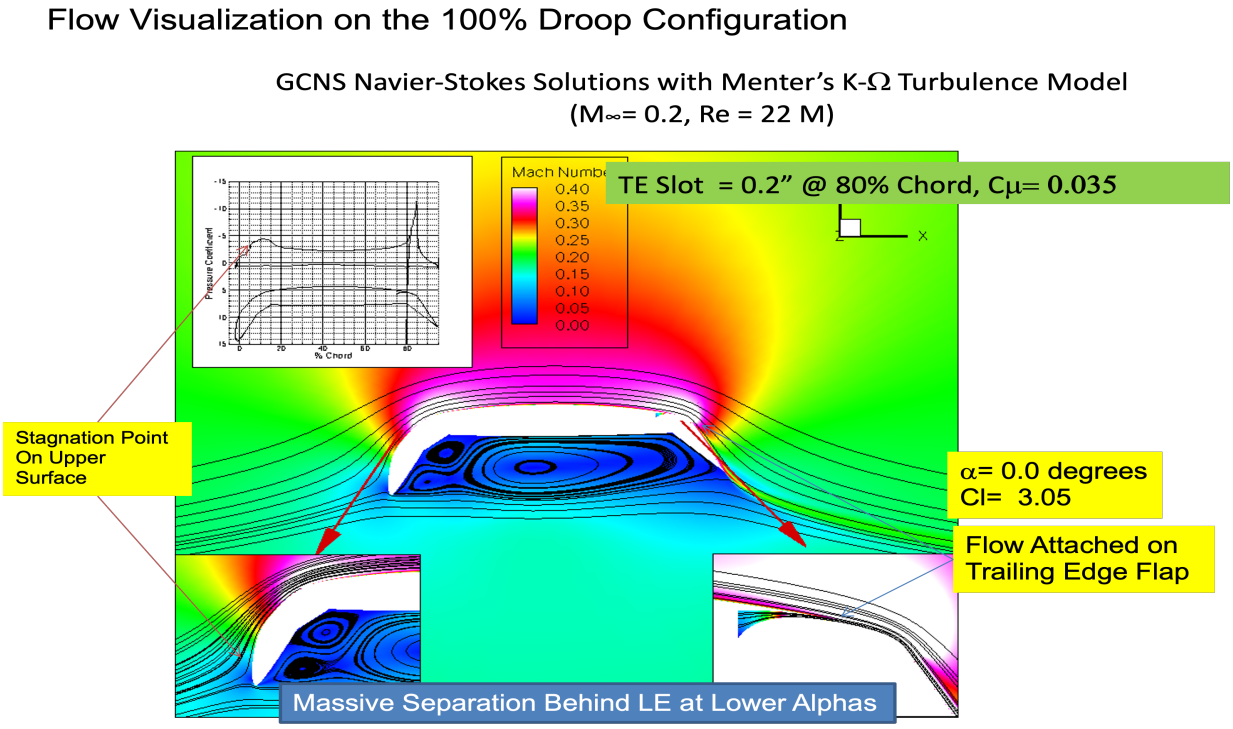


Figure 2-7. Flow visualization for MOLEC configuration at 100% droop and alpha = 0 degrees.

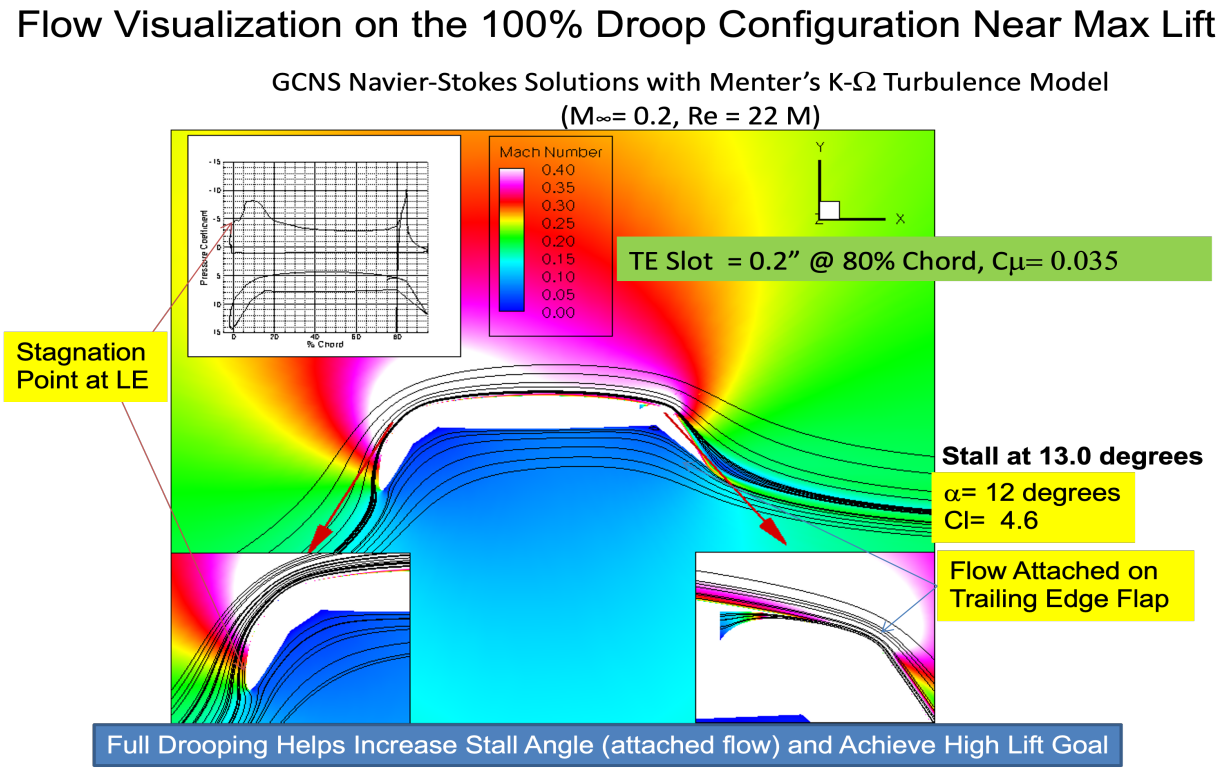


Figure 2-8. Flow visualization result for 100% droop case at alpha near stall.

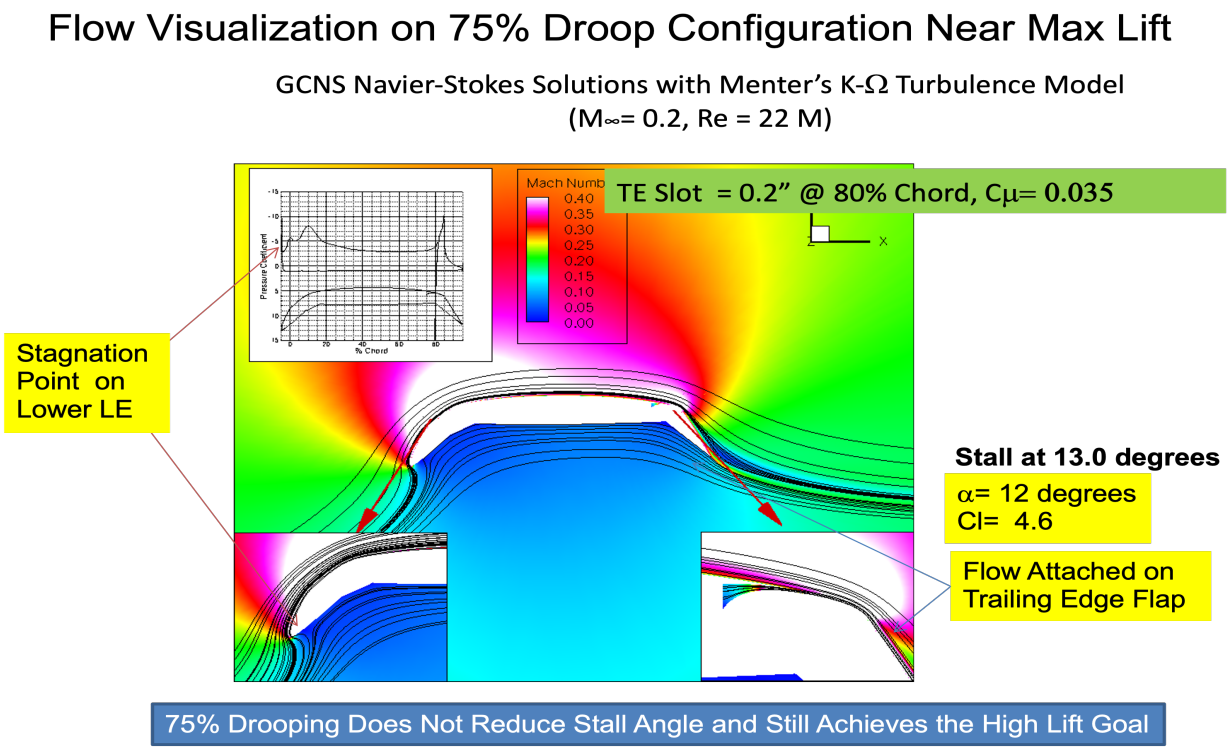


Figure 2-9. Flow visualization for 75% droop case.

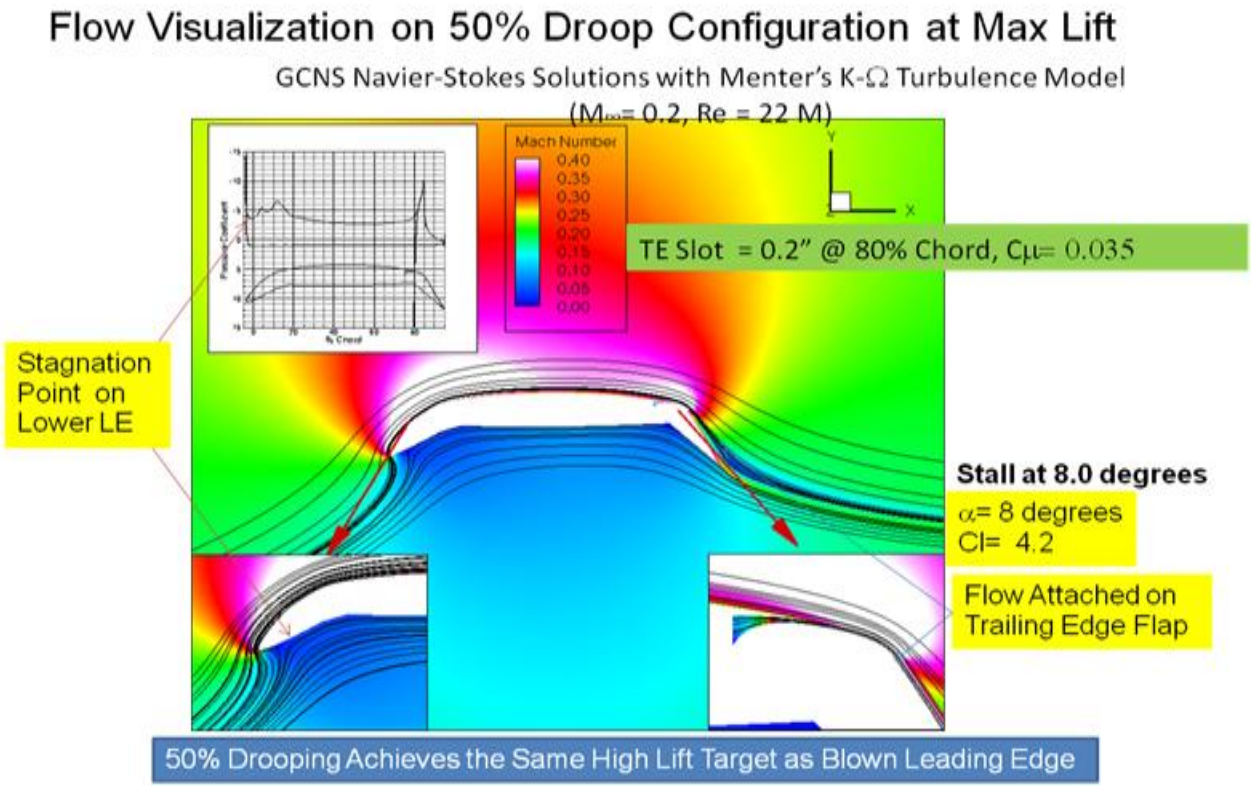


Figure 2-10. Flow visualization result for 50% droop case.

In order to recover stall angle at the takeoff and landing condition and for increased stability during those flight regimes, CFD analysis was performed using a suction patch ahead of the 15% chord location to improve the stall behavior. The results confirmed that implementation of bleed at 15% chord improved section lift to c_l = 4.5 and improved the stall angle to 12 degrees. This result is illustrated in figure 2-11. Although implementation of bleed was not realizable on this geometry, further configuration analysis led to the analysis and implementation of a blown slot at 12% and 15% chord. Those results are shown in figure 2-12.

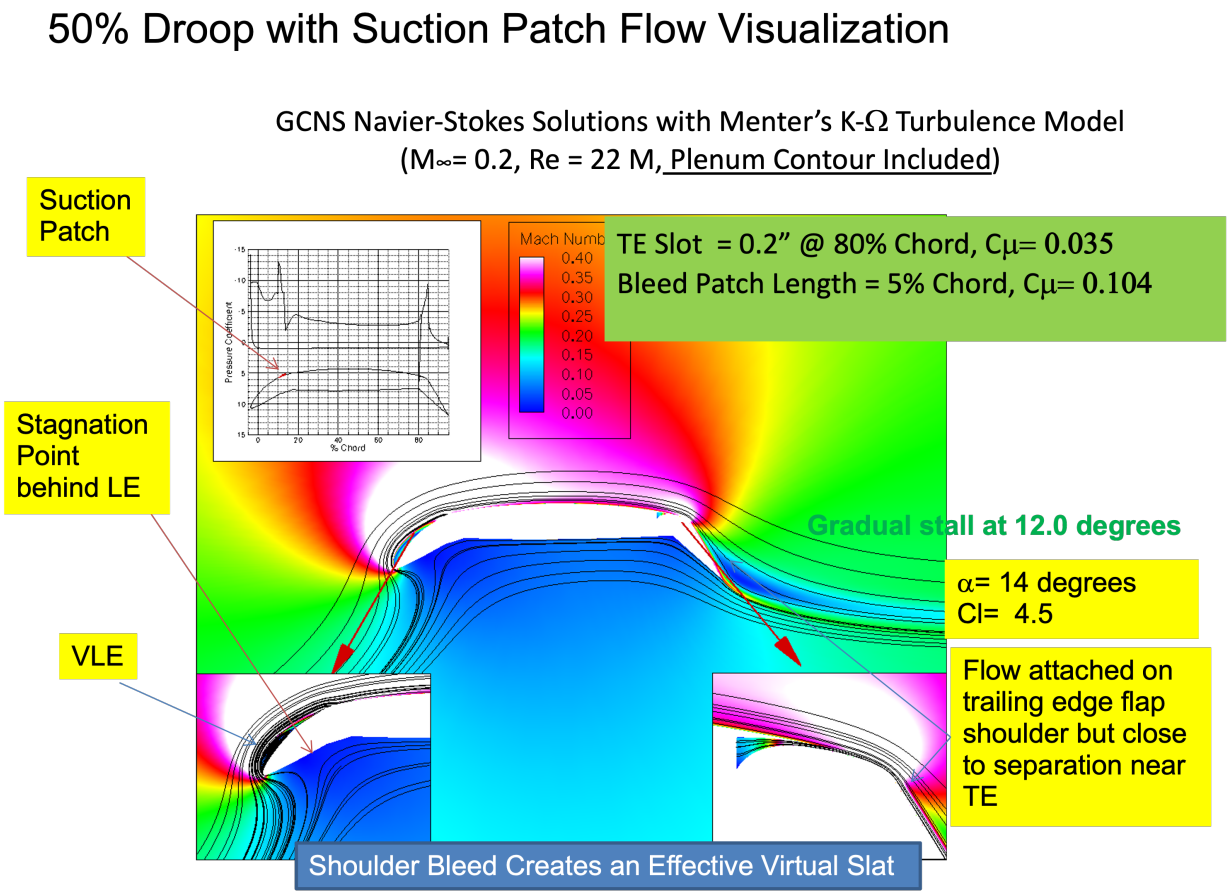


Figure 2-11. Flow visualization results for shoulder suction.

Task 1: MOLEC With Blown Shoulder at 12% Chord

- Blowing increases section lift to 5.3 and improves stall angle

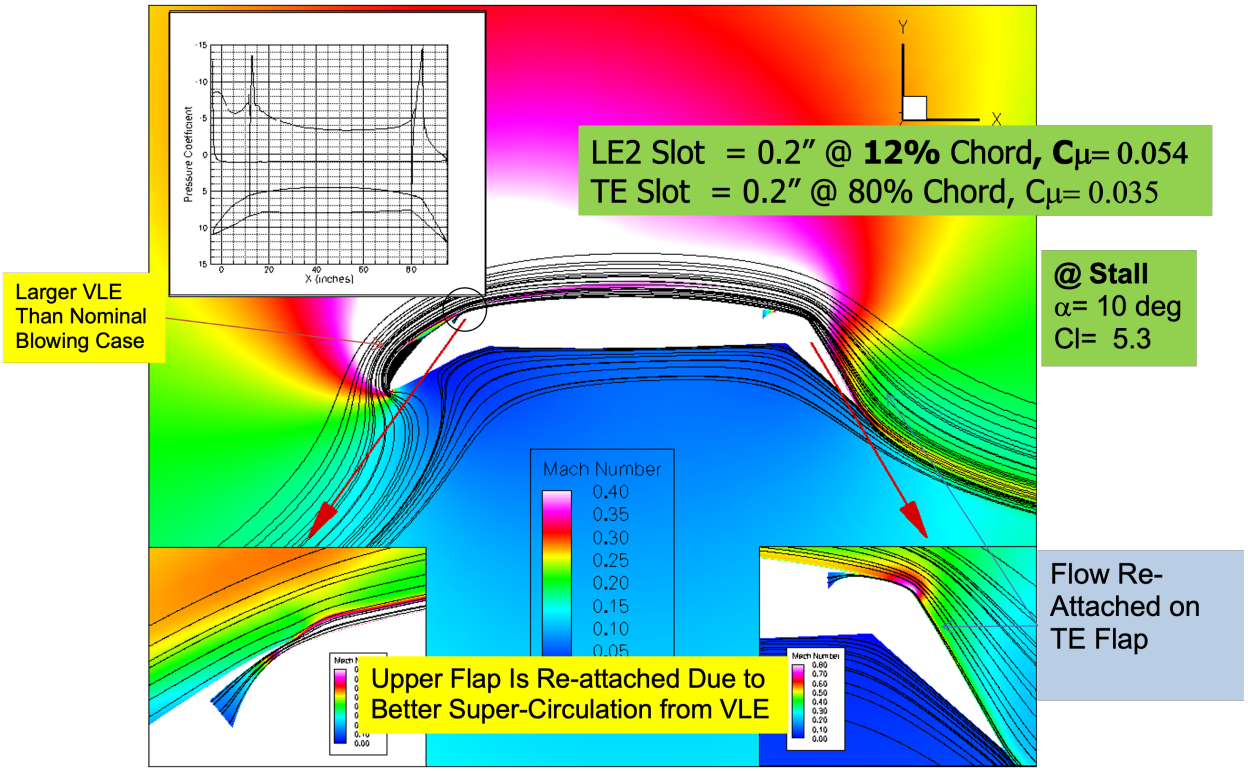


Figure 2-12. Blown shoulder CFD results.

The conceptual design task concluded with the determination of trailing-edge blowing on the fixed 45% simple flap. As expected, with increased momentum coefficient (Cμ) a higher section-lift coefficient is reached on the MOLEC configurations. That result is summarized in figure 2-13.

Task 1: MOLEC Leading Edge Results

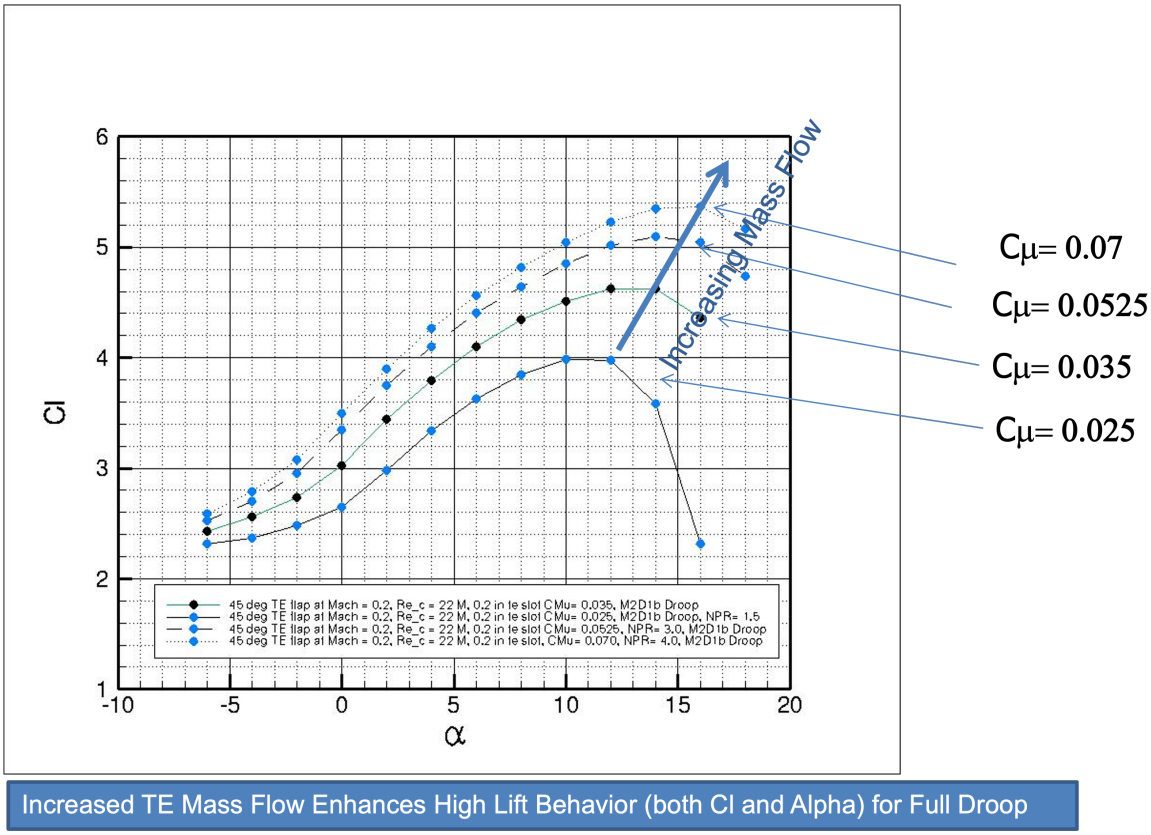
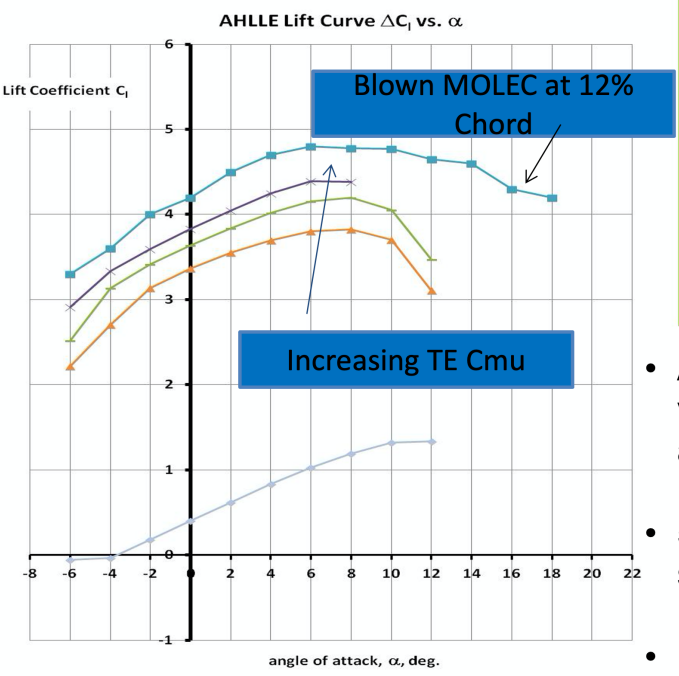


Figure 2-13. Trailing-edge blowing results on the MOLEC configuration.

A summary of the conceptual design results for the MOLEC high-lift designs is reviewed in figure 2-14. The graph represents the section c_l vs. alpha curve for increased levels of blowing on the trailing edge. The 12% chord blown slot result that achieves a predicted $c_l = 5.0$ is also shown. The 50% drooped leading-edge strategy achieves the targeted lift prediction of $c_l = 4.0$ without induction of leading-edge instabilities on the lower outer mold line (OML) surface. For these reasons, the 50% droop case is chosen over the other MOLEC configurations for further analysis and potential implementation. A summary of all the conceptual design results is highlighted in figure 2-15. These concepts will be used in the downselection for the wind tunnel test addressed in the following section.

Task 1: Morphed Leading Edge Summary



- Aerodynamic instabilities are very apparent in the 100% and 75% drooped case
- 50% droop case achieves similar section lift as LAVLET
- Blown MOLEC achieves highest section lift

Figure 2-14. Summary of MOLEC conceptual design results.

Summary of Conceptual Design Results

Configuration	Cmu1	Cmu2	Cmu3	Alpha Stall (degrees)	Cl (section)
Baseline Airfoil	n/a	n/a	n/a	10	1.4
Baseline Airfoil Deflected TE	n/a	n/a	n/a	5.5	1.67
Baseline Airfoil with Blown Deflected TE	n/a	n/a	0.035	-4	3.1
Blown Leading Edge (LAVLET)	0.035	0.035	0.035	6	4.1
MOLEC	n/a	n/a	0.035	8	4.0
MOLEC with 12% Chord Blown Slot	n/a	0.054	0.035	10	5.3

Figure 2-15. Summary of conceptual design study.

3. Model Downselect

During this Task 2 effort, the results of the conceptual design task were used to determine the best suited candidates for wind tunnel design, fabrication, and testing.

3.1.Configuration Analysis

Configuration selection was based on a quality function deployment (QFD) ranking of the available high-lift configurations identified in Task 1. The preferred concepts were selected as the candidates for further aerodynamic analysis and wind tunnel testing. The LAVLET was chosen as the optimal high-lift configuration for ground testing along with MOLEC and blown MOLEC. This decision to test two configurations is explained further in the sections below.

3.2.QFD Down Selection

Configuration selection for wind tunnel testing was based on a QFD ranking of the AHLLE conceptual designs. Based on the QFD criteria and relative weightings considered, combined with the technology scoring conducted, the two recommended AHLLE concepts were:

- LAVLET (with steady blowing)
- MOLEC: 50% deployed (with and without steady blowing located at the 12% chord location)

The team arrived at these test concepts based on a five-step process enumerated below and detailed in figure 3-1.

QFD was performed as a five-step process:

1. Develop performance and system integration criteria based on program goals
2. Develop relative weighting of these criteria based on requirements with input from subject matter experts (SMEs)
3. Develop AHLLE concepts to be considered
4. SMEs score the AHLLE concepts against each of these criteria
5. Rank the concepts based on their overall technology score

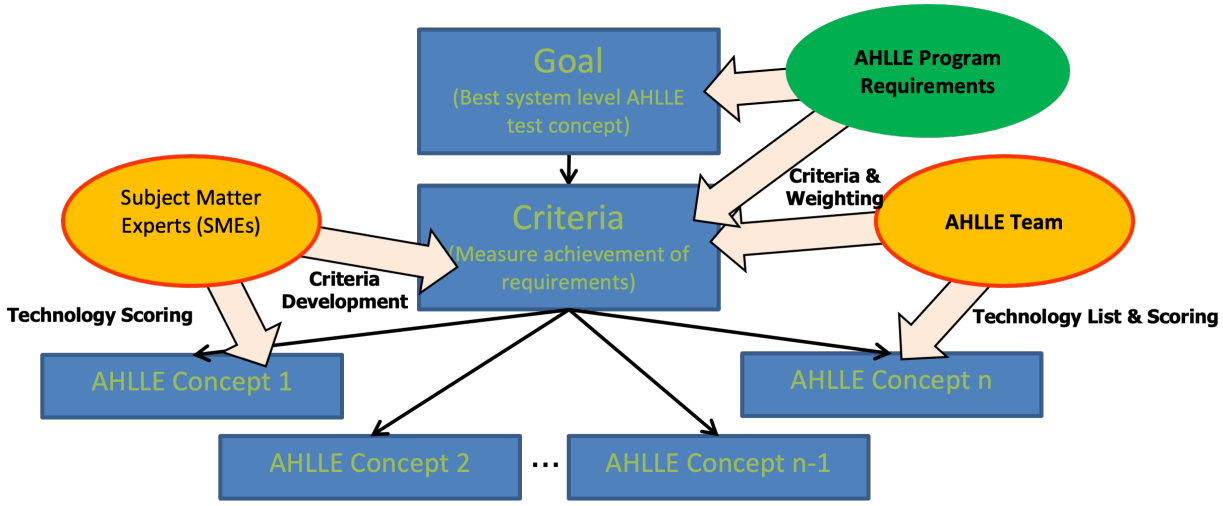


Figure 3-1. QFD analysis process.

Ten assessment criteria categories were identified and ranked. Laminar flow compatibility and lift performance have been deemed the most important parameters, followed by power/bleed requirement. In figure 3-2, error bars show ± one average deviation based on team inputs.

Weighting	Average Dev	Assessment Criteria
27.8%	3.9%	Laminar Flow Compatibility
18.3%	4.7%	Lift Performance
7.5%	2.8%	Weight
7.0%	2.6%	Noise
6.1%	1.5%	Complexity
11.8%	3.8%	Power Requirement
4.1%	2.7%	TRL Input
3.9%	0.6%	Affordability
6.9%	2.2%	Reliability
6.7%	2.4%	Maintainability

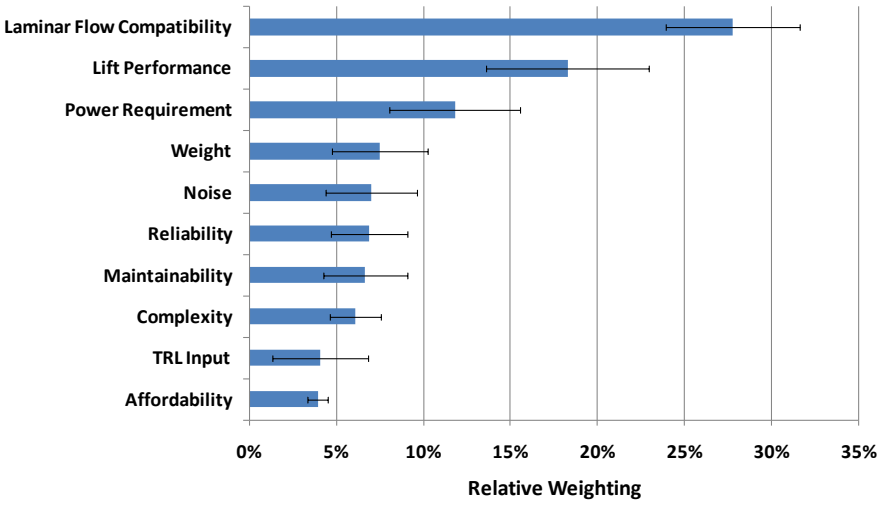


Figure 3-2. Relative rankings and weighting assessment factors for QFD

A list of the candidate leading-edge technologies is shown in figure 3-3. The candidates include MOLEC, LAVLET, MOLEC with blowing, MOLEC with suction, LAVLET with unsteady pulsation, and a Krueger flap. As shown in the results of figure 3-4, LAVLET concepts emerge as the clear winners in terms of technology score. Added complexity, weight, etc., of the unsteady LAVLET concept brings it down relative to the steady concept. MOLEC with shoulder blowing produces the next highest technology score. Tabular results from all the rankings are assembled in figure 3-4 to figure 3-14.

AHLLE Technology List		
Technology#	Description	Designation
N-AERO-01	Multi-Objective Leading Edge Concept (MOLEC) 50% Deployed	MOLEC
N-AERO-02	Laminar Virtual Leading Edge Technology (LAVLET) with Steady Blowing	LAVLET
N-AERO-03	MOLEC 50% Deployed with Leading Edge Shoulder Steady Blowing	MOLEC + Blowing
N-AERO-04	MOLEC 50% Deployed with Shoulder Suction	MOLEC + Suction
N-AERO-05	LAVLET + Unsteady Blowing	LAVLET Unsteady
N-AERO-06	Conventional Krueger Flap	Krueger

Figure 3-3. Candidate high-lift leading-edge technologies.

AHLLE Technology List		Tech Score
N-AERO-01	MOLEC	4.286
N-AERO-02	LAVLET	6.077
N-AERO-03	MOLEC + Blowing	4.368
N-AERO-04	MOLEC + Suction	4.193
N-AERO-05	LAVLET Unsteady	5.413
N-AERO-06	Krueger	4.202

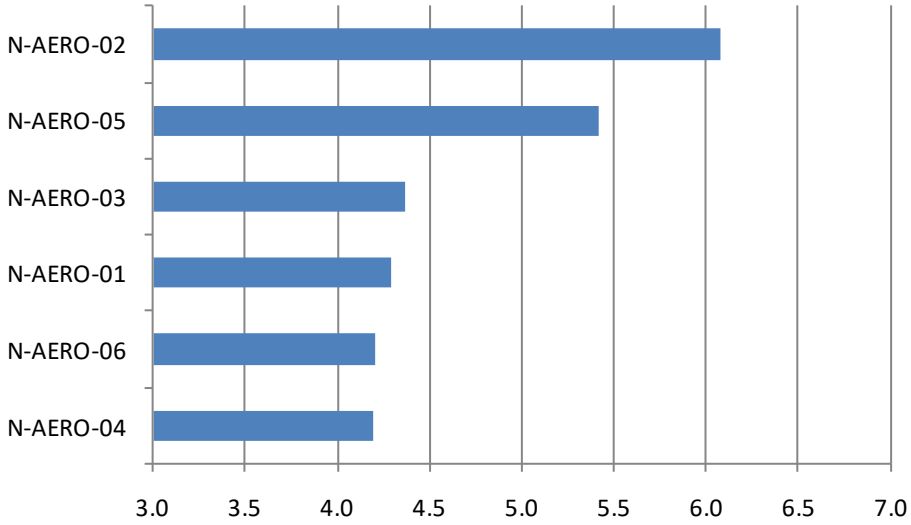


Figure 3-4. Results of the QFD analysis.

AHLLE Technology List		Score	Comments
N-AERO-01	MOLEC	7	50% MOLEC
N-AERO-02	LAVLET	9	
N-AERO-03	MOLEC + Blowing	7	
N-AERO-04	MOLEC + Suction	7	
N-AERO-05	LAVLET Unsteady	9	Assumed to have same compatibility as N-AERO-2
N-AERO-06	Krueger Flap	1	Rigid Krueger flap not designed for laminar flow compatibility – some possible w/ design

Laminar Flow Compatibility		
1	Poor	Likely to cause transition at leading edge
3	Moderate	Likely to cause transition >10% chord on both surfaces
5	Medium	Likely to cause transition >10% chord on upper surface
7	Significant	Likely to cause transition >50% chord on upper surface
9	High	Likely to support laminar flow to trailing edge control surfaces

Figure 3-5. Laminar flow compatibility scores.

AHLLE Technology List		ΔCl_{max}	Score	Comments
N-AERO-01	MOLEC	2.9	3	50% MOLEC; Stall at low AOA
N-AERO-02	LAVLET	2.8	7	Optimized from LAVLET program
N-AERO-03	MOLEC + Blowing	--	7	Assuming some benefit over N-AERO-01
N-AERO-04	MOLEC + Suction	3.2	7	Only achieved this lift increment with extreme $C\mu$
N-AERO-05	LAVLET Unsteady	2.8	7	Assume no lift benefit relative to N-AERO-02
N-AERO-06	Krueger Flap	~1.5	5	Justification based on report*

Lift Performance		
1	Poor	$\Delta CL_{max} > 0.0$ relative to clean airfoil
3	Moderate	$\Delta CL_{max} > 0.5$ relative to clean airfoil
5	Medium	$\Delta CL_{max} > 1.0$ relative to clean airfoil
7	Significant	$\Delta CL_{max} > 2.0$ relative to clean airfoil
9	High	$\Delta CL_{max} > 3.0$ relative to clean airfoil

*Englar, R., Smith, M., Kelley, S., and Rover, R., "Application of Circulation Control to Advanced Subsonic Transport Aircraft, Parts I-II", *Journal of Aircraft*, Vol. 31, No. 5, pp. 1160-1177, 1994.

Figure 3-6. Representative lift performance for technologies.

AHLLE Technology List		Score	Comments
N-AERO-01	MOLEC	5	50% MOLEC
N-AERO-02	LAVLET	1	Possible extreme bleed requirements
N-AERO-03	MOLEC + Blowing	3	Traditional slat extension plus bleed
N-AERO-04	MOLEC + Suction	1	Balance between suction pump requirements and traditional slat extension
N-AERO-05	LAVLET Unsteady	3	Mass flow benefit relative to N-AERO-02
N-AERO-06	Krueger Flap	5	Similar to conventional high-lift device

Power Requirement		
1	High	>+10% power or bleed requirement relative to traditional high-lift system
3	Significant	>+5% power or bleed requirement relative to traditional high-lift system
5	Medium	Power or bleed requirement comparable to traditional high-lift system
7	Moderate	<-5% power or bleed requirement relative to traditional high-lift system
9	Low	<-10% power or bleed requirement relative to traditional high-lift system

Figure 3-7. Power requirement QFD scoring.

AHLLE Technology List		Weight, lb/ft^{2*}	Score	Comments
N-AERO-01	MOLEC	+29%	1	50% MOLEC
N-AERO-02	LAVLET	-22%	9	Should fall into the 9 bucket, but weight estimate does not include
N-AERO-03	MOLEC + Blowing	>29%	1	Will be greater than 50% MOLEC
N-AERO-04	MOLEC + Suction	>29%	1	Will be greater than 50% MOLEC
N-AERO-05	LAVLET Unsteady		7	Will be greater than N-AERO-02, with additional weight for devices
N-AERO-06	Krueger Flap	-9.5 %	7	Rigid Krueger flap

Weight		
1	High	Heavier than traditional high-lift device
3	Significant	Comparable to traditional high-lift device
5	Medium	<5% weight savings compared to traditional high-lift device
7	Moderate	<10% weight savings compared to traditional high-lift device
9	Low	<15% weight savings compared to traditional high-lift device

*Measured relative to a traditional three-position slat without slave tracks (5.80 lb/ft^2)

Figure 3-8. Relative QFD scores due to weight.

AHLLE Technology List		Score	Comments
N-AERO-01	MOLEC	7	50% MOLEC – designed for takeoff noise reduction
N-AERO-02	LAVLET	1	Slow blowing through high AR slots will produce excessive high-frequency noise
N-AERO-03	MOLEC + Blowing	3	Slow blowing will produce excessive high-frequency noise, though fewer slots
N-AERO-04	MOLEC + Suction	5	Quieter than blowing, but addition of suction system still generates noise
N-AERO-05	LAVLET Unsteady	1	Acoustically similar to N-AERO-02
N-AERO-06	Krueger Flap	5	Comparable to traditional device

Noise		
1	High	+6 dB relative to traditional high-lift device
3	Significant	+3 dB relative to traditional high-lift device
5	Medium	Noise comparable to traditional high-lift device
7	Moderate	-3 dB relative to traditional high-lift device
9	Low	-6 dB relative to traditional high-lift device

Figure 3-9. Relative weightings due to noise.

AHLLE Technology List		Score	Comments
N-AERO-01	MOLEC	3	50% MOLEC – based on number of parts and complexity
N-AERO-02	LAVLET	7	based on number of parts and complexity
N-AERO-03	MOLEC + Blowing	3	More parts to fail than N-AERO-01
N-AERO-04	MOLEC + Suction	3	More parts to fail than N-AERO-01
N-AERO-05	LAVLET Unsteady	5	Balance between simplicity of blowing system and complexity of actuation
N-AERO-06	Krueger Flap	5	Estimated to be same as traditional high-lift device

Reliability		
1	Low	<-10% MTBF* relative to traditional high-lift device
3	Moderate	<-5% MTBF relative to traditional high-lift device
5	Medium	MTBF comparable to traditional high-lift device
7	Significant	>+5% MTBF relative to traditional high-lift device
9	High	>+10% MTBF relative to traditional high-lift device

Figure 3-10. Relative weightings due to reliability.

AHLLE Technology List		Score	Comments
N-AERO-01	MOLEC	3	50% MOLEC
N-AERO-02	LAVLET	3	No mechanical moving parts, though thinness of blade seals implies easy damage
N-AERO-03	MOLEC + Blowing	1	Additional systems relative to N-AERO-01
N-AERO-04	MOLEC + Suction	1	Additional systems relative to N-AERO-01
N-AERO-05	LAVLET Unsteady	1	Additional systems relative to N-AERO-02
N-AERO-06	Krueger Flap	5	Assumed same MTTR as traditional device

Maintainability		
1	High	>+10% MTTR* relative to traditional high-lift device
3	Significant	>+5% MTTR relative to traditional high-lift device
5	Medium	MTTR comparable to traditional high-lift device
7	Moderate	<-5% MTTR relative to traditional high-lift device
9	Low	<-10% MTTR relative to traditional high-lift device

Figure 3-11. Relative weightings due to maintainability.

AHLLE Technology List		Score	Comments
N-AERO-01	MOLEC	1	Two actuated sections would at least double the part count
N-AERO-02	LAVLET	7	Greatly reduced part count, few moving parts
N-AERO-03	MOLEC + Blowing	1	> Part count than MOLEC alone
N-AERO-04	MOLEC + Suction	1	> Part count than MOLEC alone
N-AERO-05	LAVLET Unsteady	3	N-AERO-2 plus part count associated with unsteady devices
N-AERO-06	Krueger Flap	5	~2100 parts for fixed-camber Krueger

Complexity		
1	High	>+25% part count relative to traditional high-lift system*
3	Significant	>+10% part count relative to traditional high-lift system
5	Medium	Part count comparable to traditional high-lift system
7	Moderate	<-10% part count relative to traditional high-lift system
9	Low	<-25% part count relative to traditional high-lift system

Figure 3-12. Relative weightings due to complexity.

AHLLE Technology List		Technology Readiness Level	Technology Risk Index	Comments
N-AERO-01	MOLEC	3	1.3	Extensive CFD analysis demonstrating high-lift/reduced noise
N-AERO-02	LAVLET	3	1.3	Extensive CFD analysis demonstrating high lift
N-AERO-03	MOLEC + Blowing	3	1.3	Some CFD analysis demonstrating high lift under AHLLE program
N-AERO-04	MOLEC + Suction	3	1.3	Some CFD analysis demonstrating high lift under AHLLE program
N-AERO-05	LAVLET Unsteady	2	1.1	Concept formulated
N-AERO-06	Krueger Flap	9	9.0	Used on variants of the 727, 737, and 747

Technology Readiness Level*	
9	Flight System Proven
8	Flight System Qualified
7	Prototype Demonstrated In Airborne Environment
6	Prototype Demonstrated In Relevant Environment
5	Component/Breadboard Validated In Relevant Environment
4	Component/Breadboard Validated In Laboratory
3	Critical Function Demonstrated(POC)
2	Technology Concept Formulated
1	Basic Principle Observed

Figure 3-13. Technology readiness level (TRL) assessment.

AHLLE Technology List		Score	Comments
N-AERO-01	MOLEC	3	D*- moderate advance to traditional technology P** - more parts than traditional device O&S*** - more moving parts than traditional device
N-AERO-02	LAVLET	7	D - leading edge blowing is advancing state of traditional technology P - fewer parts than traditional device O&S - fewer moving parts than traditional device
N-AERO-03	MOLEC + Blowing	3	D - leading edge blowing is advancing state of traditional technology P - more parts than MOLEC O&S - more parts than MOLEC
N-AERO-04	MOLEC + Suction	1	D - suction is state of art P - more parts than traditional plus holes in skin O&S - more moving parts than traditional plus holes in skin require more frequent maintenance
N-AERO-05	LAVLET Unsteady	5	D - leading edge blowing is advancing state of traditional technology P - more parts than LAVLET O&S - more parts than LAVLET
N-AERO-06	Krueger Flap	5	Comparable to traditional high-lift deice

Affordability		
1	Poor	+10-20% vehicle life cycle cost relative to traditional high-lift device
3	Moderate	+5-10% vehicle life cycle cost relative to traditional high-lift device
5	Medium	Vehicle life cycle cost comparable to traditional high-lift device
7	Significant	-5-10% vehicle life cycle cost relative to traditional high-lift device
9	High	-10-20% vehicle life cycle cost relative to traditional high-lift device

***D- Development, **P - Production, ***O&S – Operations & Support**

Figure 3-14. Affordability QFD assessment.

In summary, the affordability, maintainability, reliability, weight and noise were similarly weighted in this study. The stand-out technologies for wind tunnel testing were ranked as blown MOLEC, LAVLET and MOLEC without blowing. The test planning and coordination to bring these configurations to ground test are discussed in the following section.

4. Wind Tunnel Test Plan

4.1 Introduction

The wind tunnel test plan Task 3 is a culmination of several test planning and coordination activities. This section will provide a description of the wind tunnel test facility, the conceptual design considerations and the logistics involved with the test article design, fabrication,

instrumentation, and assembly. A description is provided of the desired model configurations, the anticipated test conditions and the resulting detailed test matrix.

4.2 Test Guidelines

The overall success of this program could be attributed to a talented, hard-working team and frequent review of action items. The schedule was closely followed, as shown in figure 1-1, to achieve a successful wind tunnel test starting in January 2012. The only significant delay was at the start of the test due to an anomaly in the high-pressure flow delivery system. Eventually the problem was identified and corrected, but it caused a three-week delay in testing. Fortunately, the facility extended the test by three full weeks and all test objectives (including all priority 1 and 2 runs) were met. Preliminary design considerations for the wind tunnel test portion of the program were coordinated with our NASA Langley point of contact and our test and evaluation (T&E) personnel. The following definitions have been outlined as guidelines for the test:

1. Test article will be an infinite swept 2D model, mounted vertically in the 7×10 ft LSWT, similar in concept to the HiLDA model (2003)
2. The design approach is to use a common "center body" (machined from aluminum) with interchangeable leading edges (stereolithography)
3. Guidelines for the test matrix will entail:
    - Buildup: Baseline AHLLE with no flap deflection and no blowing
    - Buildup: Baseline AHLLE with 45° trailing-edge (TE) flap, no blowing
    - Reference Configuration: Baseline AHLLE with blown 45° TE flap
    - AHLLE Concept 1 with blown 45° TE flap
    - AHLLE Concept 2 with blown 45° TE flap
    - Angle of Attack for all configurations, approx. –5 deg to +20 Deg
4. Test conditions
    - Nominal dynamic pressure: 30 psf (maximum 60 psf)
    - Angle of attack (yaw table) range: –5° to 20°
    - Nozzle pressure ratio (NPR) range: Off to 2.0
    - Maximum total $C\mu$: 0.39 (0.13 per slot)
    - Expected c_{lmax}: 4.5
5. Preliminary Instrumentation will follow the approach of:
    - Two-three rows of static pressure taps installed in test article, to compute lift force and possibly pitching moment
    - Mass flow meter, external to test article, to measure airflow supplied to the test article

Based on CFD for leading-edge and trailing-edge blowing, the model will require 1.8 pps for the 3 slot configuration. Figure 4-1 details the ground rules and assumptions for the wind tunnel test.

Task 3 – Design Considerations

- Conceptual design considerations
  - Description of test article
    - Test article will be an infinite 2-D model, mounted vertically in the 7'x10' LSWT, similar in concept to the HiLDA model except wall liners not required for AHLLE
    - AHLLE model to have 0° leading edge sweep
    - Common "centerbody" (machined from aluminum) with interchangeable leading and trailing edges
  - Model sizing to be based on mass flow requirements, slot heights, and load considerations
  - Preliminary instrumentation considerations
    - One dense row of static pressure taps to compute section lift and pitching moment coefficients
    - Two sparse rows of monitor spanwise uniformity
    - Mass flow meter, external to test article, to measure airflow supplied to the test article
    - Hand-help total pressure probe
    - Possible use of boundary layer rake (time permitting)



HiLDA Model in 7'x10' LSWT (2003)



AHLLE Model in 7'x10' LSWT (2012)

Figure 4-1. Design considerations.

4.3 Wind Tunnel Facility

The Low-Speed Wind Tunnel (LSWT) test facility at Northrop Grumman is located in Hawthorne, CA. The tunnel is 7×10×20 ft in size with a closed loop recirculating return. Tunnel capabilities and photos are highlighted in figure 4-2.

Task 3 – Test Facility

NGC 7'x10' Low Speed Wind Tunnel

- General
  - Located in Hawthorne, CA
  - Constructed in 1956 to support X-21 laminar flow research studies



- Specifications
  - Atmospheric, closed-return circuit with test section measuring 7'*x*10'*x*20'
  - Dynamic pressures up to 200 *psf* (Mach 0.37) with clear test section
  - Highly versatile support system capable of the (model installed wings level)
    - Pitch range of -14° to +85°
    - Yaw range of -24° to +24°
  - Auxiliary high-pressure air supply capable of up to *psi* at 2 *lb/sec* continuous
    - Bottle field can supply up to 300 *lbm/sec* for 20*s*

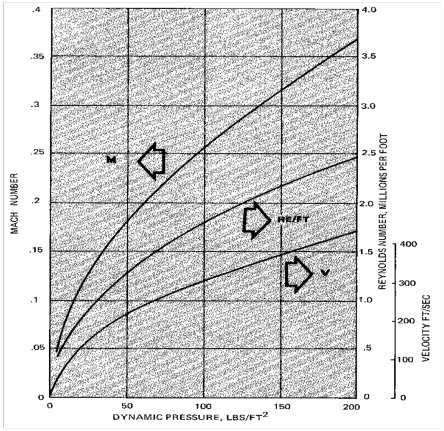
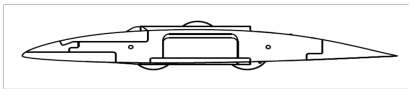


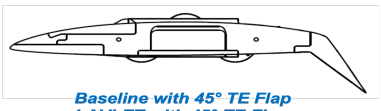
Figure 4-2 Northrop Grumman LSWT.

Task 3 – Model Configurations

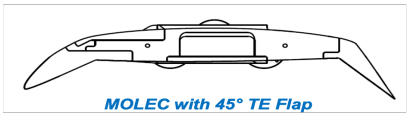
- Buildup of clean model to baseline configuration
  - Model common to LAVLET config, but with 1% and 10% chord slots taped over
  - 0° TE Flap
  - 45° TE Flap (without and with steady blowing at 80% chord slot)
- LAVLET concept with blown 45° TE flap
  - With steady blowing at 1% and/or 10% chord slots
- MOLEC concept with blown 45° TE flap
  - Without and with steady blowing at 12% chord slot



Baseline with 0° TE Flap



Baseline with 45° TE Flap
LAVLET with 45° TE Flap



MOLEC with 45° TE Flap

Figure 4-3. Model configurations identified for the test.

A majority of Task 3 was dedicated to test planning and coordination of the model design with the T&E personnel. Additionally, a preliminary test matrix was defined in order to specify test requirements/objectives and to define the anticipated model performance in the wind tunnel. The ground rules for the test are detailed below:

- Nominal dynamic pressure: 30 psf (maximum 60 psf)
- Angle of attack (yaw table) range: –5° to 20°
- NPR range: Off to 2.0
- Maximum total Cμ: 0.39 (0.13 per slot)
- Expected c_{lmax}: 4.5

The summary of test configurations is detailed below:

- Baseline AHLLE with 0° TE flap, no blowing
- Baseline AHLLE with 45° TE flap, no blowing
- Baseline AHLLE with blown 45° TE flap
- Blown LAVLET with blown 45° TE flap
- MOLEC with blown 45° TE flap
- Blown MOLEC with blown 45° TE flap

The detailed test matrix included 155 runs originally planned over 5–7 days. During the planned model build-up time, a system shakedown, instrumentation leak checks, and pressurize/leak check plenums, etc., were established. The test matrix also included a zero-degree TE flap (baseline configuration) so stagnation point is on the nose of the airfoil.

For each configuration listed in the test matrix, a series of alpha sweeps at fixed NPR, the effect of dynamic pressure on alpha sweeps, and data repeatability was addressed. For blown configurations, the test matrix included choke plate calibration, survey blowing slots with a handheld total pressure probe, NPR sweeps at fixed alpha, and checks for hysteresis

5. Aerodynamic Analysis

The Northrop Grumman Hawthorne LSWT was used for the ground test portion of the program. The Aerodynamic Analysis and Pretest Prediction (Task 4) was performed to address several items imperative to the model design process. Task 4 was completed in parallel with Task 5, Wind Tunnel Model Design, as the two processes were intertwined. The Aero-Analysis Task included the following subtasks:

- Validation of model sizing (2D and 3D)
- Placement of static pressure taps
- CFD pretest predictions (3D)
- Wall corrections
  - Trip dot sizing

The first objective was to validate the AHLLE model size through CFD analysis prior to model fabrication. Specifically, 2D and 3D CFD was performed to assess and examine possible wall effects, blockage, and blown jet interactions.

5.1.Validation of Model Sizing

Our approach was to use two types of aero analysis. First, a 2D CFD was used to generate "free air" C_P distributions and aero coefficients. Next, a 3D CFD analysis was performed to generate "installed" C_P distributions and aero coefficients. Finally, a comparison of "installed" results to "free air" results determined adverse effects due to the presence of the wind tunnel walls. For this task, the starting CFD geometry was the LAVLET configuration with a 45° TE flap. A 3D model is an 84-inch extrusion of a 2D section cut. The grid of the test section, shown in figure 5-1, is of the Northrop Grumman 7×10 ft LSWT test section. Reference parameters used are: S_{ref} = 17.5 ft^2; c = 30 in; b = 84 in; and T_t = 518.7°R.

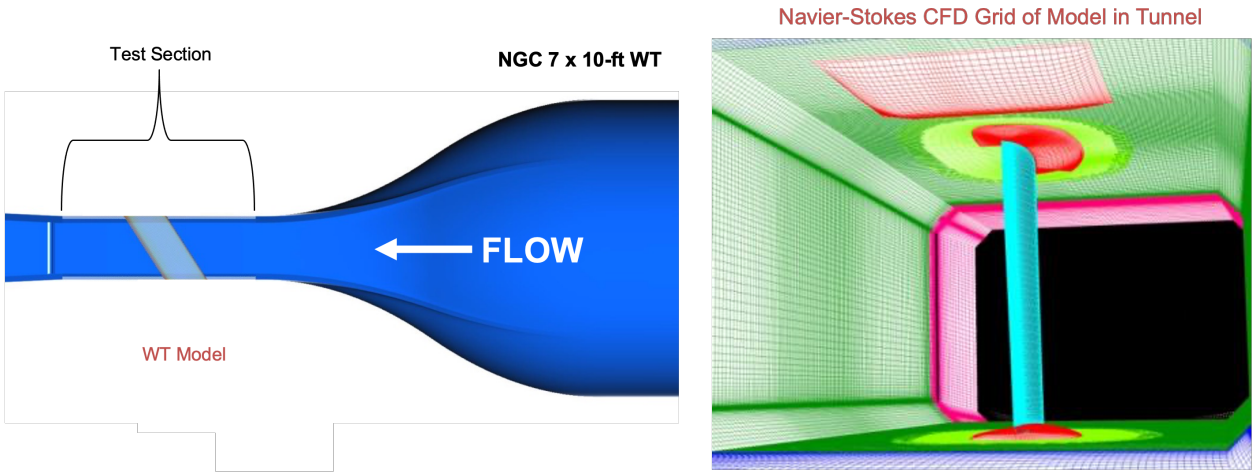
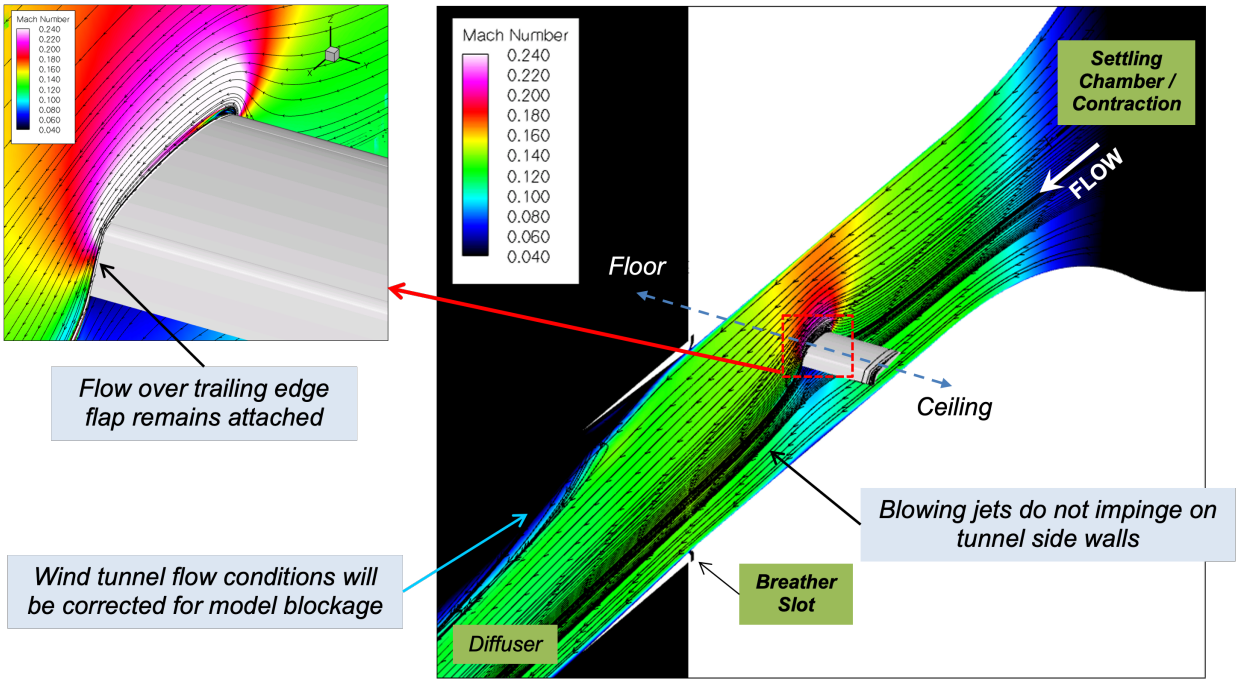


Figure 5-1. Wind tunnel model grid.

Task 4 – Validation of Model Sizing Results



3D LAVLET Model in WT; NPR 2.0 (All Slots); Alpha 4°
Image cut made at ~b/2

Figure 5-2. Model sizing results of 3D CFD.

Task 4 – Validation of Model Sizing Results

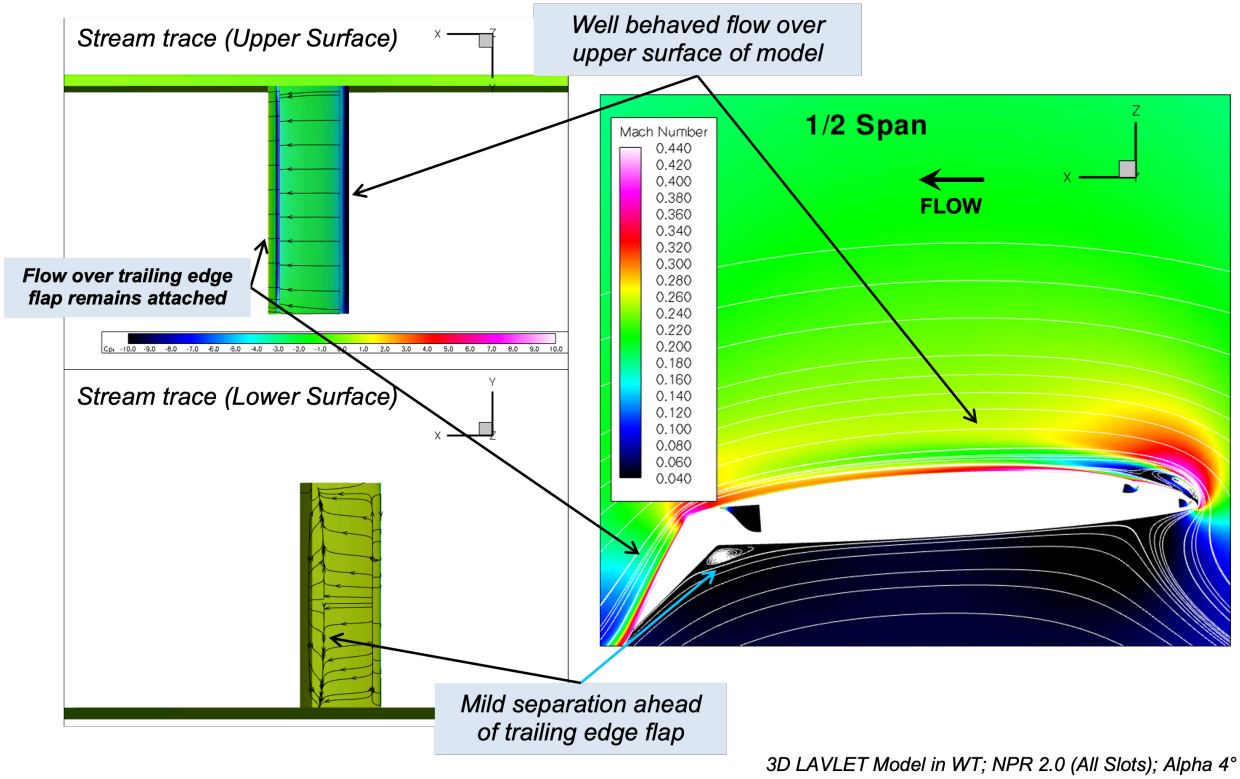


Figure 5-3. Validation of model sizing from 3D analysis.

Task 4 – Validation of Model Sizing Results

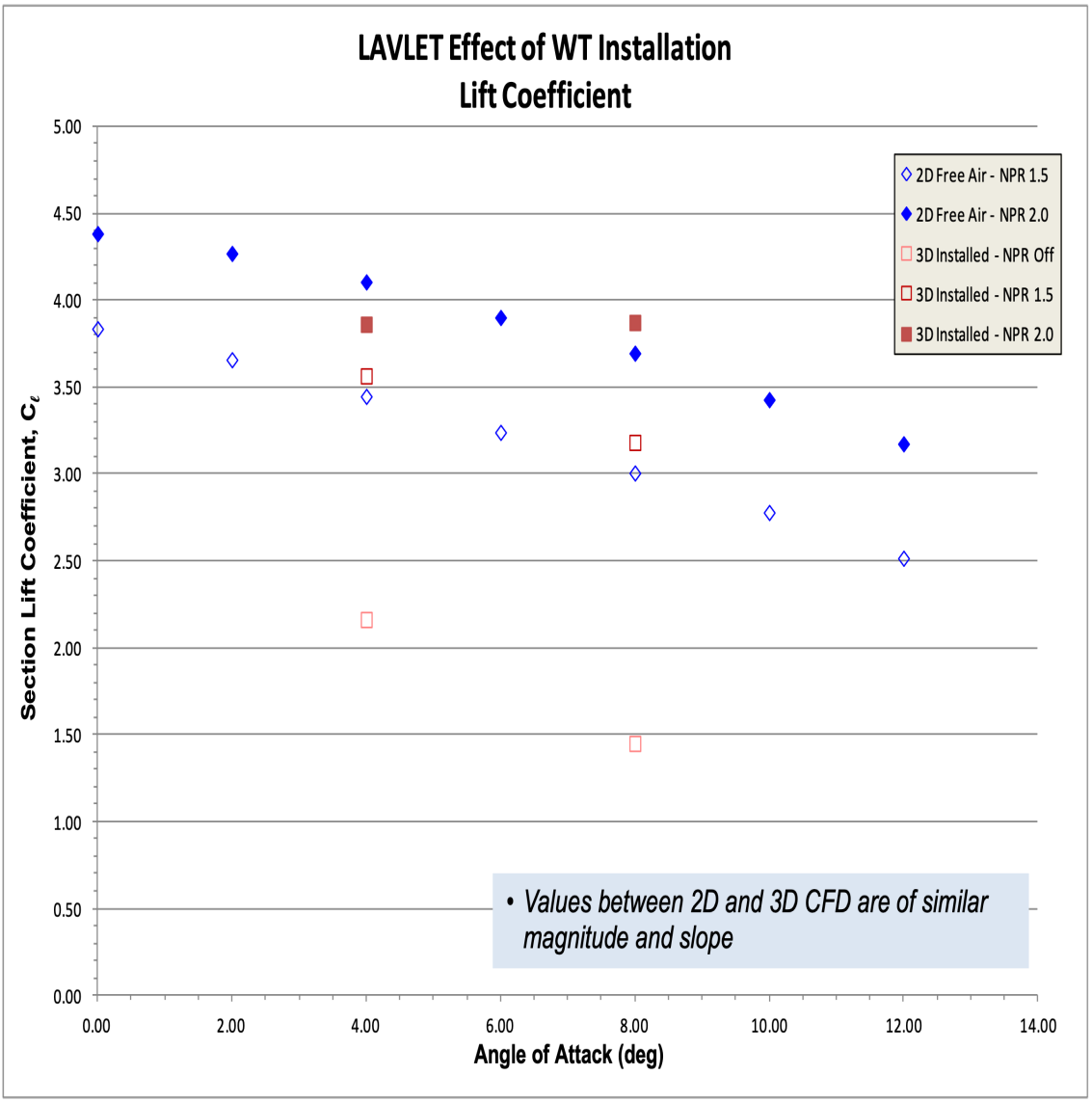


Figure 5-4. Comparison of 2D and 3D predicted lift results.

Task 4 – Validation of Model Sizing Results

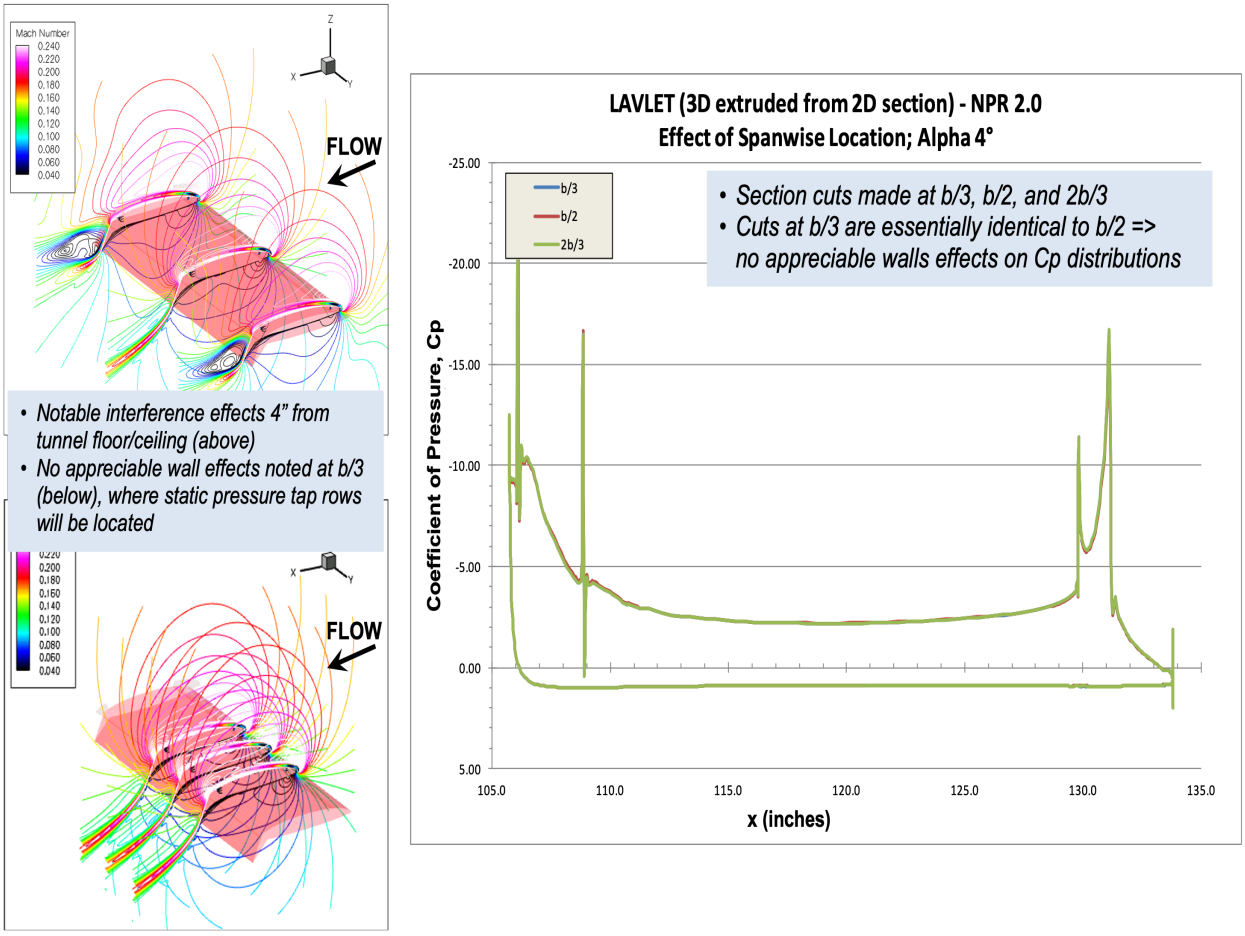


Figure 5-5. Predicted effects wall effects on C_P distributions.

For the model sizing aerodynamic analysis effort, there were several conclusions based on the 3D installed CFD. First, the blown jets do not appear to impinge on the wind tunnel walls. In general, all the model blockage effects can be accounted for by correcting the wind tunnel flow conditions (q, alpha, etc.) during the test. As shown in figure 5-5, wall interference effects in the planned measurement regions appear (between b/3 and b/2) to be negligible. The negligible wall effects allow us to plan static pressure tap placement based on the predicted CFD C_P distributions for baseline, LAVLET, and MOLEC configurations. Additionally, based on comparison of 3D installed to 2D Free Air CFD, no obvious installation effects are present in the C_P distribution comparisons. The section lift coefficient values are of similar magnitude and

slope. This provides confidence that measurement taps located at any of the 1/3, 1/2 or 2/3 span locations will provide favorable comparisons during the measurement of C_P.

5.2.Static Tap Placement

Static pressure taps were used to compute lift and pitching moment coefficients during wind tunnel testing. The static taps were distributed on OML with the objective of minimizing errors in the computed section lift coefficient compared to 3D CFD predictions. Static tap configurations were designed with a single dense row at b/2 for force/moment computations and a sparse row of taps at ~b/3 and ~2b/3 for spanwise uniformity checks. The total number of installed static pressure taps is 65. Due to the limited quantity of taps the anticipated error in integrated forces/moments was estimated to be errors in C_l < ~3.5% and C_m < ~8.5% (based on limited CFD data).

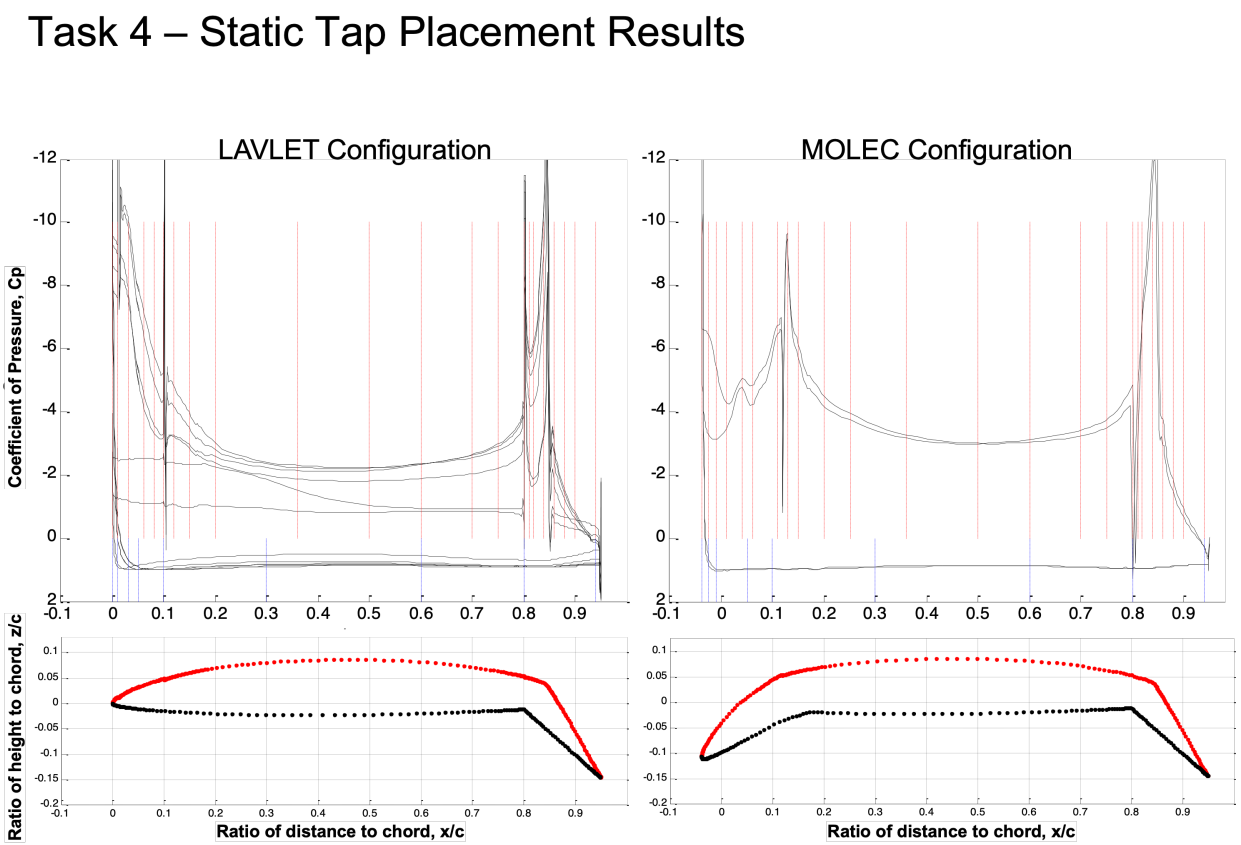


Figure 5-6. Static tap placement on model.

5.3. Pretest CFD Predictions

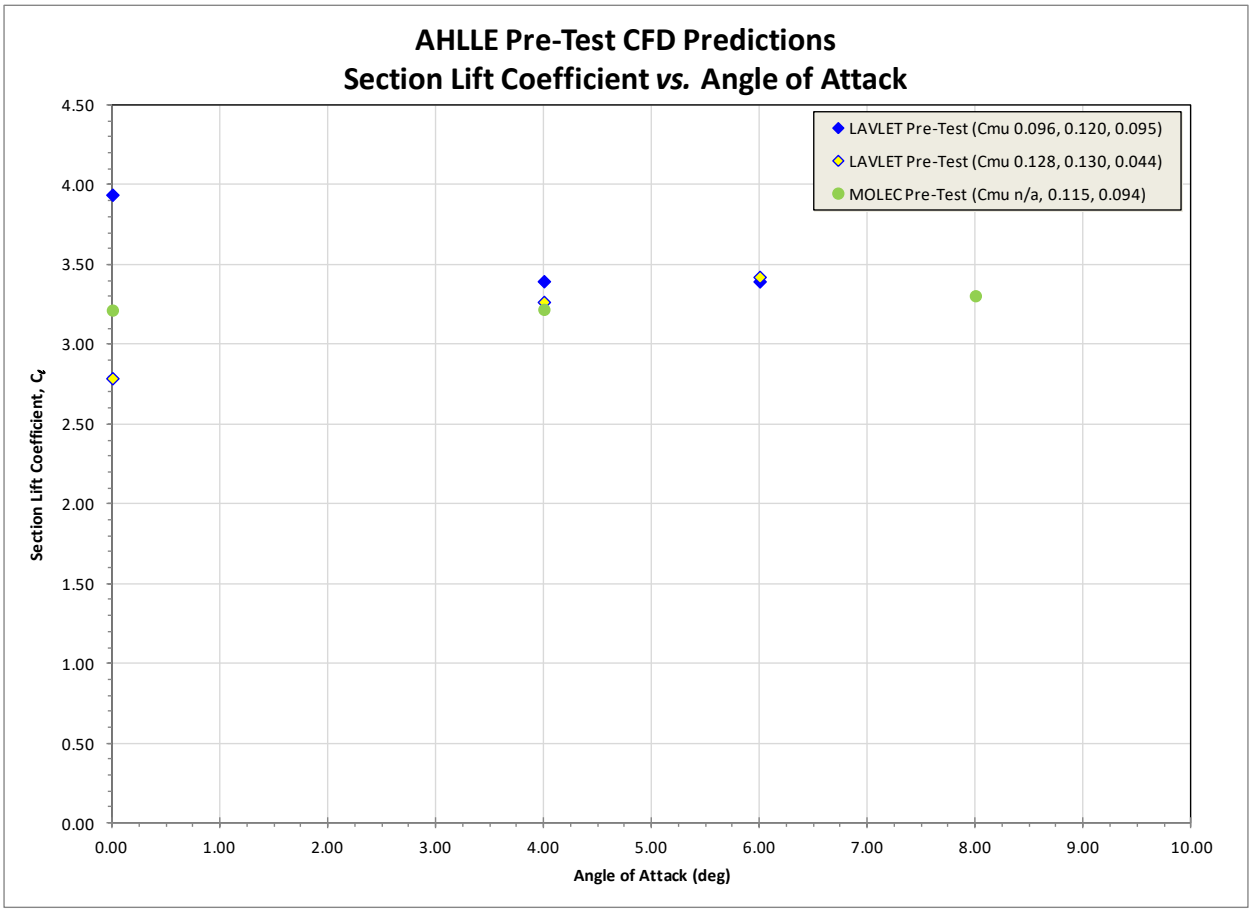


Figure 5-7. Pretest CFD predictions.

Figure 5-7 provides the result of the pretest CFD predictions of the installed 3D model in the wind tunnel. The analysis examined the wind tunnel model OML as designed for the experiment. Based on the aero analysis of section 5.1, it was determined that no slot blowing would occur within 4 inches of the tunnel ceiling and floor. For the pretest predictions, the turbulence model was Menter's SST k-omega. Initial conditions assumed nominal flow conditions in the wind tunnel with dynamic pressure of Q = 31 psf (assumes empty test section) and Mach number of 0.145. The Reynolds number is 2.53×10^6. Pretest predictions were performed on the following run matrix:

		1%	10%/12%	80%	1%	10%/12%	80%	
	Alpha	**$C\mu_1$**	**$C\mu_2$**	**$C\mu_3$**	**NPR_1**	**NPR_2**	**NPR_3**	
	deg	-	-	-	-	-	-	
LAVLET w/ Blown 1%+10%	0	0.096	0.120	0.095	1.610	1.884	1.680	"Nominal" blowing
	4	0.098	0.119	0.093	1.650	1.884	1.680	
	6	0.975	0.119	0.093	1.640	1.884	1.680	
LAVLET w/ Blown 1%+10%	0	0.128	0.130	0.044	2.000	2.000	1.250	"Reduced" blowing
	4	0.129	0.130	0.044	2.000	2.000	1.250	
	6	0.129	0.130	0.043	2.000	2.000	1.250	
MOLEC w/ Blown 12%	0	n/a	0.115	0.094	n/a	1.884	1.680	"Nominal" blowing
	4	n/a	0.115	0.093	n/a	1.884	1.680	
	8	n/a	0.115	0.093	n/a	1.884	1.680	

To summarize the results in figure 5-7, CFD predictions are comparable to previous CFD results validating model sizing. There is no exact overlap in pretest prediction and model sizing validation CFD cases, however, general shapes and magnitudes of C_P distributions are comparable. Nominal blowing conditions on LAVLET were predicted to result in a negative lift curve slope; however, a reduction in trailing-edge slot blowing was found to produce a favorable lift curve slope. Sensitivities to various slot NPRs and freestream dynamic pressures will be examined in detail during the wind tunnel test. CFD predictions (c_l, c_m, and C_P) were taken to the wind tunnel and were available for comparisons to test data during the ground test.

The aerodynamic analysis also showed that wall corrections due to solid blockage and streamline curvature will be applied to correct tunnel dynamic pressure, tunnel velocity, Reynolds number, section lift and pitching moment coefficients, and model angle of attack during the test. Wake blockage is negligible given the average predicted drag coefficient over the angle-of-attack range is zero. The actual wake in the test will be minimized due to the presence of blowing slots.

5.4. Trip Dot Sizing

A determination was made regarding the necessity and size/location of boundary layer transition dots for the test. An assessment of the upper and lower surfaces of all configurations (baseline, LAVLET, and MOLEC) was performed analytically using Northrop Grumman design methods. A review of test conditions determined the need and/or desirability for fixed transition. After reviewing the predicted pressure distributions and previous work to evaluate effectiveness of fixed transition on the wing w/ blown slots, the following determinations were made. First, it was decided to forego transition dots on all upper surfaces, allowing free transition for all blown and unblown configurations. The large NPR variations would make it difficult to identify a single location for fixed transition. The use of grit has previously shown to have no effect on test data for a comparable high-lift LSWT test. The natural transition location with blowing is expected to be less than 1 inch aft of the slot. The natural transition location without blowing is expected to be near the slot due to the aft-facing step created by the slot. The application of 0.0114 inch trip dots on the baseline/LAVLET lower surface, ~1.75 inch aft of the leading edge was deemed necessary from the predictions since the lower surface is susceptible to laminar flow, due to smooth, flat pressure distributions. A decision was also made to forego transition dots on the MOLEC lower surface since the effective leading-edge deflection will likely result in separated flow on the lower surface at test Re conditionsch.

6. Wind Tunnel Model Design

This section will describe the Task 5 Wind Tunnel Model Design and Drawings work. The model design task included the definition of all the design parameters in conjunction with the aero analysis work from Task 4. This section will detail the model configurations and design approach, the plenum layout, the high-pressure air system and hardware, the model instrumentation, the stress analysis, model fabrication, and model inspection criteria and tolerances.

6.1.Model Design Parameters

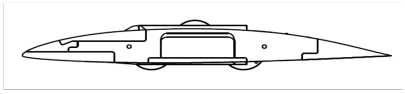
From Northrop Grumman's extensive experience as an aircraft manufacturer, our model design and fabrication expertise are internationally recognized as the leader in the industry. The processes detailed in the following sections ensured that the wind tunnel model would meet the cost, schedule and stringent aerodynamic performance requirements for the complex design. To start, the model sizing activity was performed hand in hand with the CFD analysis. The model requirements were specified below:

- Model dimensions
  - Span is full height of tunnel (7 ft) minus ~1/8 inch gaps at floor/ceiling for clearance
  - Chord is 30 inches (baseline/LAVLET configurations with 0° TE flap)
  - Each blowing slots span 76 inches of model, with height of 0.041 inches (S_{slot} = 3.1395 in^2)
- Design loads and attitude limits
  - Nominal dynamic pressure: 30 psf (maximum 60 psf)
  - Angle of attack (yaw table) range: –5° to 20°
  - Maximum NPR: 2.0
  - Maximum total Cμ: 0.39 (0.13 per slot) at Q = 30 psf and NPR = 2.0
  - Predicted c_{lmax}: 4.5
- High-pressure (HP) air system
  - Maximum HP plenum pressure: 450 psi
  - Three control valves used to deliver HP air to each of three model plenums
    - Minimum C_v = 1.45 and Maximum C_v = 9.32
  - Maximum pressure in each model plenum = 150 psi

Figure 6-1 provides our detailed design approach and an overview of the various model configurations for testing.

Task 5 – Model Configurations/Design Approach

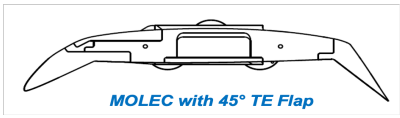
- Overview of model configurations
  - Baseline configuration with LAVLET leading edges
    - 1% and 10% chord slots taped over
    - 0° TE Flap
    - 45° TE Flap (without and with steady blowing at 80% chord slot)
  - LAVLET concept with blown 45° TE flap
    - With steady blowing at 1% and/or 10% chord slots
  - MOLEC concept with blown 45° TE flap
    - Without and with steady blowing at 12% chord slot
- Design approach
  - Aluminum centerbody, common to all configurations, with interchangeable leading and trailing edges
  - Trailing edge pieces grown from Bluestone
  - Leading edge pieces were either aluminum (LAVLET) or Bluestone (MOLEC)
  - Aluminum (fwd/mid) and steel (aft) choke plates deliver uniform flow to slots
    - LAVLET at 1%, 10% and 80% chord; MOLEC at 12% and 80% chord



Baseline with 0° TE Flap



Baseline with 45° TE Flap
LAVLET with 45° TE Flap



MOLEC with 45° TE Flap

Figure 6-1. Wind tunnel model design approach.

Figure 6-2 illustrates the first of the configurations designed. This is the all-aluminum center body design that allows for build-up of the leading-edge and trailing-edge components and was common to all configurations. The trailing-edge pieces were grown from Bluestone, a rapid prototyping material, and the leading-edge pieces were either aluminum (LAVLET) or Bluestone (MOLEC). Aluminum (fwd/mid) and steel (aft) choke plates were manufactured to deliver uniform flow to the slots. Flex lines attached through the floor of the wind tunnel to supply high-pressure air to each of the individual plenum cavities for the three slots: 1% and 10% chord LE slots on LAVLET, 12% chord slot on MOLEC, and the common 80% TE slot on all configurations.

Task 5 – Model Configurations: Centerbody

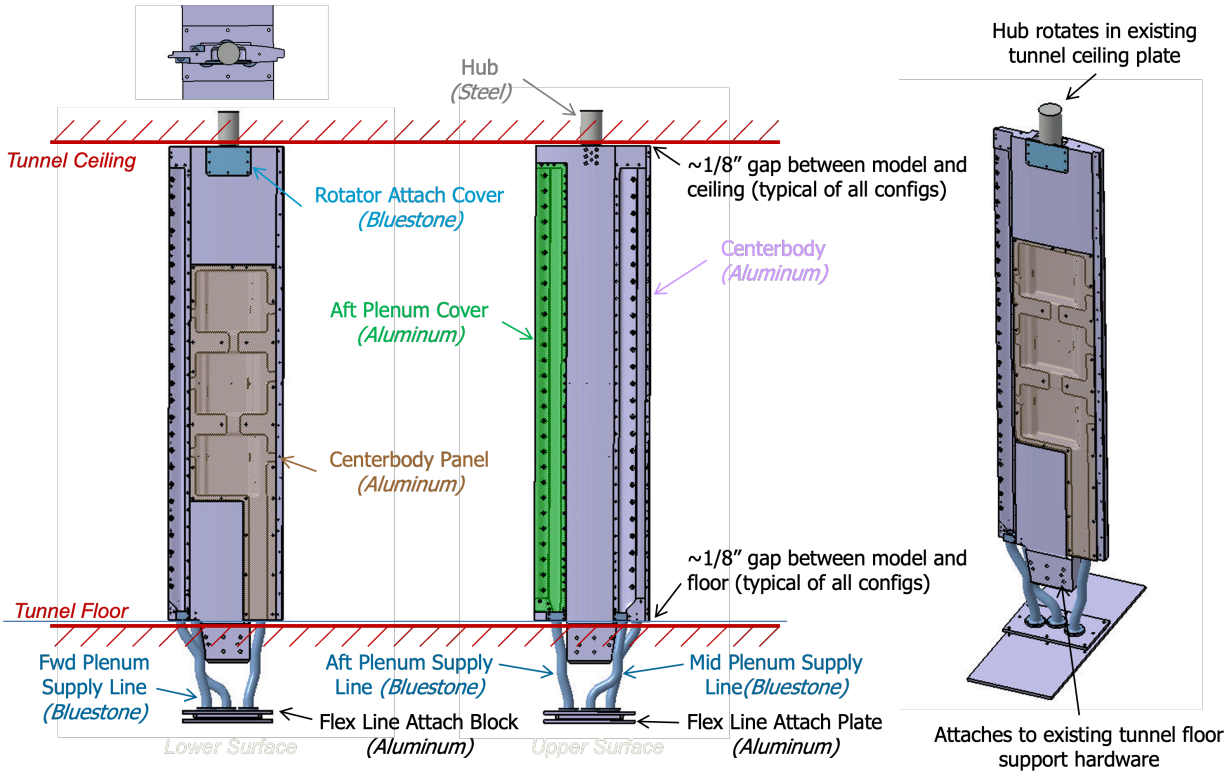


Figure 6-2. Aluminum center body design.

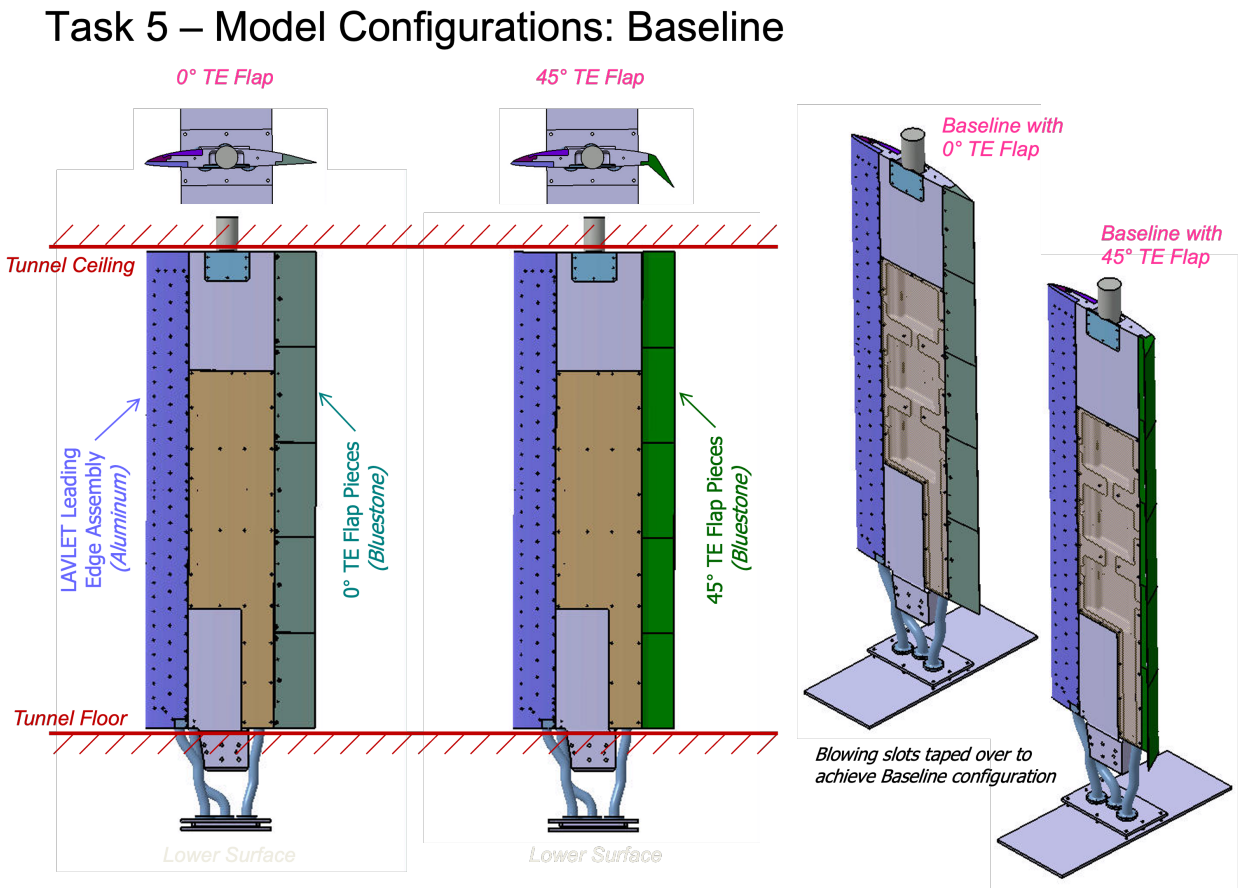


Figure 6-3. Baseline model configuration.

The baseline configuration shown in figure 6-3 now reveals the leading-edge and trailing-edge pieces installed on the aluminum center body. Figure 6-4 pictorially shows the buildup of the models for the deflected trailing edge, the LAVLET, and the MOLEC designs. For all baseline runs, the slots are taped over, and then the tape is removed during blown runs.

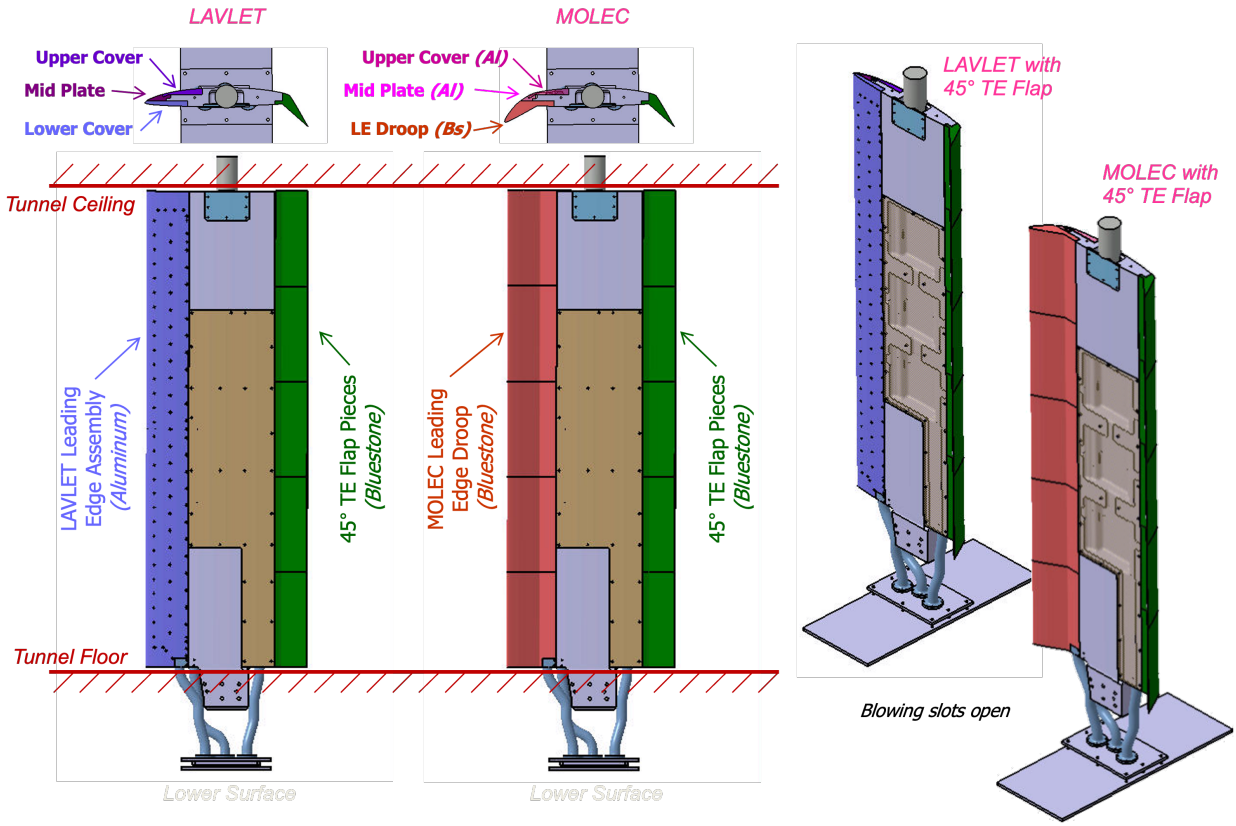
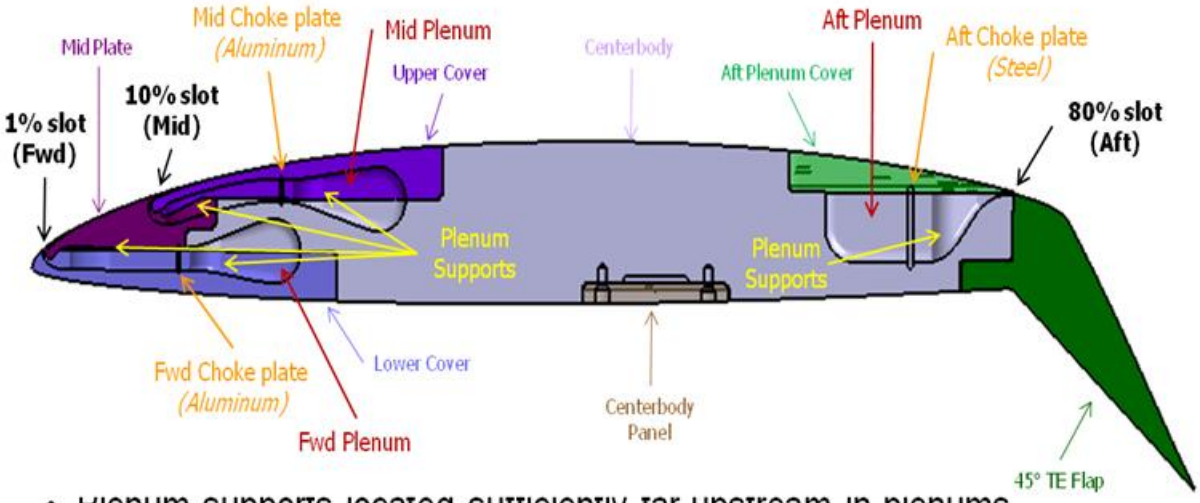


Figure 6-4. LAVLET and MOLEC configurations.

Figure 6-5 illustrates a sideview of the model with the plenum layouts. Each slot is pressurized by a dedicated continuous plenum. Supporting structure inside each plenum ensures that the model slot will remain contiguous under pressurization, but the supporting struts are sufficiently placed upstream of each slot so as to not distort the exit slot flow. The tunnel floor and ceiling are shown in each of the configurations. The entire model rotates on a turntable to achieve changes in alpha.

Task 5 – Plenum Layout

- Each slot location is pressurized by a dedicated continuous plenum
  - Layout of model plenums shown below for LAVLET configuration



- Plenum supports located sufficiently far upstream in plenums

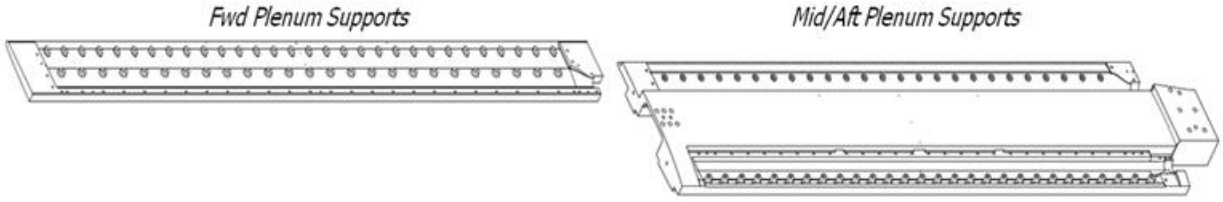
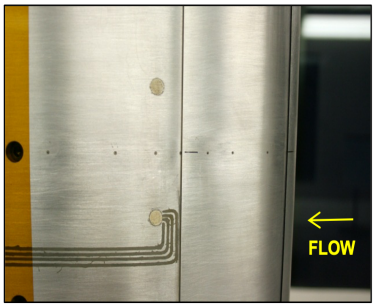


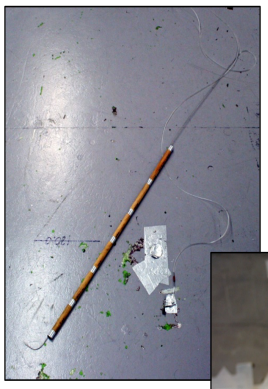
Figure 6-5. Plenum layout and sideview of model.

Task 5 – Model Instrumentation (External)

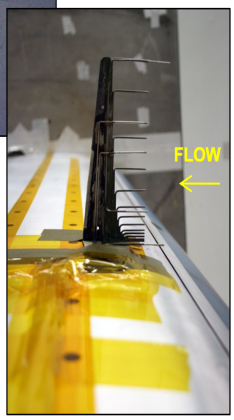
- Static pressure taps on model OML
  - 70 taps distributed along three rows
    - 1 sparse rows at b/3 (offset towards b/2 by 0.9")
    - 1 dense row at b/2
      - Pressure data integrated to obtain lift/pitch
    - 1 sparse rows at 2b/3 (offset towards b/2 by 0.9")
  - Measured using three 32-port 15 *psid* multiducers
- Hand-held total pressure probe
  - Curved 0.040" ID pressure hardline mounted on a wooden dowel for rigidity
  - Measured using a 50 *psid* transducer
- Boundary layer rake
  - Existing rake having 18 total pressure tubes and 3 static tubes
    - Secured to model OML using double-sided tape and superglue
  - Measured using a 32-port 15 *psid* multiducer



Dense static tap row at b/2



Hand-held probe



Installed boundary layer rake

Figure 6-6. Instrumentation on the model OML.

Figure 6-6 represents the OML instrumentation used for the wind tunnel test inch all configurations. Static pressure taps on the OML included 70 taps distributed along three rows. There were two sparse rows offset by 0.9 inches from the 1/3 and 2/3 chord locations (due to structural concerns) and a dense row on tap instrumentation at 1/2 chord. This instrumentation provided the integrated lift and pitch information. All instrumentation was fed to three 32-port, 15 psid multiducers. Additionally, a handheld total pressure probe installed with a 50 psid transducer was used to check slot flow uniformity throughout the test. An existing boundary layer rake was used that consisted of 18 total pressure tubes and 3 static pressure tubes. This was secured to the OML of the model using double-sided tape and superglue.

Task 5 – Model Instrumentation (Internal)

- Internal model instrumentation
  - Static taps in slot plenums, upstream of choke plate
    - Located at b/2 (3 total)
    - Used to monitor plenum pressures
    - Measured using 500 *psid* transducers
  - Static taps in slot plenums, downstream of choke plate
    - Located at b/2 and 2b/3 for each slot (6 total)
    - Treated as the total pressure of the slot jet
    - Measured using 50 *psid* transducers
  - Static taps in slot exits to measure NPR
    - Located at b/2 and 2b/3 for each slot (6 total)
    - Measured using a 15 *psid* multiducer

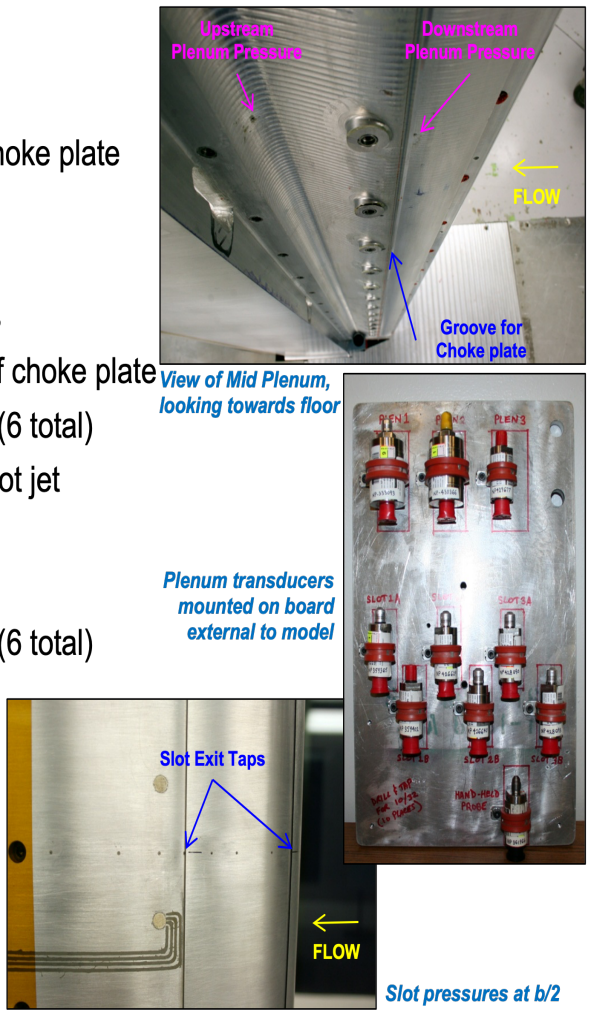


Figure 6-7. Internal model instrumentation.

Internal to the model was additional instrumentation that is highlighted in figure 6-7. Static taps were located in the slot plenums upstream of the choke plate and were used to monitor plenum pressures. This instrumentation required 500 psid transducers. Static taps were also located in the slot plenums, downstream of the choke plates. A total of six slot transducers capable of measuring 50 psid were used to measure total pressure of the slot jet. Static taps were also located at the slot exits at the 1/2 and 2/3 span locations to measure NPR.

Task 5 – Stress Analysis

- Stress analysis/report was completed prior to model installation by J. Whitehead and S. Bieck
- Design loads
  - Max q = 60 *psf*
  - Max NPR = 2.0
  - Aero loads based on CFD/analytical predictions
- Resulting safety factors
  - Minimum safety factor (4.1 upper hub) exceeds wind tunnel requirements
  - Representative safety factors
    - Centerbody >16.5
    - Centerbody cover > 4.6
    - Choke plates > 4.4
    - Trailing edge flap > 8.8
    - Bluestone supply lines 16.7 (burst)

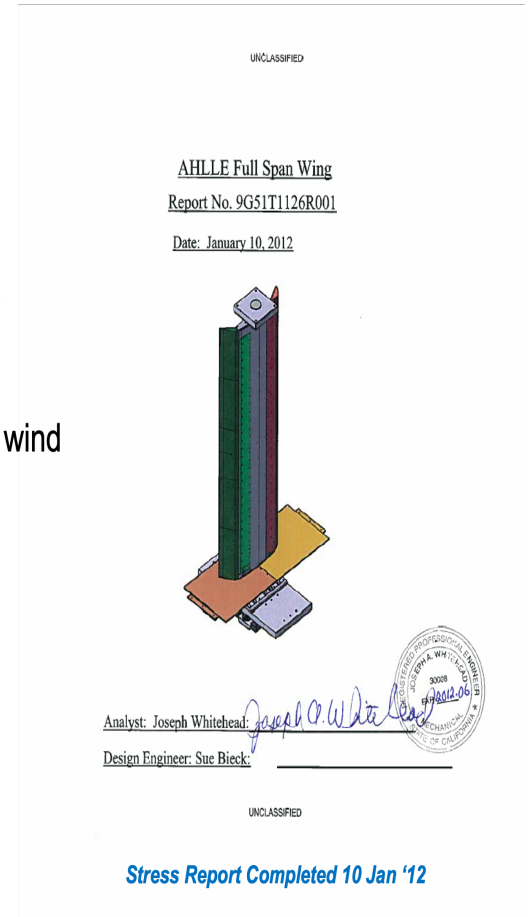


Figure 6-8. Stress analysis report.

A stress analysis report was completed prior to model installation. This ensured design load operation up to a maximum of Q = 60 psf in the tunnel. This stress analysis was based on the ground rule that the model would not be pressurized beyond an NPR = 2.0. All aero loading was determined based on CFD and analytical predictions. Resulting safety factors from the stress analysis far exceeded wind tunnel requirements. The signed report seal is shown in figure 6-8.

Task 5 – Model Fabrication



Clockwise from top left

1) Birds eye view of AHLLE components, ready for assembly and final inspection
2) Lower surface of machined centerbody
3) Trailing edge surfaces, having 0° and 45° deflections (5 pieces per configuration)
4) Support hardware used to mount model to tunnel floor and ceiling
5) HP air supply lines leading to centerbody

Figure 6-9. Model fabrication.

Figure 6-9 and figure 6-10 show our model fabrication process of all the manufactured parts for the wind tunnel test. Figure 6-9 shows, from clockwise top left, a birds-eye view of the AHLLE components ready for assembly and final inspection, the lower surface of the machined center body, the trailing-edge surfaces using five pieces per configuration, the support hardware used to mount the model to the tunnel floor and ceiling, and the high-pressure supply lines leading to the center body.

Task 5 – Model Fabrication



Clockwise from top left

1) LAVLET upper & mid leading edge components
2) Detail of LAVLET LE with static pressure tap hard lines protruding from IML
3) LAVLET lower leading edge component
4) Detail of three choke plates (2 Al + 1 Steel)
5) Bluestone MOLEC leading edge droop components
6) Aluminum MOLEC mid & upper leading edge components

Figure 6-10. Model fabrication pictures.

Figure 6-10 shows photos of the LAVLET upper and mid leading-edge components, the detail of LAVLET leading-edge static pressure tap hardlines protruding from the inner mold line (IML), the LAVLET lower leading-edge component, a detail of three choke plates, Bluestone MOLEC leading-edge droop components, and the aluminum MOLEC mid and upper leading-edge components.

Task 5 – Model Inspection Criteria & Tolerances

- Inspection of outer mold lines (OML)
  - Lower OML inspected using FARO Arm (4 pts/in)
  - Upper OML inspected using FARO Arm
    - 10 pts/in between model leading edge and mid slot
    - 4 pts/in between mid slot and model trailing edge
  - Specified OML tolerances of:
    - ±0.010 at model leading edge
    - ±0.030 aft of leading edge
- Inspection of blowing slots
  - Slot height inspected using feeler gauges
    - Specified tolerance of 0.041 ±0.002
  - Rigging of slot trailing edge inspected using FARO Arm (4 pts/in)
- Model buy-off occurred on 18 Jan, with delivery of model to tunnel on 19 Jan
  - Only 2 days later than originally scheduled

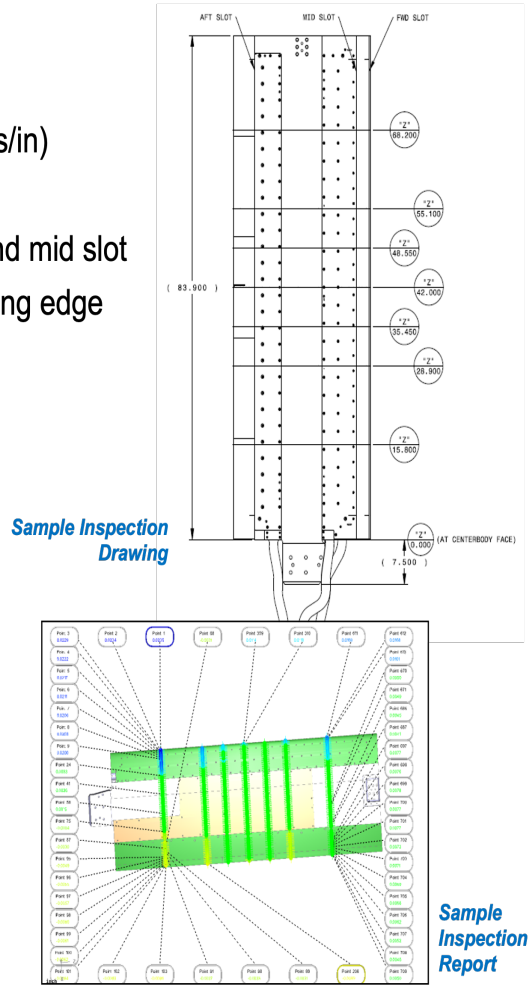


Figure 6-11. Model inspection criteria and tolerance reports.

Prior to installation of all hardware components and delivery to the wind tunnel, Northrop Grumman held a test readiness review and model inspection review in early January 2012. The model inspection, as shown in figure 6-11, included an upper and lower OML inspection using the FARO Arm (4 pts/inch). The specified OML tolerances were dictated at ±0.010 at the model leading edge and ±0.030 aft of the leading edge. The slot heights were inspected using feeler gauges with a specified tolerance of 0.041 ± 0.002 inches. The inspection reports were examined by the principal investigator and lead aero test engineer, and the model buy-off occurred on January 18. The model was then delivered to the wind tunnel on January 19, two days later than originally scheduled.

7. Wind Tunnel Model Installation

This section describes the installation of the inspected wind tunnel models and the high-pressure air system.

7.1.High-Pressure Air System Installation

Figure 7-7-1 describes the high-pressure air flow paths and installation of the high-pressure air components. Facility high-pressure air is delivered to and stored in a test-specific HP plenum. The flow branches from HP plenum to three supply arms, each with a control valve to vary slot NPR from Off to 2.0 (minimum control of 1.05). A safety valve is connected to each control valve to prevent over pressurization of the model. Downstream of each control valve is a choke, critical-flow venturi to meter the mass flow. Each venturi is connected to a flex line that in turn is connected to a model supply line (Bluestone, metallic). All supply lines reside beneath the tunnel floor. The model supply lines mount directly to each of the model plenums. Flow in each plenum passes through a choke plate to achieve uniform flow along the span of the slot.

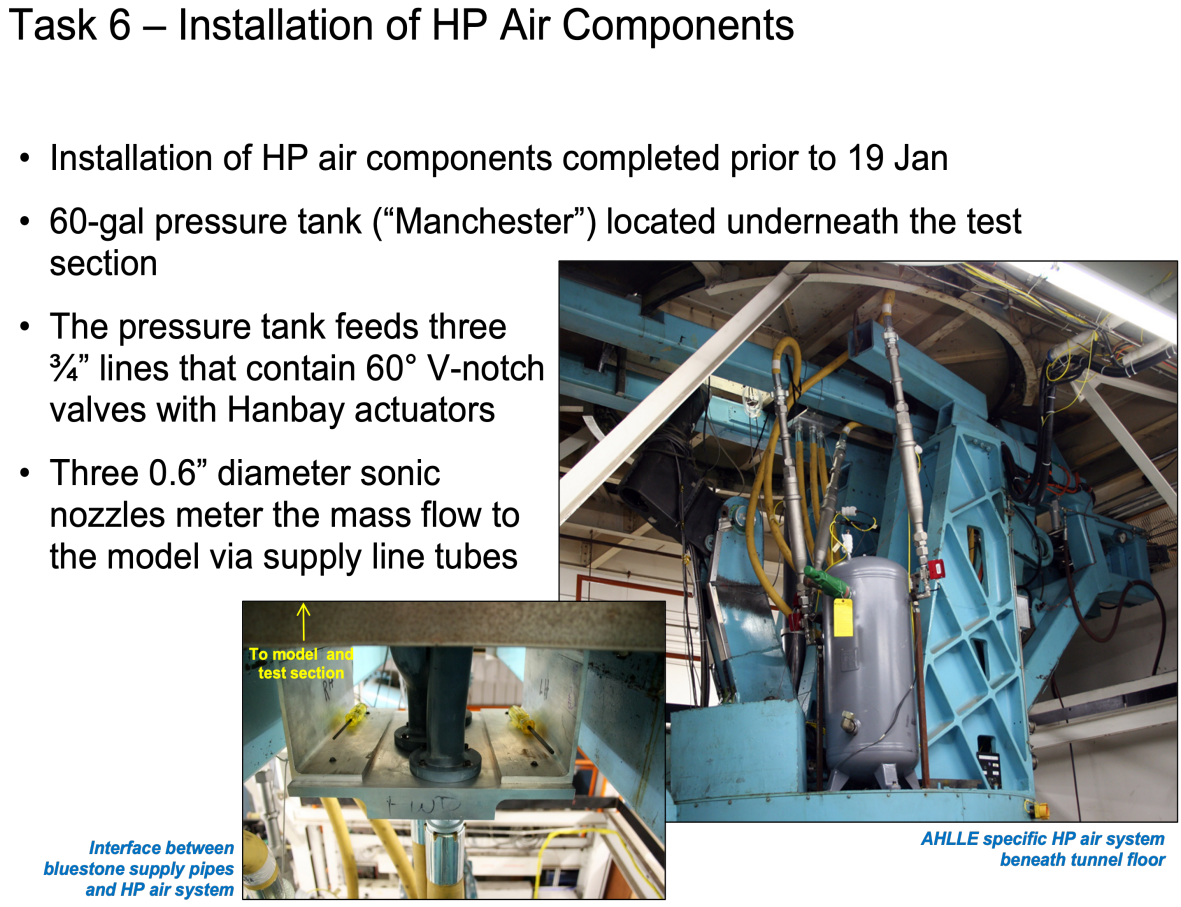


Figure 7-7-1. Installation of the high-pressure air system.

Task 6 – Model Installation

- Initial model installation occurred between 19 Jan - 01 Feb



Figure 7-2. Model installation in the 7×10 tunnel.

Model installation photos are shown in figure 7-2. The initial model installation occurred January 19 through February 1, 2012. Photographs show the installation of the model in the wind tunnel, the complex instrumentation, the procedure for sealing the high-pressure plenums, the externally mounted pressure transducers, and the fully assembled model.

During the course of installation of the model a failure occurred of the Bluestone supply lines. As shown in figure 7-3, the model assembly was removed for redesign of supply lines. No obvious defects were detected during installation and all safety factors indicated sufficient design margin. Because the cause of the failure remains unknown, an entirely new all-metallic solution was designed, fabricated, and reinstalled within two weeks of the failure. Figure 7-3 details the new high-pressure supply line installation.

Task 6 - Failure of Bluestone Supply Lines

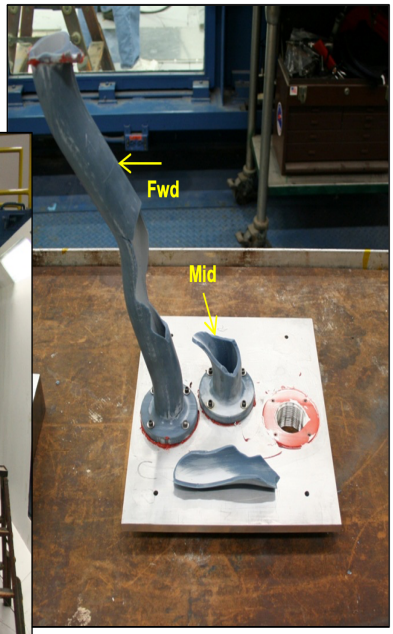
- Bluestone high pressure supply line ruptured during testing on 06 Feb
  - No injuries or damage to the model when Mid line burst
  - Safety factors indicate sufficient design margin; cause of failure unknown
    - Possible pre-load applied during installation and/or material defects
- Model assembly was removed for redesign of supply lines
  - Customer visited on 07 Feb



Mid supply line absent after failure



Removal of assembled model to gain access to supply lines



Fwd line damaged; mid line mostly absent; aft line not shown (attached to model)

Figure 7-3. Failure of high-pressure supply lines.

Task 6 – New Metallic Supply Lines to Model

- New all-metallic high pressure supply line solution was designed and fabricated on short notice; install complete 20 Feb
  - Included design/fab of new floor plate to simplify the mechanical design solution
  - Also included a hydrostatic test of line assemblies

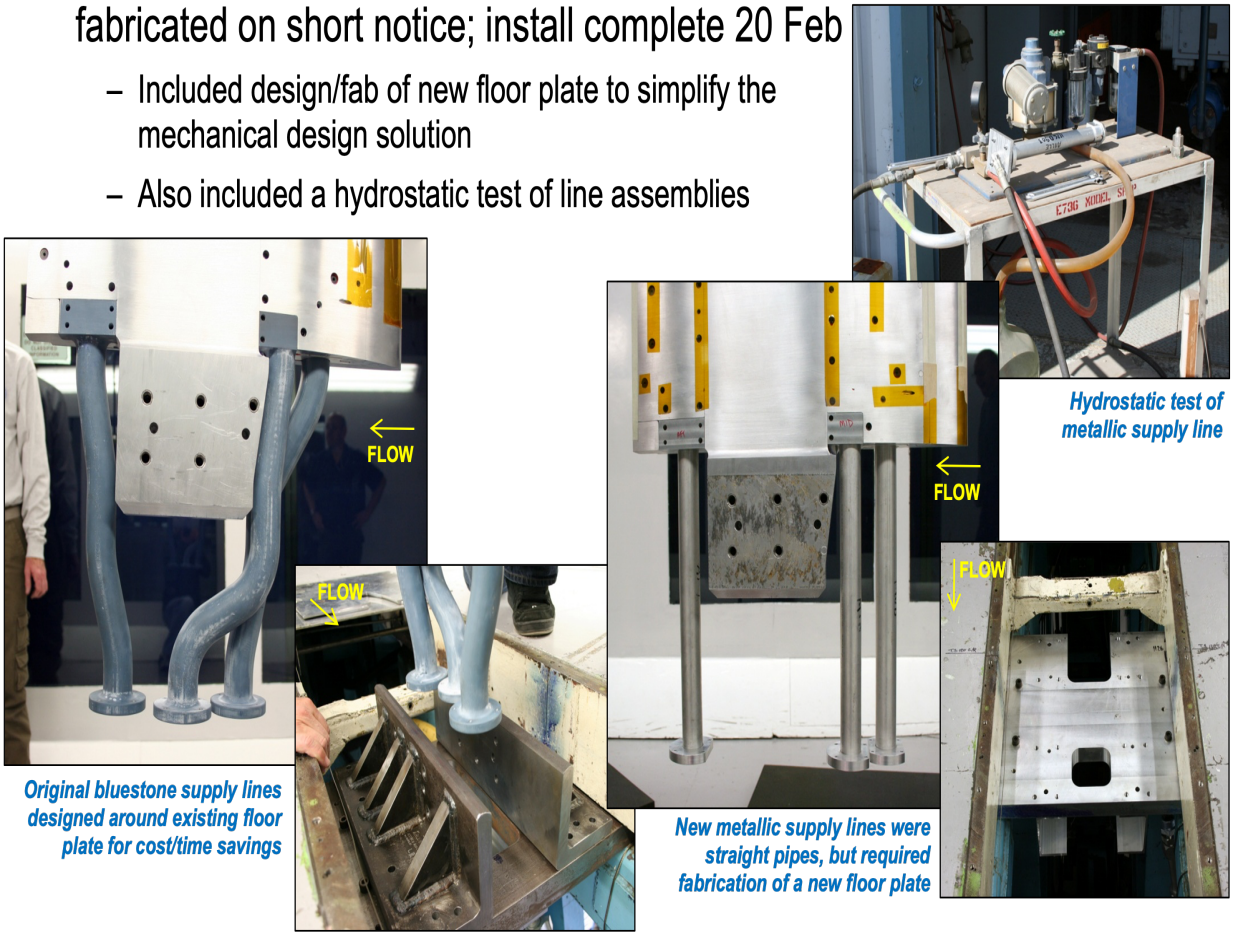


Figure 7-4. New metallic supply line installation.

7.2.Wind Tunnel Test Plan Execution

The wind tunnel test restarted on February 20, 2012 and concluded March 6, 2012. The duration of the test included baseline model test, deflected and blown trailing-edge flaps, and all high-lift configurations. Photos from the wind tunnel test and data collection are given in figure 7-5.

Task 6 – Execution of WT Test Plan

- Duration of wind tunnel test 20 Feb thru 06 Mar
  - Baseline model with 0° and 45° TE flaps
  - High lift configurations of LAVLET and MOLEC

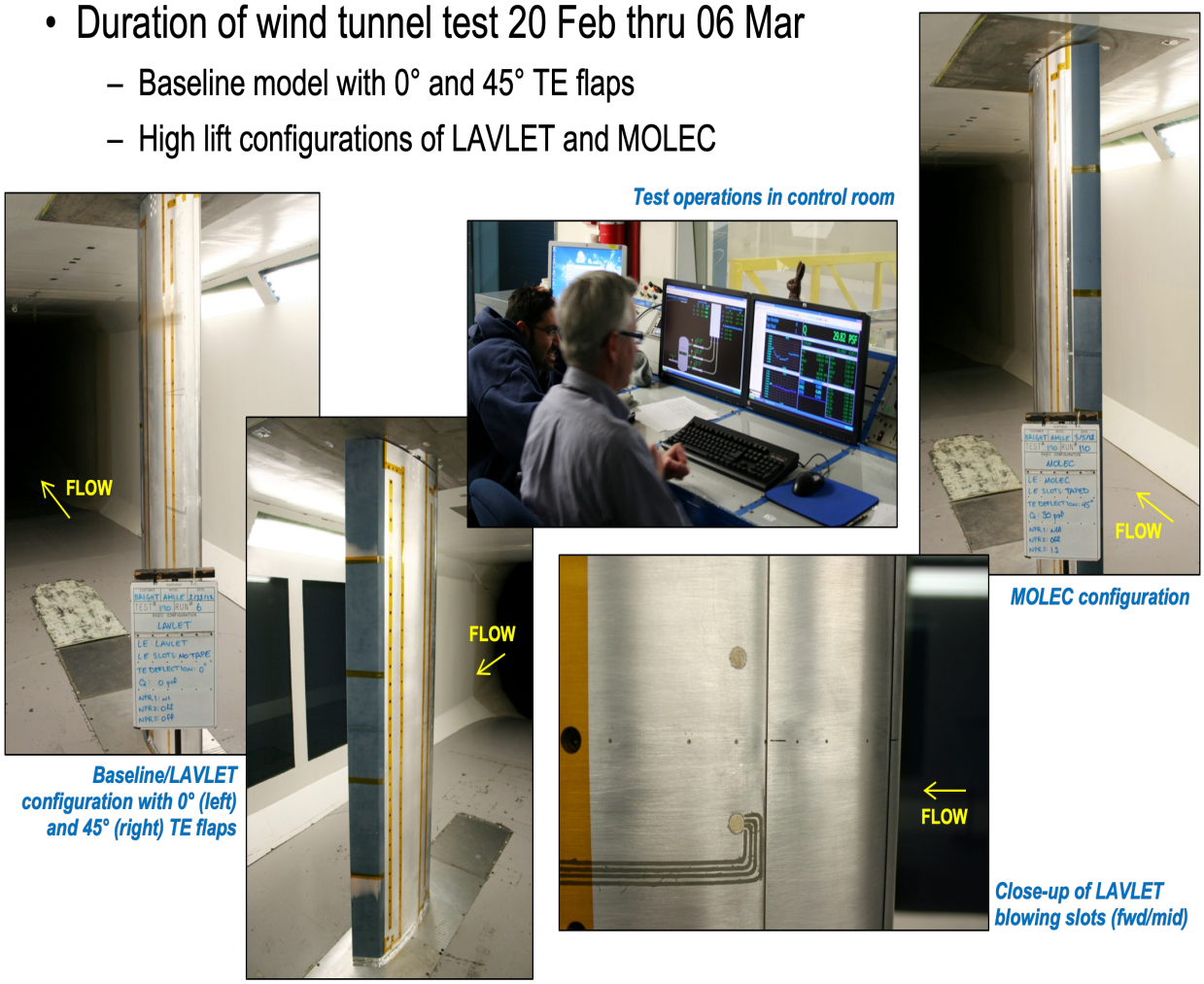


Figure 7-5. Execution of the wind tunnel test plan.

Task 6 – Model Un-Install & Test Summary

- Model un-installed and packed in storage crate on 08 Mar 2012
  - Model delivered to storage on 02 Apr 2012
- Test Summary
  - 135 valid data runs (155 planned)
  - 8 days of air-on testing
  - 27 days of occupancy (includes facility down days)



Figure 7-6. Model uninstall and test summary.

The wind tunnel Task 5 concluded after a total of 135 valid data runs of all priority data collection. A total of 8 days of air-on testing occurred for a total of 27 days of occupancy including facility down days. Raw data were produced by the facility in the form of *.csv files. That data included freestream test conditions, model attitude, and static/total pressure readings from pressure transducers. HP air supply parameters were also collected (mass flow, temperatures, pressures). Post processing, which will be described in the next section, was performed using MATLAB to compute a myriad of internal flow parameters (Cμ, discharge coefficients, etc.). MATLAB code was also generated to integrate static pressure data to obtain section c and c_m, correct model attitude and model solid blockage, correct aerodynamic data for streamline curvature, and plot raw and corrected wind tunnel data.

8. Data Analysis

The baseline configuration for the AHLLE model is shown in figure 8-1. This baseline airfoil is the cruise configuration of the AHLLE laminar airfoil with leading-edge slots and trailing-edge slots sealed with aluminum tape. Shakedown of the model included a series of tests at wind tunnel condition Q = 30.0, the nominal operating condition, to determine the 0-degree alpha condition and stagnation point for the installed model. An additional series of runs calibrated the choke plate settings for the leading-edge slots. These runs included variations of Cμ and NPR.

In order to assess the quality of the data, the first tests involved the calibration of blowing slots. This was performed through a pressure survey of the blowing slots and a check of spanwise uniformity using the handheld pressure probe. Additionally, checks for hysteresis and data repeatability were performed.



Figure 8-1. Baseline AHLLE configuration.

Sample data are shown in figure 8-2 for aft choke plate calibration. These were used to verify the choke plate was choked and performing as expected. The discharge coefficient was expected to be between 0.6 and 0.8. These parameters were monitored throughout the test to detect any gross changes in plenum performance. This data calibration was performed for the forward choke plate in the LAVLET with blown 45° TE flap, the mid choke plate for LAVLET with blown 45° TE flap and MOLEC with blown 45° TE flap, and the aft choke plate in the baseline configuration with blown 45° TE flap.

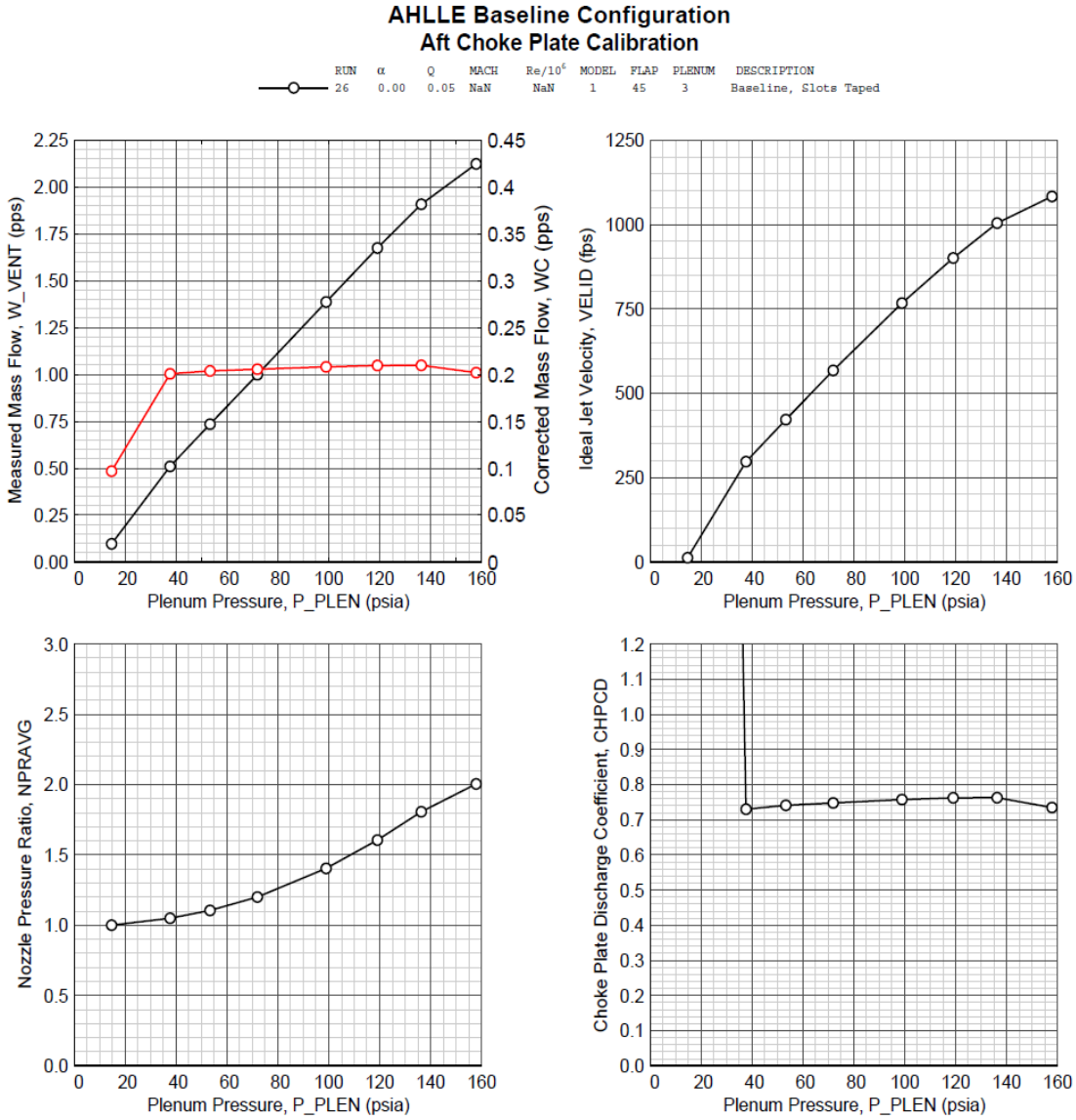


Figure 8-2. AHLLE choke plate calibration.

Slot flow documented through use of a handheld total pressure probe inserted into the blown slot is shown in figure 8-3. The purpose of the handheld probe surveys was to validate our instrumentation assumptions by placing the total pressure probe in a slot at b/w and sweeping NPR. The handheld surveys were used to document slot flow uniformity by moving total probe

along the length of the slot at a fixed NPR. These surveys were performed at the forward, mid, and aft choke plates.

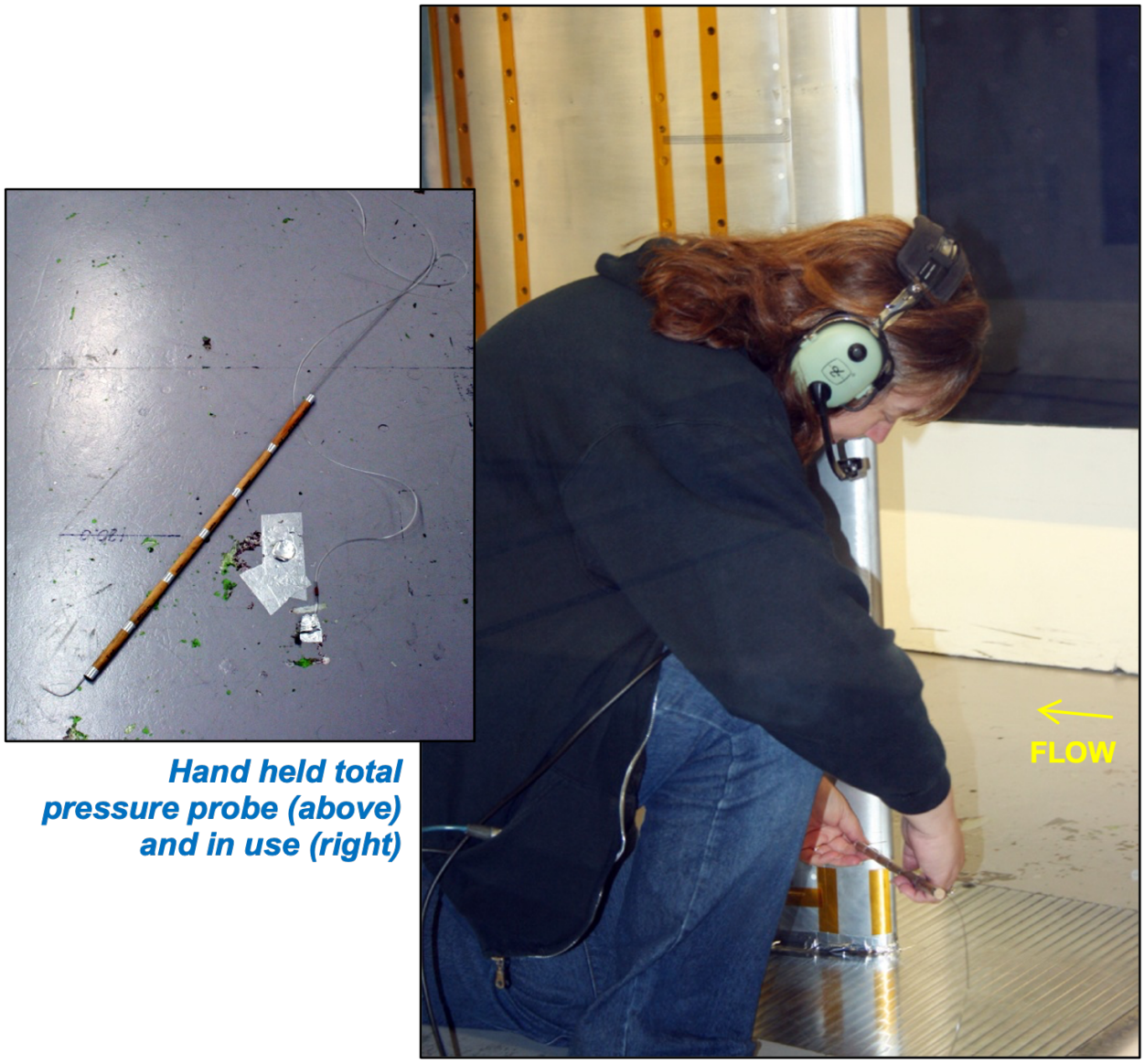


Figure 8-3. Handheld probe surveys.

- Sample survey shown for Aft Slot (Baseline w/ 45° TE Flap)

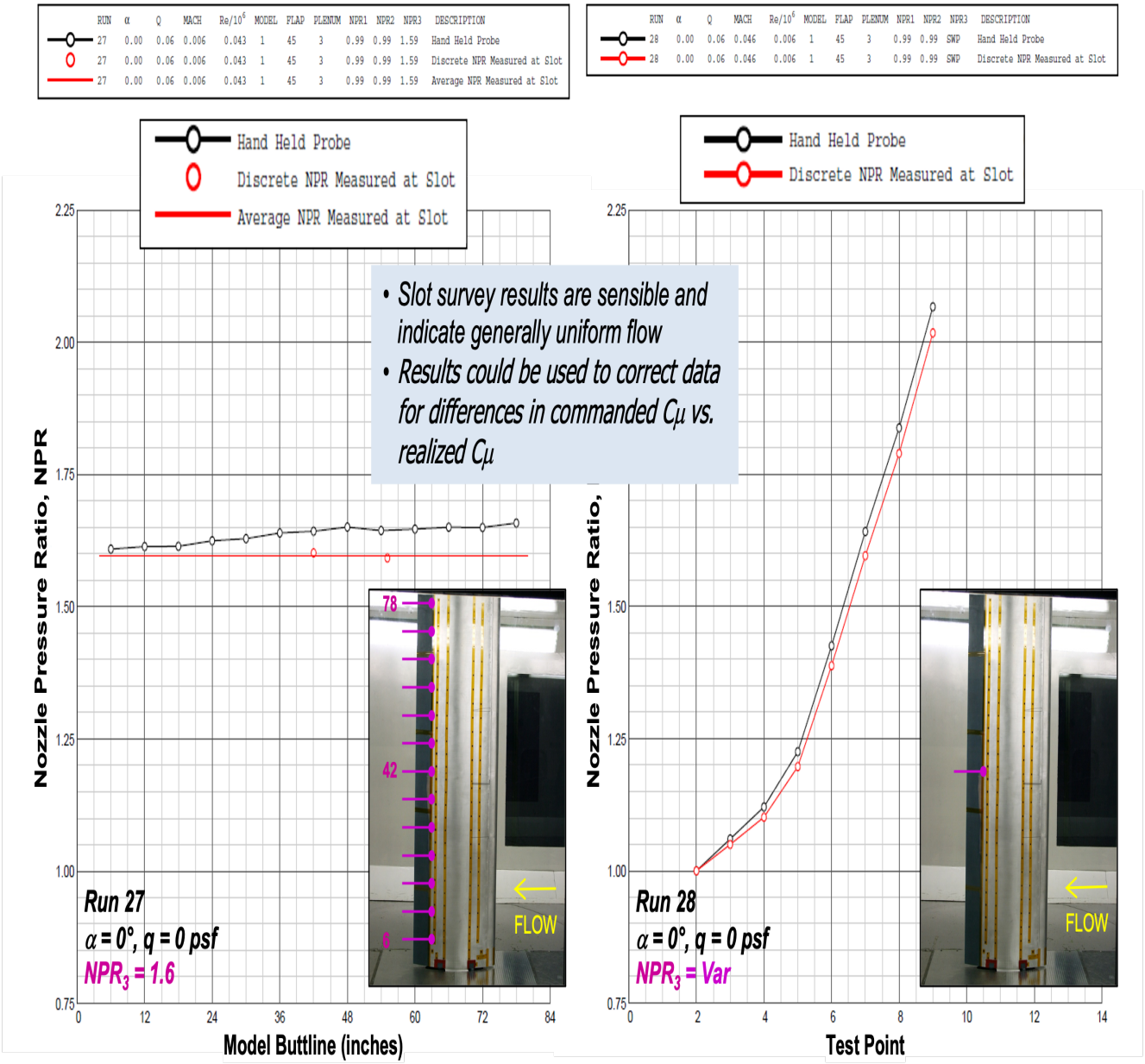
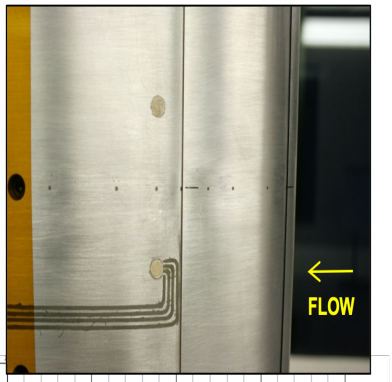


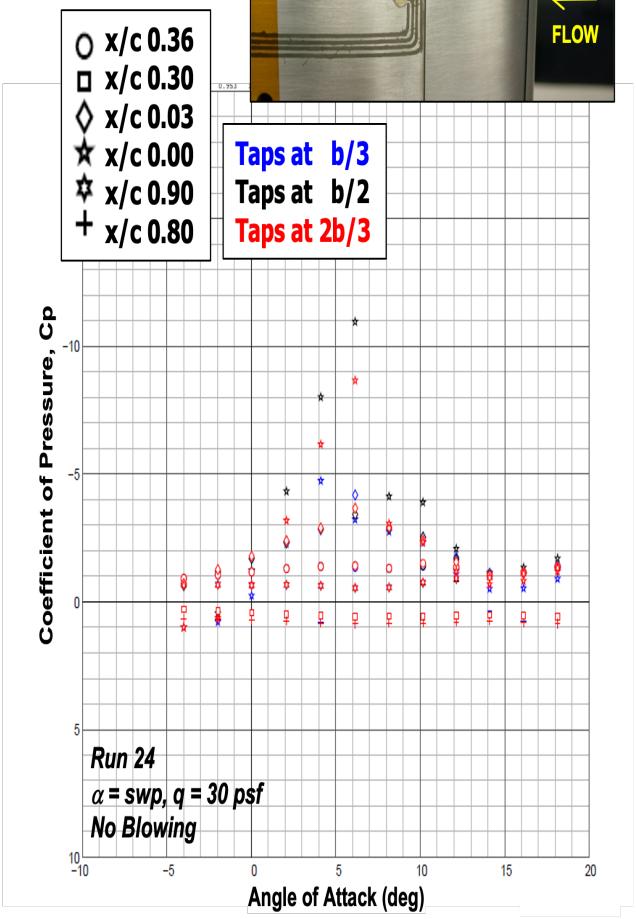
Figure 8-4. Slot survey data results.

Figure 8-4 documents the slot survey results for the aft slot. The slot surveys at fixed NPR and during an NPR sweep show general uniformity.

Task 7 – Data Quality: Spanwise Uniformity

- Spanwise uniformity documented through analysis of static pressure data taken at the three rows of static taps (b/3, b/2, 2b/3)
- Pressure data recorded every run; analyzed for all major model configurations
- Sample uniformity shown for Baseline w/ 45° TE flap





- *Non-uniformities are present on the very nose of the model, as the stagnation point moves around for a variety of possible reasons*
- *Otherwise, results indicate good uniformity across instrumented span of the model*

Figure 8-5. Data quality results.

During the test for spanwise uniformity, static pressure data were taken at the three rows of static taps. These are shown in the blue, black, and red data of figure 8-5. The data lie on top of each other except for the data taken at the very nose of the model. This stagnation point moved around very slightly during examination. Otherwise, results indicate good uniformity across the instrumented span of the model.

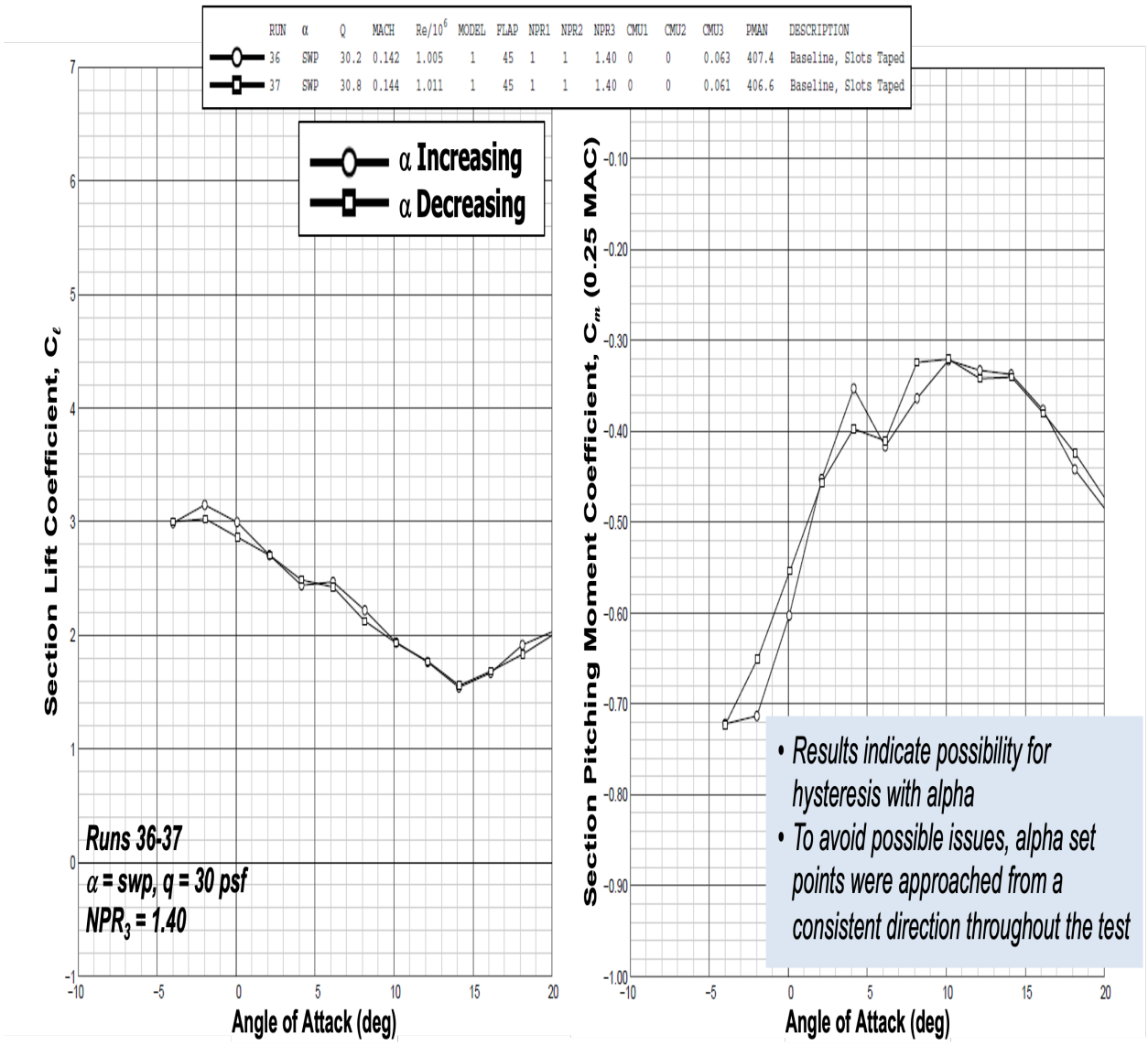


Figure 8-6. Data results for hysteresis sweeps.

Wind tunnel runs were made to look for possible hysteresis in sweeping model angle of attack. The results are shown in figure 8-6 for the baseline configuration with blown 45° TE flap. Results indicate a possibility for hysteresis with alpha. To avoid any possible issues, the test was run in a consistent manner and all alpha set points were approached from one direction.

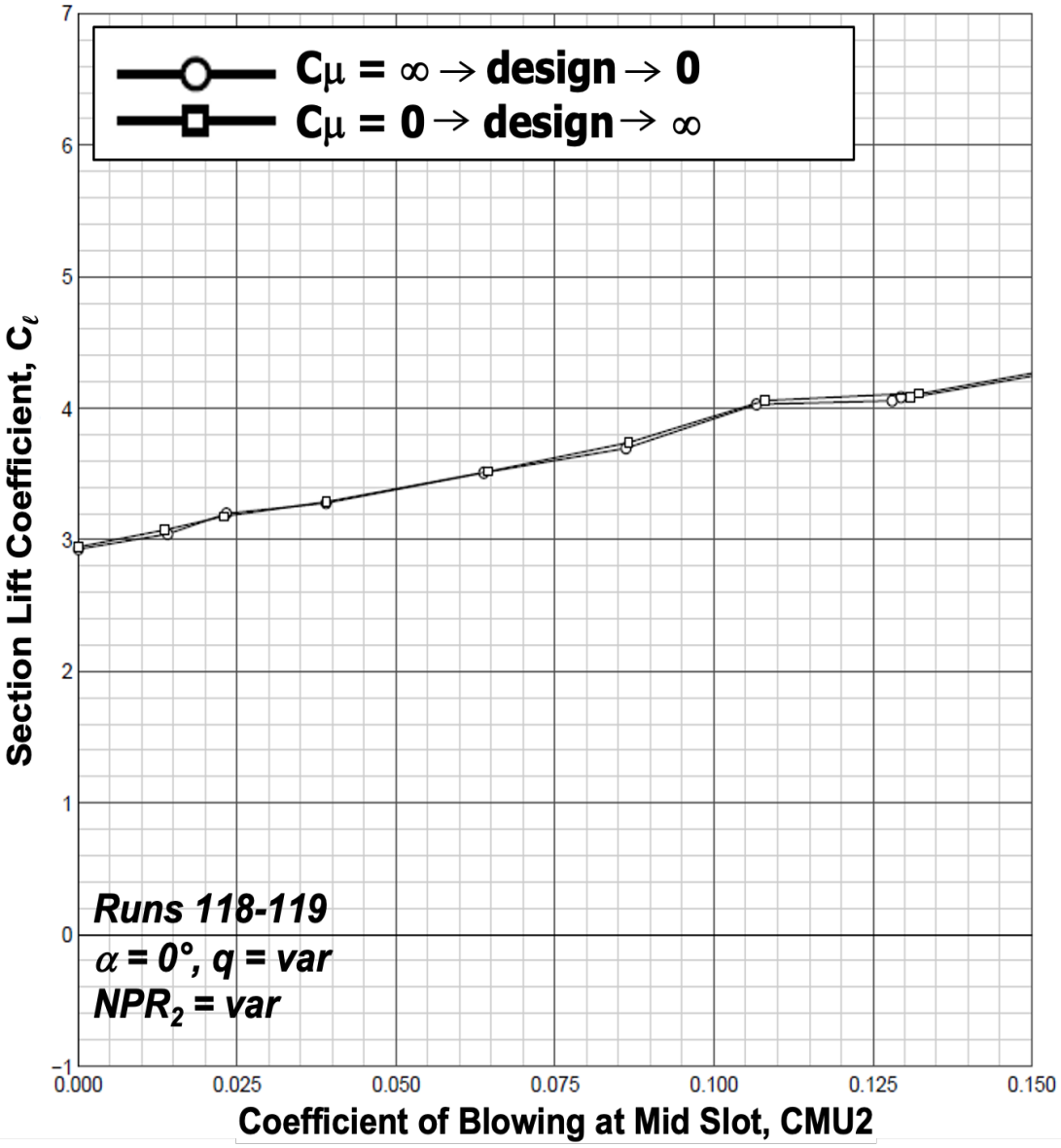


Figure 8-7. Data quality: Cμ hysteresis results.

Wind tunnel runs were made to look for possible hysteresis in varying Cμ. During the test to assess data quality, the following procedure was performed. With NPR = 2.0, ramp Q from 0 to 30 psf, then at Q = 30 psf, ramp NPR to Off (*Cμ = inf -> design -> zero*). Next, with Q = 30 psf, ramp NPR from Off to 2.0, then at NPR = 2.0, ramp Q to 0 psf (*Cμ = zero -> design -> inf*). This procedure was performed for the baseline configuration with blown 45° TE flap and showed no hysteresis effects. The test was also performed on LAVLET 10% slot with 1% slot fixed. This configuration showed slight hysteresis likely due to complex flow interactions. Results showed a slight variation in c_l ~0.1. For the MOLEC 12% slot configuration no hysteresis appeared. Figure 8-7 is a sample data set shown for the MOLEC 12% slot.

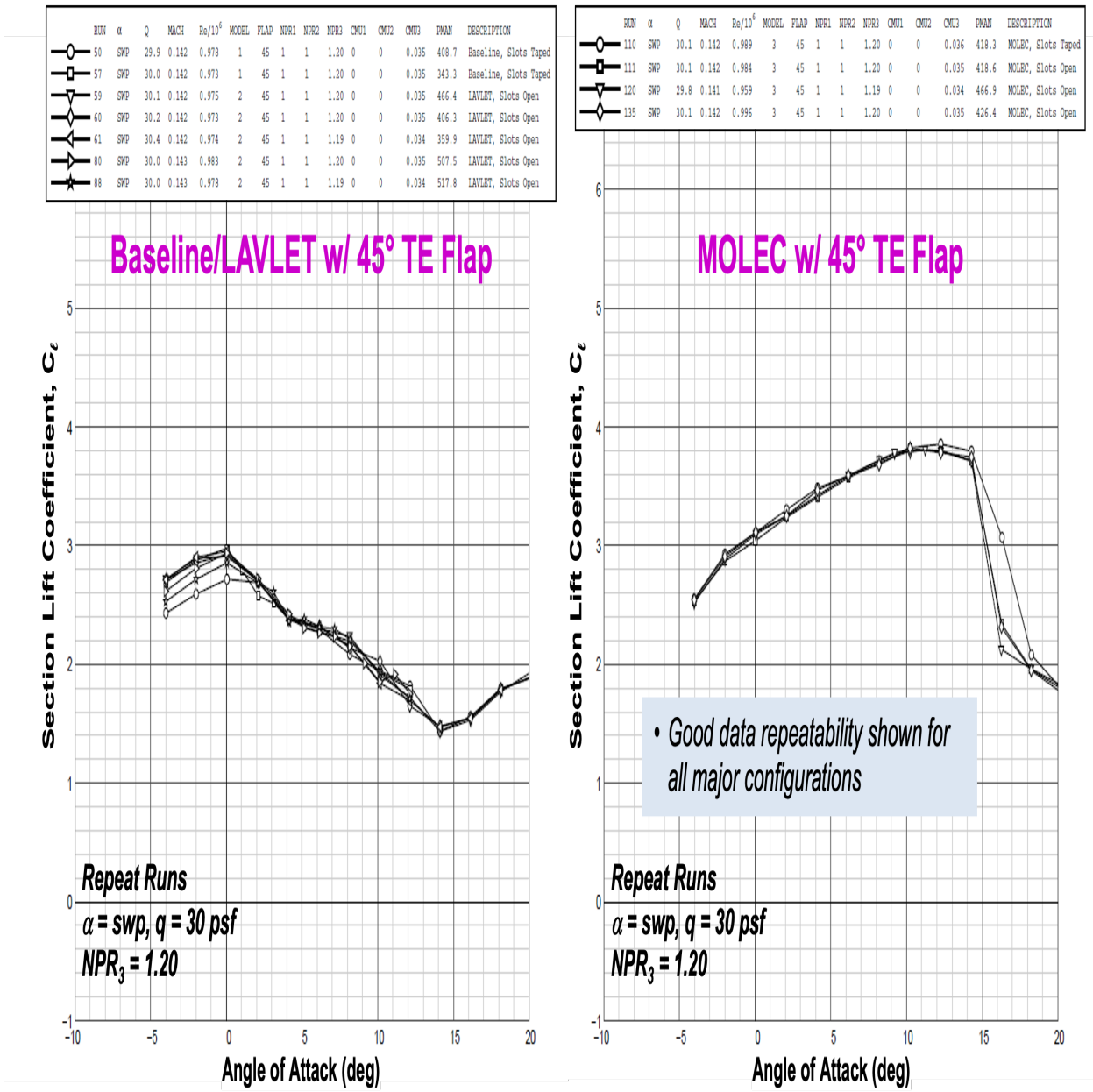
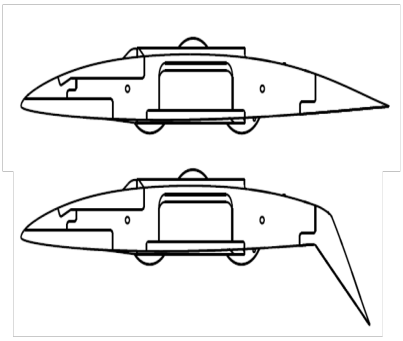


Figure 8-8. Data quality: data repeatability.

Data repeatability was analyzed for consistency in data throughout the test. Figure 8-8 shows results of good data repeatability for all major configurations. They are:

- Baseline/LAVLET with blown 45° TE flap
- MOLEC with blown 45° TE flap

Task 7 – Baseline: Effect of Q



- Effect of freestream dynamic pressure
  - Baseline with 0° TE flap
  - Baseline with 45° TE flap (data shown below)

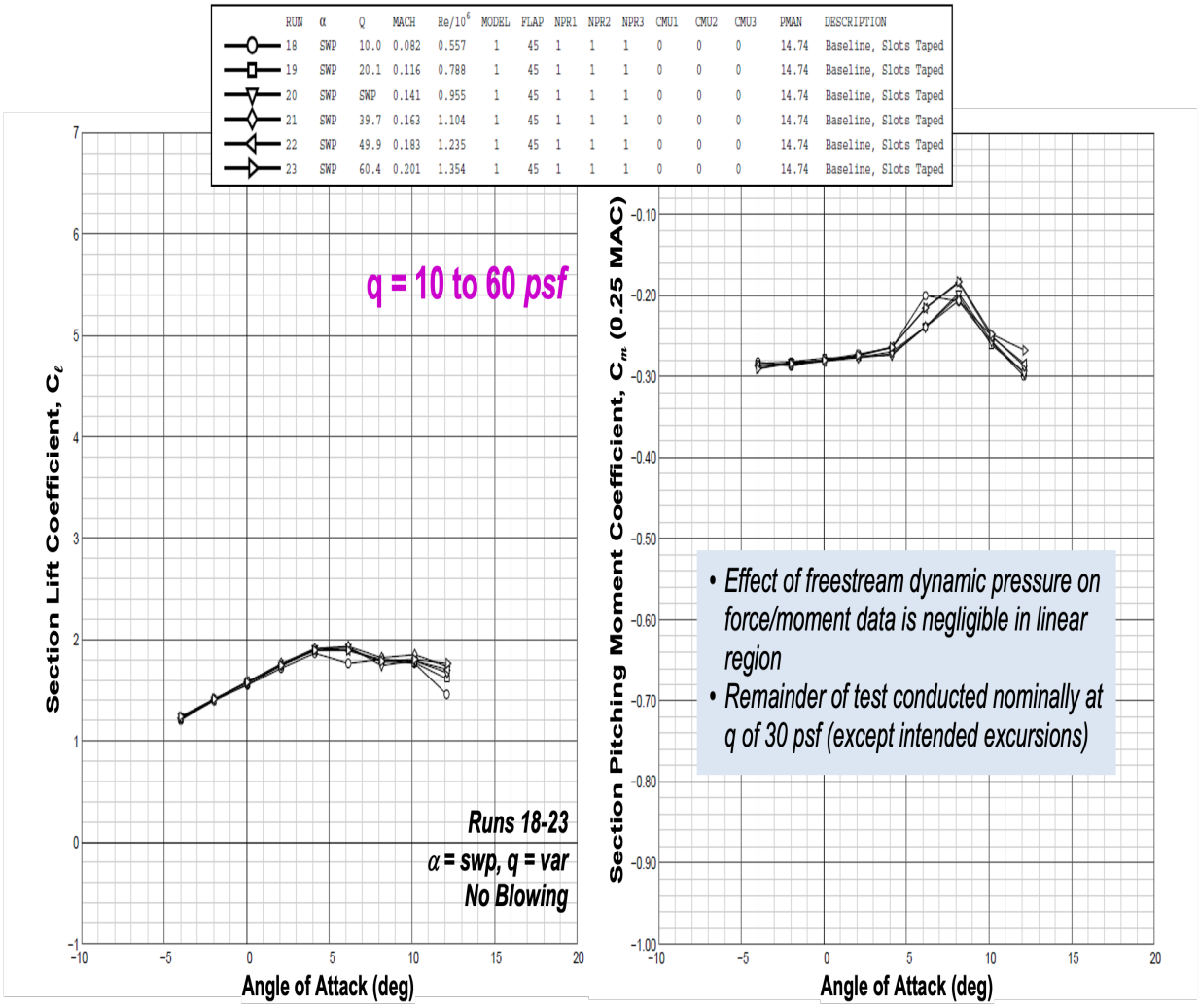


Figure 8-9. Effect of freestream dynamic pressure.

The effect of freestream dynamic pressure on force and moment data is negligible. This is shown in figure 8-9. The remainder of the tests are conducted at a nominal Q = 30 psf.

Figure 8-10 shows the results on the baseline model with the flap deflected and that they are consistent with CFD pretest predictions.

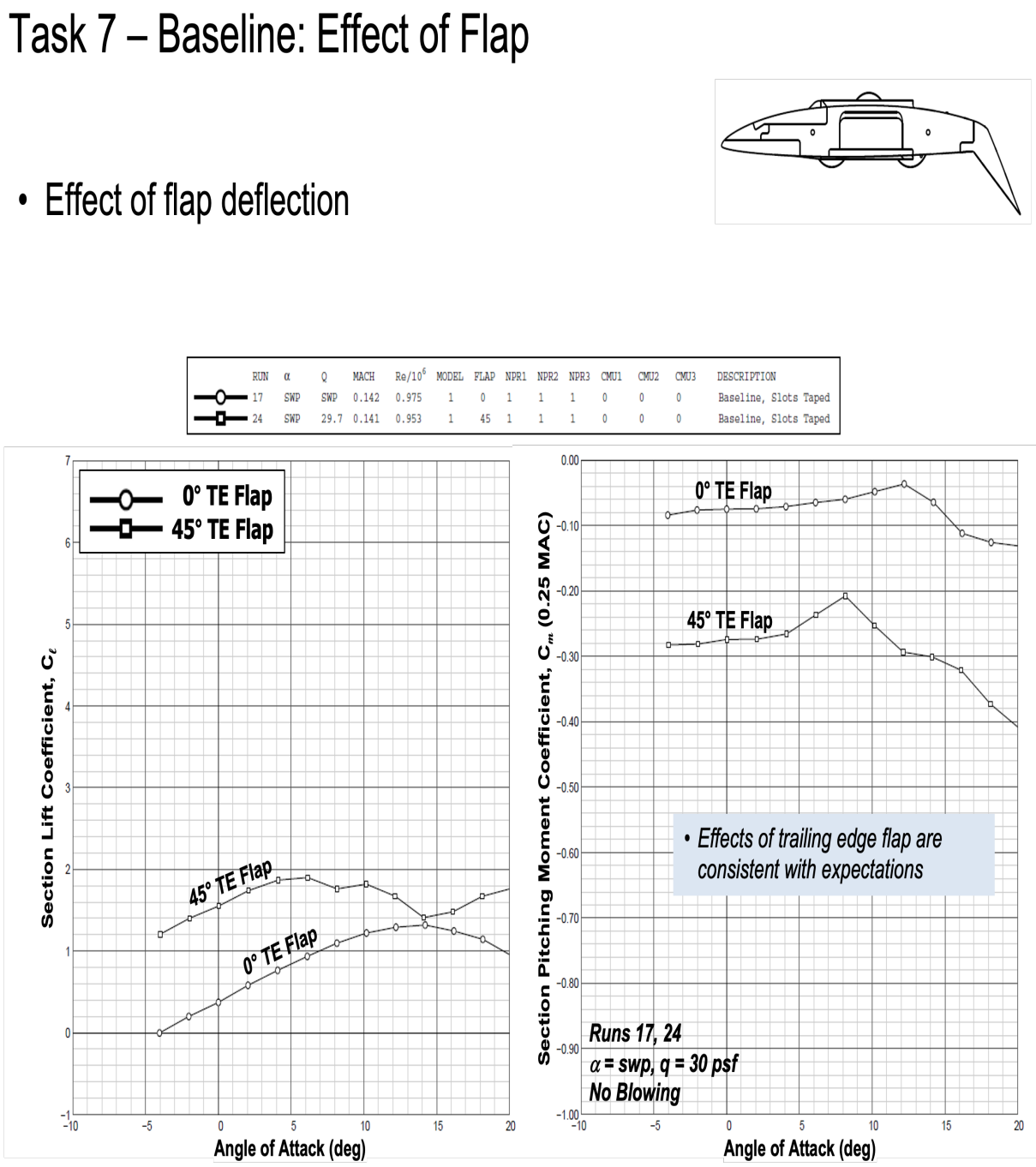


Figure 8-10. Effect of flap deflection.

Task 7 – Baseline: CFD Comparisons

- Comparison of WT test data to CFD predictions – force/moment data
  - Comparisons made where configurations overlapped

	RUN	α	Q	MACH	$Re/10^6$	MODEL	FLAP	NPR1	NPR2	NPR3	CMU1	CMU2	CMU3	DESCRIPTION
○	17	SWP	SWP	0.142	0.975	1	0	1	1	1	0	0	0	Baseline, Slots Taped
□	24	SWP	29.7	0.141	0.953	1	45	1	1	1	0	0	0	Baseline, Slots Taped
○	1	SWP	30	0.142	1.008	1	0	0	0	0	0	0	0	CFD Pre-Test 2D Baseline
○	1	SWP	999	0.2	22	1	0	0	0	0	0	0	0	CFD Conceptual Design Baseline
□	2	SWP	999	0.2	22	1	45	0	0	0	0	0	0	CFD Conceptual Design Baseline
▽	3	SWP	999	0.2	5	1	0	0	0	0	0	0	0	CFD Conceptual Design Baseline

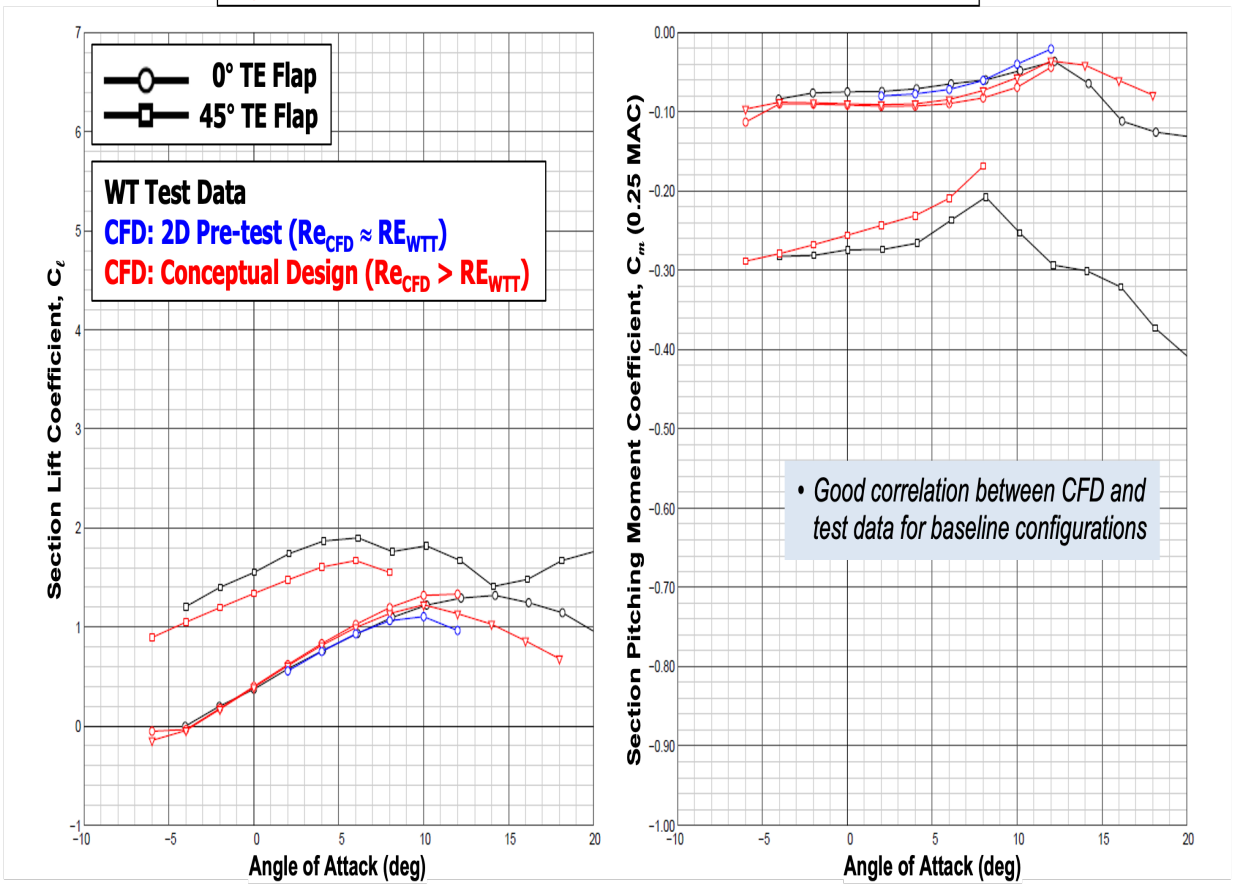


Figure 8-11. CFD correlation with test data.

Figure 8-11 compares wind tunnel test data, shown in black, with pretest CFD predictions and CFD conceptual design (Re = 22 M). All data trend similarly and predict alpha and section lift.

Task 7 – Baseline: CFD Comparisons

- Comparison of WT test data to CFD predictions – Cp distribution

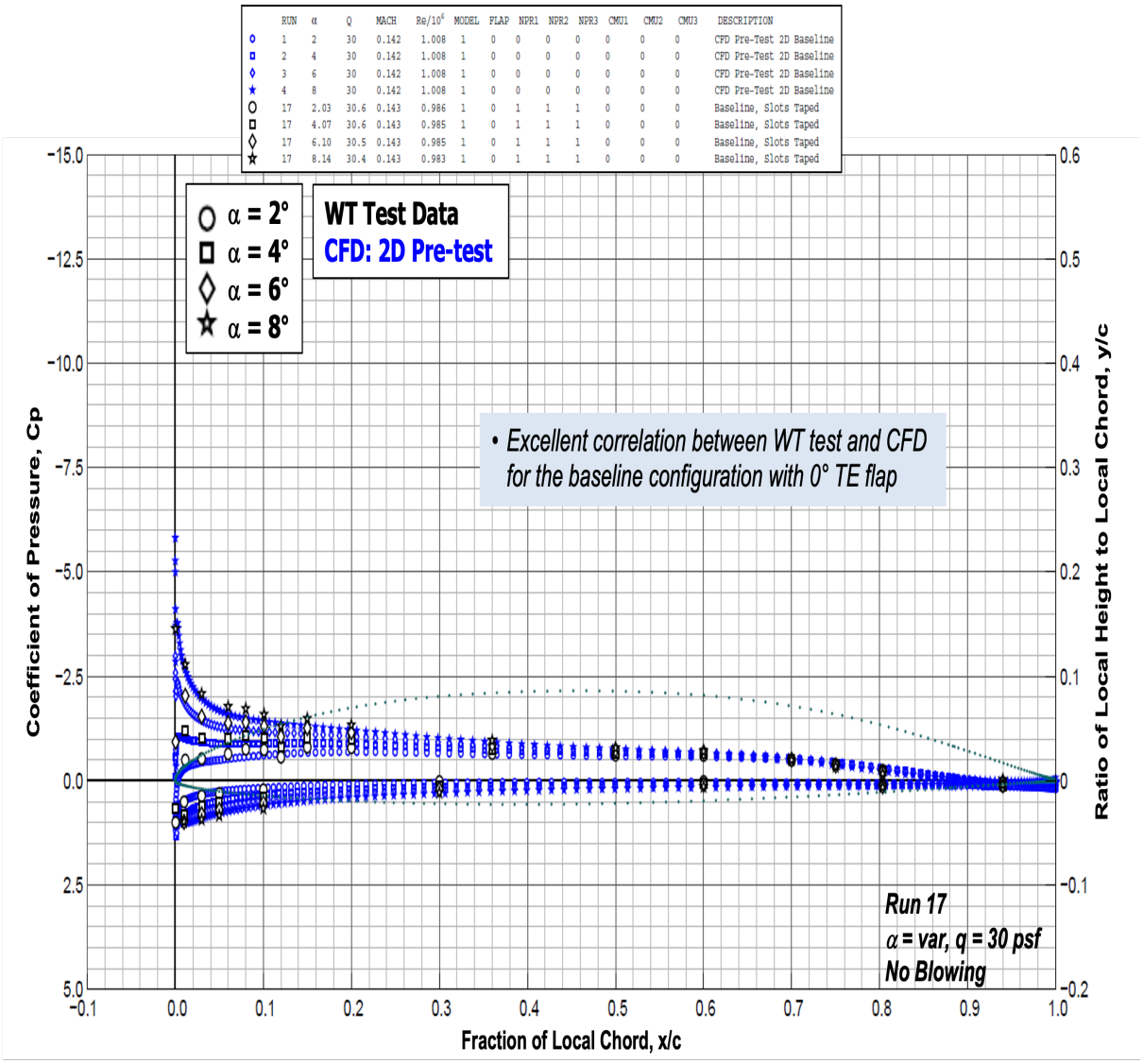
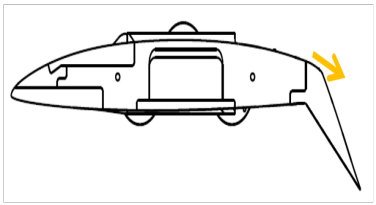


Figure 8-12. C_P distribution comparison with CFD prediction.

Figure 8-12 shows excellent correlation between wind tunnel test data shown in black and CFD for the baseline configuration with zero-degree TE flap.

Task 7 – Baseline: Effect of Flap Blowing



- Effect of blowing on 45° TE flap
  - NPR_3 varied from 1.0 to 2.0 (No blowing at Fwd/Mid slots)

RUN	α	Q	MACH	$Re/10^6$	MODEL	FLAP	NPR1	NPR2	NPR3	CMU1	CMU2	CMU3	DESCRIPTION
46	SWP	29.9	0.142	0.989	1	45	1	1	1	0	0	0	Baseline, Slots Taped
48	SWP	30.2	0.142	0.986	1	45	1	1	1.05	0	0	0.010	Baseline, Slots Taped
49	SWP	30.1	0.142	0.983	1	45	1	1	1.10	0	0	0.018	Baseline, Slots Taped
50	SWP	29.9	0.142	0.978	1	45	1	1	1.20	0	0	0.035	Baseline, Slots Taped
51	SWP	30.2	0.142	0.982	1	45	1	1	1.39	0	0	0.062	Baseline, Slots Taped
52	SWP	29.9	0.142	0.976	1	45	1	1	1.59	0	0	0.088	Baseline, Slots Taped
53	SWP	30.1	0.142	0.978	1	45	1	1	1.79	0	0	0.110	Baseline, Slots Taped
54	SWP	30.1	0.142	0.978	1	45	1	1	1.99	0	0	0.133	Baseline, Slots Taped

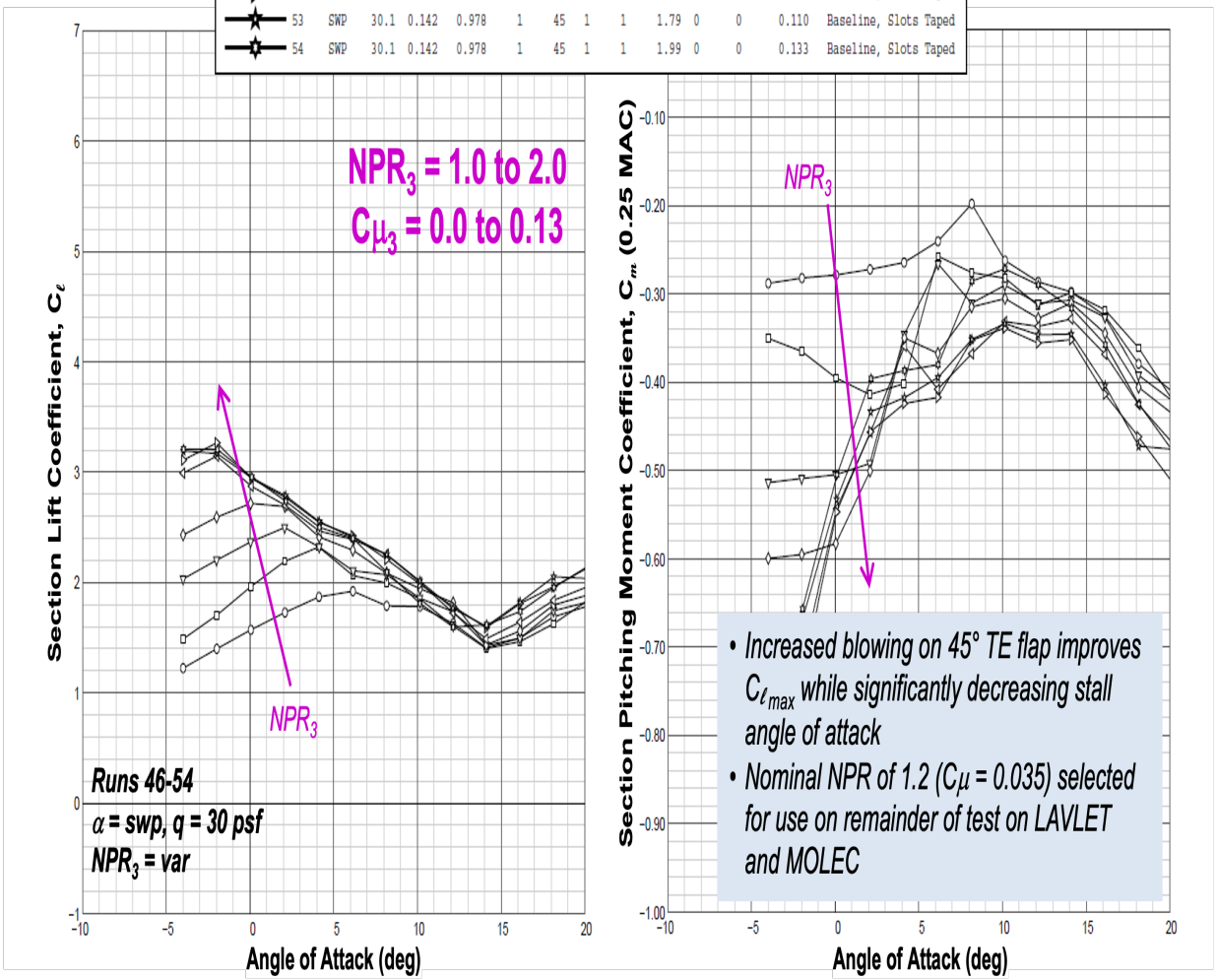


Figure 8-13. Effect of flap blowing.

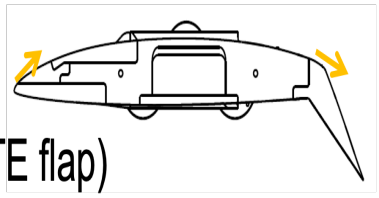
Figure 8-13 displays results for section lift versus angle of attack to show the effectiveness of TE flap blowing. In the curve on the left, NPR on the trailing edge is adjusted by increments of 0.05 to achieve a nominal blown flap value. Increased blowing on the 45 TE flap improves c_{lmax} while significantly decreasing the stall angle of attack. This was predicted by our CFD during pretest aerodynamic analysis and the result is expected. A nominal NPR = 1.2 ($C\mu$ = 0.035) was selected for use on the remainder of the test on both the LAVLET and MOLEC configurations. As this was a proof-of-concept experiment for leading-edge high-lift concepts, the trailing-edge blowing was not the emphasis of the study. Once a nominal NPR was achieved that maintained a positively sloped lift curve and a positive stall angle, that value was fixed.

In figure 8-14, the results are shown for the effectiveness of single slot blowing at the 1% chord location on the LAVLET model. This study was performed to assess and fix the blowing coefficient ($C\mu$) on the leading-edge slot. Again, the TE slot NPR is fixed to 1.2. The 10% chord slot is off. The NPR for the 1% chord slot is varied every 0.05 from 1.0 to 2.0. The lift curves and pitching moment curves versus alpha are shown. As NPR is increased from the single slot, the lift curve increases, and the stall angle of attack improves commensurately.

Figure 8-15 shows the results for both the 1% chord and the 10% chord slots varied equally in NPR in 0.05 increments from NPR = 1.0 to 1.9. (NPR of 2.0 was not achievable on the 10% chord slot.) The results of lift and moment versus alpha are shown in the figure. As equal NPRs are achieved on the forward slots, a section lift of $c_l = 4.6$ is achieved. Stall becomes less delayed and is more benign with increased $C\mu$.

The final LAVLET configuration test is shown in figure 8-16. These results are reported for 1% chord and 10% chord slots varied differentially in NPR. $C\mu$ was incrementally adjusted from NPR = 1.0 to 1.9 on the second slot. NPR on the 1% chord slot was fixed at 1.4. This value was set based on the equal blowing results from figure 8-15. Figure 8-16 shows that differential blowing achieves a lift coefficient $c_l = 4.6$ and improves the stall angle to nearly 10 degrees with a gradual stall.

Task 7 – LAVLET: Effect of Fwd Slot Blowing



- Effect of 1% slot blowing on LAVLET (blown 45° TE flap)
  - NPR_1 varied from 1.0 to 2.0 (NPR_3 fixed at 1.2)

RUN	α	Q	MACH	Re/10^6	MODEL	FLAP	NPR1	NPR2	NPR3	CMU1	CMU2	CMU3	PMAN	DESCRIPTION
80	SWP	30.0	0.143	0.983	2	45	1	1	1.20	0	0	0.035	507.5	LAVLET, Slots Open
81	SWP	30.1	0.143	0.984	2	45	1.05	1	1.19	0.014	0	0.034	519.7	LAVLET, Slots Open
82	SWP	29.9	0.143	0.981	2	45	1.09	1	1.20	0.021	0	0.035	503.8	LAVLET, Slots Open
83	SWP	30.2	0.143	0.985	2	45	1.20	1	1.20	0.035	0	0.034	488.4	LAVLET, Slots Open
84	SWP	30.1	0.143	0.982	2	45	1.39	1	1.19	0.057	0	0.034	499.9	LAVLET, Slots Open
85	SWP	30.0	0.143	0.979	2	45	1.59	1	1.19	0.077	0	0.033	497.5	LAVLET, Slots Open
86	SWP	30.2	0.143	0.981	2	45	1.79	1	1.20	0.096	0	0.035	509.0	LAVLET, Slots Open
87	SWP	29.9	0.142	0.976	2	45	1.99	1	1.20	0.117	0	0.035	509.9	LAVLET, Slots Open

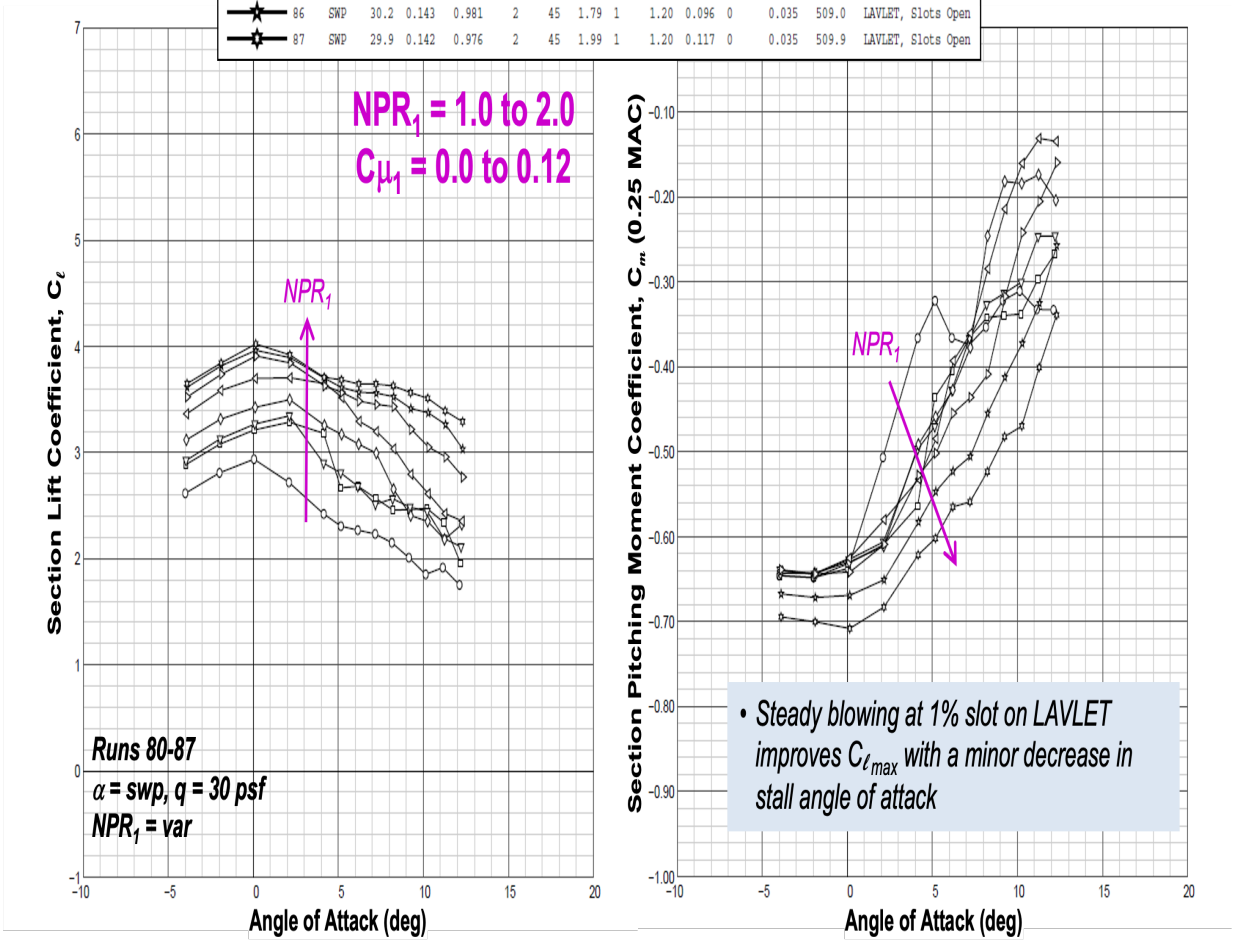
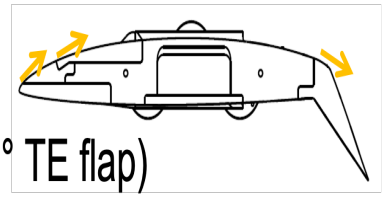


Figure 8-14. Effect of 1% chord slot blowing on LAVLET.

Task 7 – LAVLET: Effect of Fwd/Mid Slot Blowing



- Effect of equal slot blowing on LAVLET (blown 45° TE flap)
  - NPR_1 equal to NPR_2, varied from 1.0 to 1.9 (NPR_3 fixed at 1.2)

	RUN	α	Q	MACH	$Re/10^6$	MODEL	FLAP	NPR1	NPR2	NPR3	CMU1	CMU2	CMU3	PMAN	DESCRIPTION
○	88	SWP	30.0	0.143	0.978	2	45	1	1	1.19	0	0	0.034	517.8	LAVLET, Slots Open
□	89	SWP	30.3	0.143	0.981	2	45	1.04	1.04	1.19	0.012	0.014	0.034	505.4	LAVLET, Slots Open
▽	90	SWP	29.8	0.142	0.972	2	45	1.10	1.09	1.19	0.021	0.024	0.034	510.2	LAVLET, Slots Open
◇	91	SWP	30.0	0.143	0.976	2	45	1.20	1.19	1.20	0.035	0.042	0.036	496.2	LAVLET, Slots Open
◁	92	SWP	29.6	0.142	0.969	2	45	1.39	1.39	1.20	0.058	0.072	0.036	499.6	LAVLET, Slots Open
▷	93	SWP	29.5	0.142	0.968	2	45	1.60	1.59	1.20	0.079	0.098	0.036	508.6	LAVLET, Slots Open
☆	94	SWP	SWP	0.143	0.978	2	45	1.80	1.79	1.19	0.096	0.120	0.034	512.7	LAVLET, Slots Open
☆	95	SWP	29.4	0.141	0.966	2	45	1.89	1.89	1.19	0.108	0.134	0.036	507.8	LAVLET, Slots Open

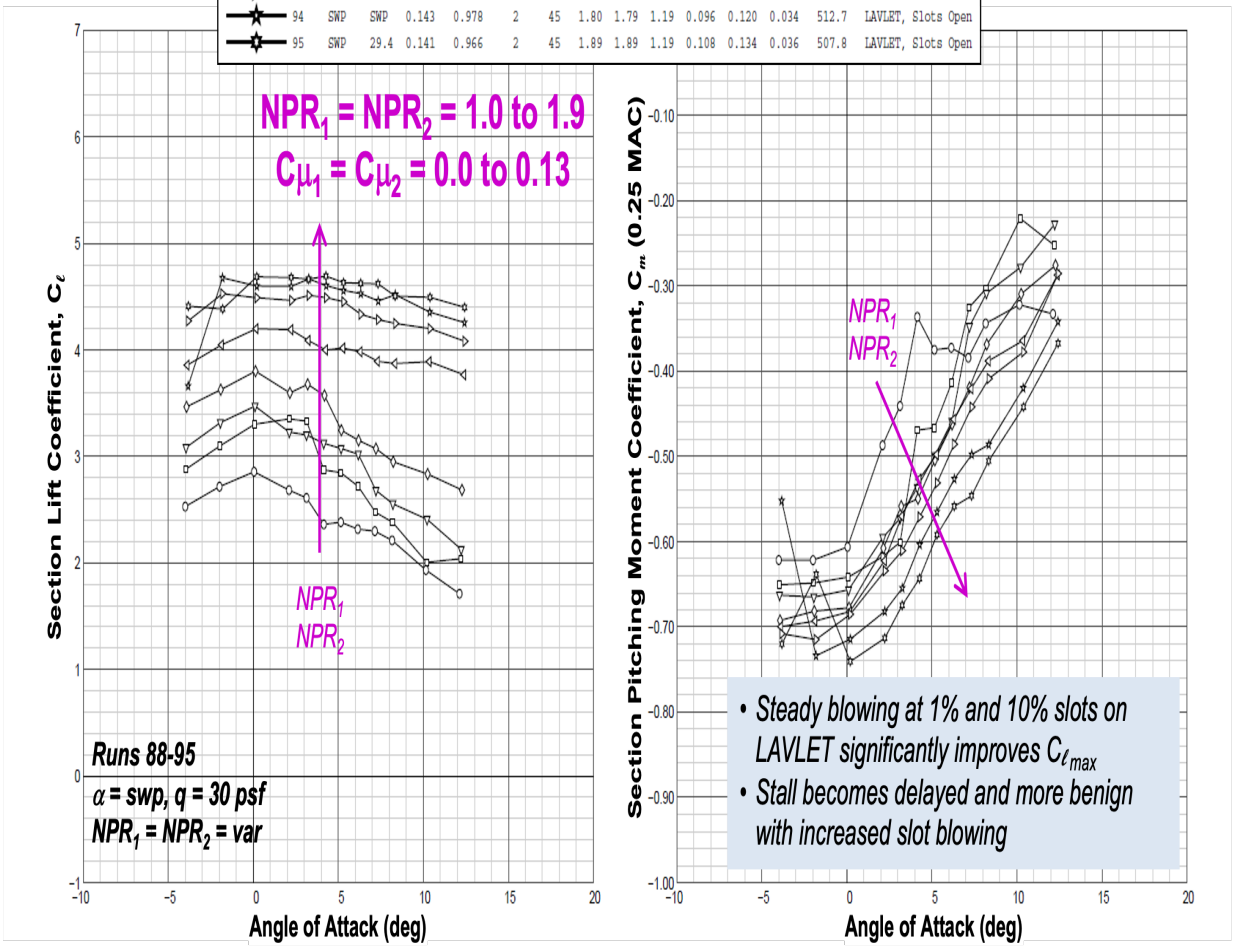
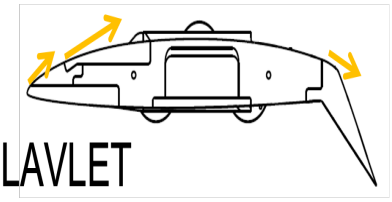


Figure 8-15. Effect of equal slot blowing on forward slots.

Task 7 – LAVLET: Effect of Fwd/Mid Slot Blowing



- Effect of (fixed 1%, variable10%) slot blowing on LAVLET
  - NPR_1 fixed at 1.4, NPR_2 varied from 1.0 to 1.9 (NPR_3 fixed at 1.2)

RUN	α	Q	MACH	$Re/10^6$	MODEL	FLAP	NPR1	NPR2	NPR3	CMU1	CMU2	CMU3	PMAN	DESCRIPTION
96	SWP	29.9	0.143	0.976	2	45	1.39	1	1.20	0.056	0	0.036	502.3	LAVLET, Slots Open
97	SWP	29.8	0.142	0.973	2	45	1.39	1.03	1.19	0.056	0.013	0.035	486.2	LAVLET, Slots Open
98	SWP	30.1	0.143	0.978	2	45	1.39	1.08	1.20	0.055	0.023	0.035	486.2	LAVLET, Slots Open
99	SWP	29.8	0.142	0.972	2	45	1.39	1.19	1.20	0.055	0.042	0.036	471.9	LAVLET, Slots Open
100	SWP	29.7	0.142	1.003	2	45	1.39	1.39	1.19	0.055	0.070	0.035	506.5	LAVLET, Slots Open
101	SWP	29.7	0.142	0.999	2	45	1.39	1.59	1.20	0.055	0.096	0.035	502.2	LAVLET, Slots Open
102	SWP	29.7	0.142	0.996	2	45	1.40	1.78	1.19	0.056	0.119	0.035	502.3	LAVLET, Slots Open
103	SWP	29.5	0.141	0.985	2	45	1.40	1.87	1.20	0.060	0.134	0.037	511.1	LAVLET, Slots Open
104	SWP	29.8	0.142	0.988	2	45	1.40	1.86	1.20	0.059	0.132	0.036	509.0	LAVLET, Slots Open

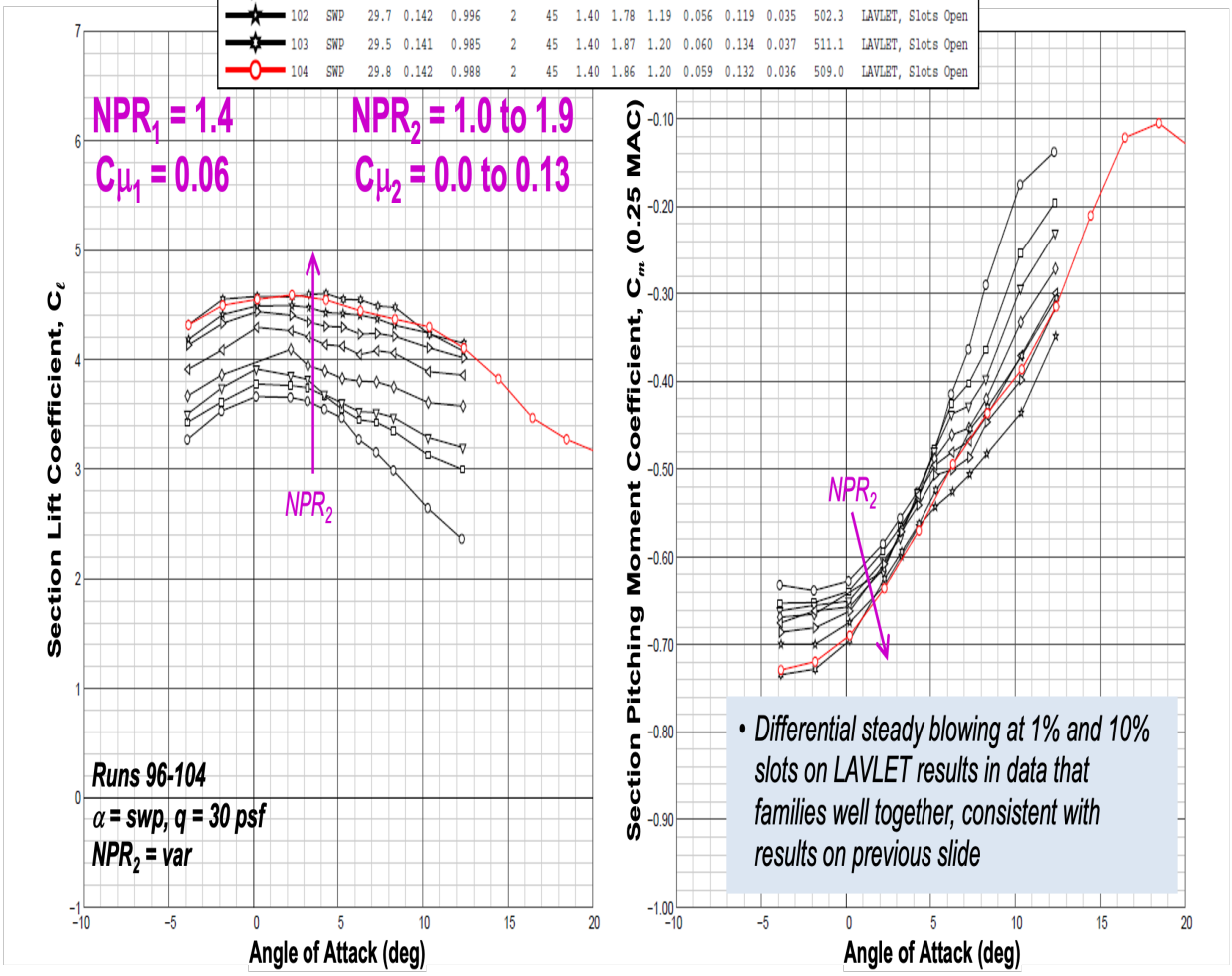


Figure 8-16. Effect of differential blowing on forward slots.

Task 7 – LAVLET: CFD Comparisons

- Comparison of WT test data to CFD predictions – force/moment data
  - Comparisons made where blowing settings overlapped

RUN	α	Q	MACH	Re/10^6	MODEL	FLAP	NPR1	NPR2	NPR3	CMU1	CMU2	CMU3	DESCRIPTION
106	SWP	29.6	0.142	0.979	2	45	1.99	1.90	1.24	0.120	0.134	0.043	LAVLET, Slots Open
104	SWP	29.8	0.142	0.988	2	45	1.40	1.86	1.20	0.059	0.132	0.036	LAVLET, Slots Open
1	SWP	30	0.142	1.008	2	45	1.68	1.84	1.2	0.12	0.135	0.041	CFD Post-Test 2D LAVLET
3	SWP	30	0.142	1.008	2	45	1.3	1.84	1.15	0.066	0.134	0.03	CFD Post-Test 2D LAVLET

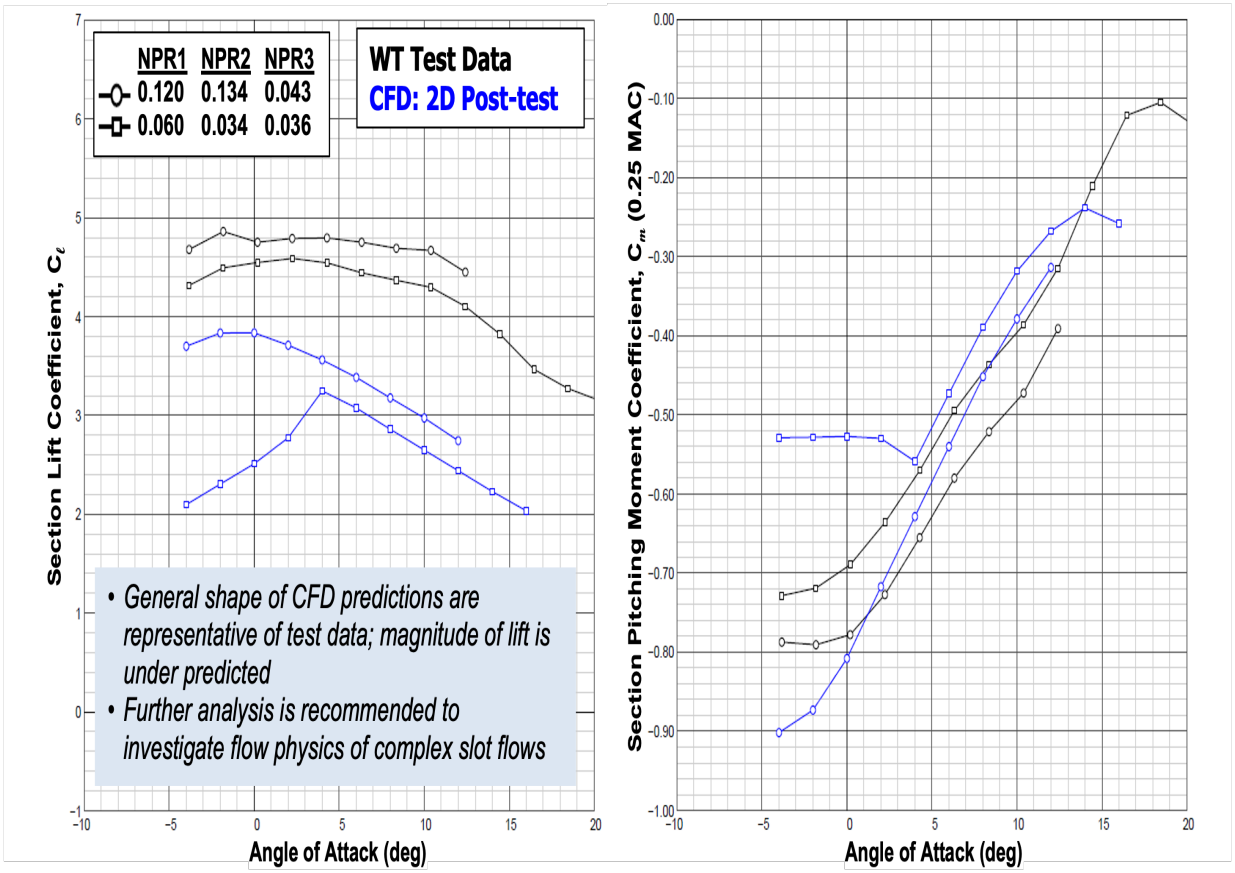


Figure 8-17. Wind tunnel test data to CFD comparisons.

Figure 8-17 examines wind tunnel test data, plotted in black, versus CFD predictions. The general shape of the curves is representative of the test data, although the magnitude of lift is underpredicted. Further analysis is recommended to investigate flow physics of the complex flow regions between the first and second slots.

Task 7 – LAVLET: CFD Comparisons

- Comparison of WT test data to CFD predictions – Cp distribution

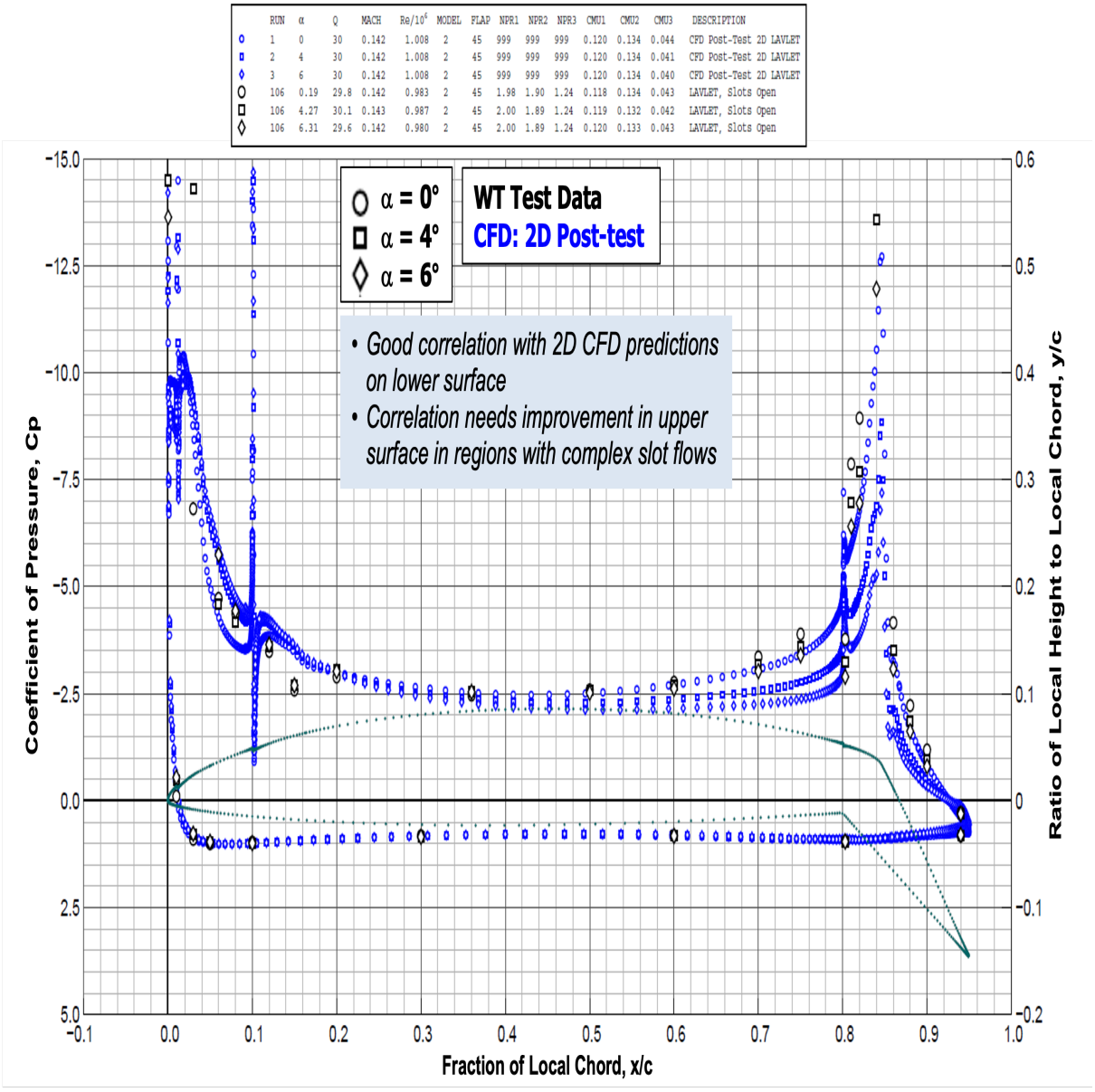


Figure 8-18. C_P comparison of wind tunnel data to CFD.

Figure 8-18 also examines the correlation of wind tunnel data compared to CFD predictions. Good correlation exists between the data and the lower surface predictions. As was seen with the

lift and moment data, the integrated C_P distributions require further analysis between the first and second slots.

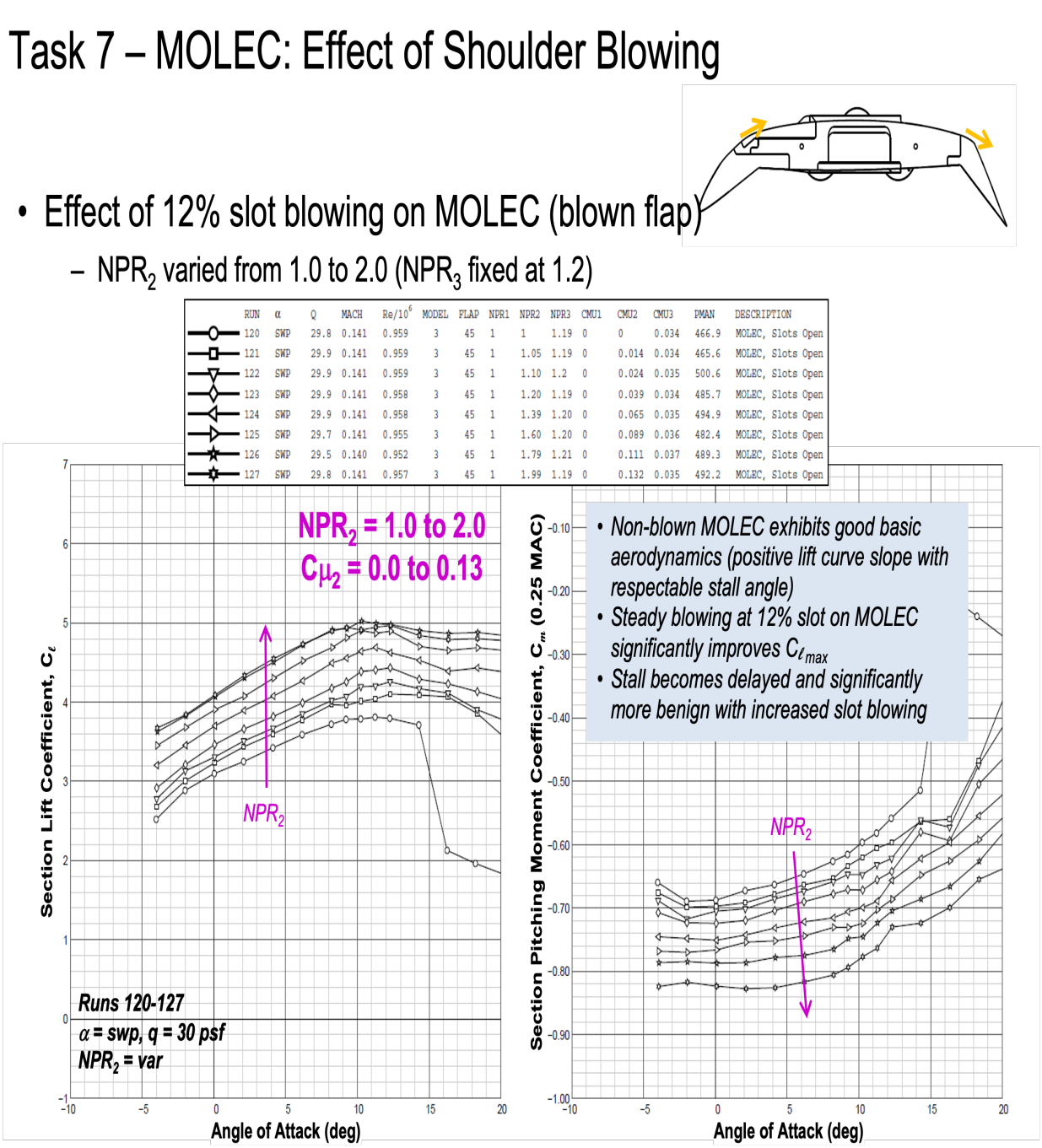


Figure 8-19. MOLEC configuration results.

Figure 8-19 shows the results for slot blowing at 12% chord on the MOLEC configuration. The slot blowing is fixed at an NPR = 1.2 as was the case for LAVLET. NPR was varied on the 12% chord slot from 1.0 to 2.0. The section lift and section moment versus angle-of-attack curves are

shown. With shoulder blowing, MOLEC achieves a remarkable Cl = 5.0. Stall becomes significantly delayed with increased Cmu.

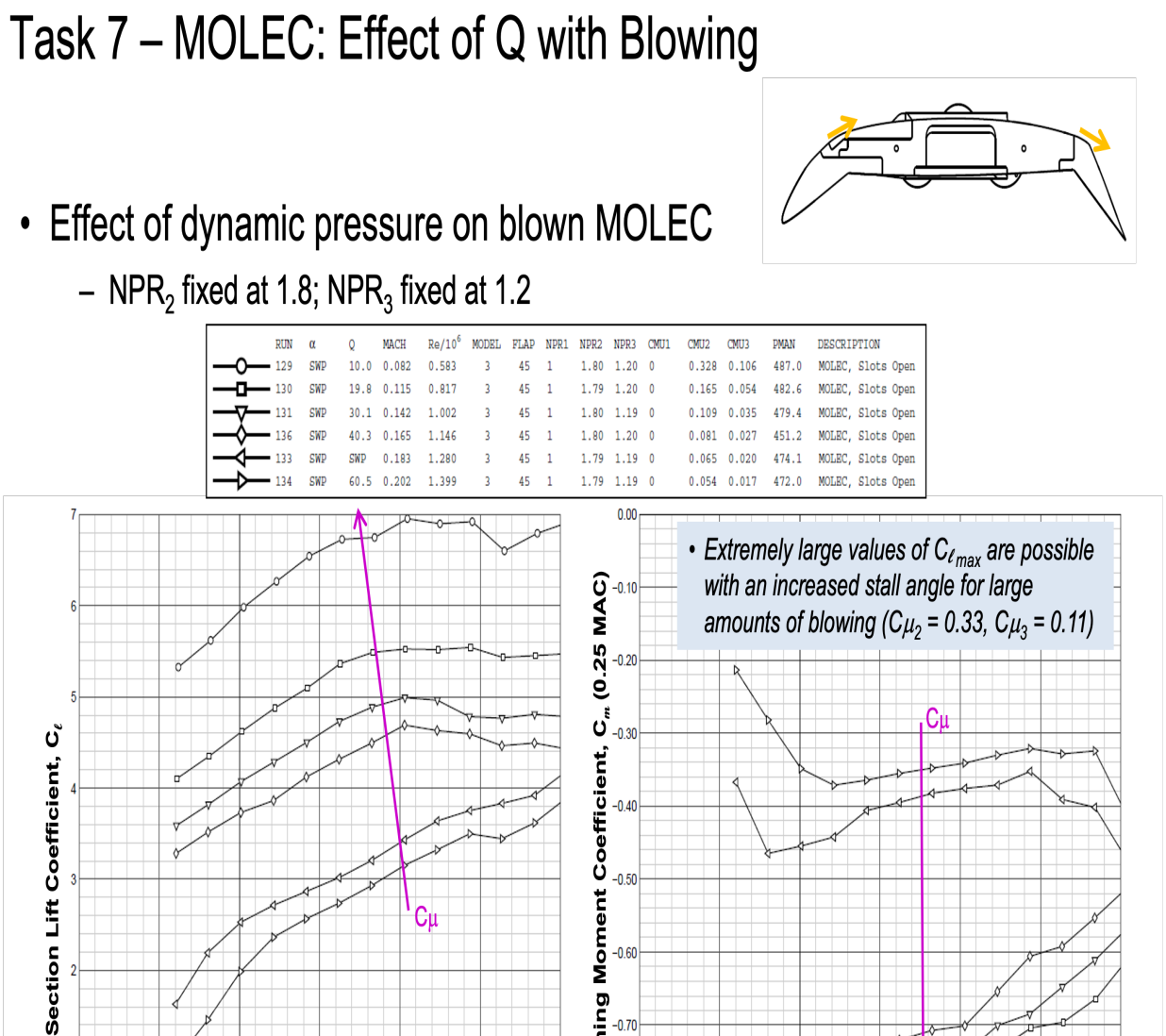


Figure 8-20. Effect of q on MOLEC configuration.

The final assessment was performed on the MOLEC configuration to examine the effect of q variation. In this test, the dynamic pressure, q, was varied from 10 psf to 60 psf while the NPR

on the 12% chord slot was fixed at 1.8 and the NPR on the TE slot was fixed at 1.2. An extraordinary high-lift value $c_l = 7.0$ was achieved during the q sweep.

Task 7 – MOLEC: CFD Comparisons

- Comparison of WT test data to CFD predictions – force/moment data
  - Comparisons made where blowing settings overlapped

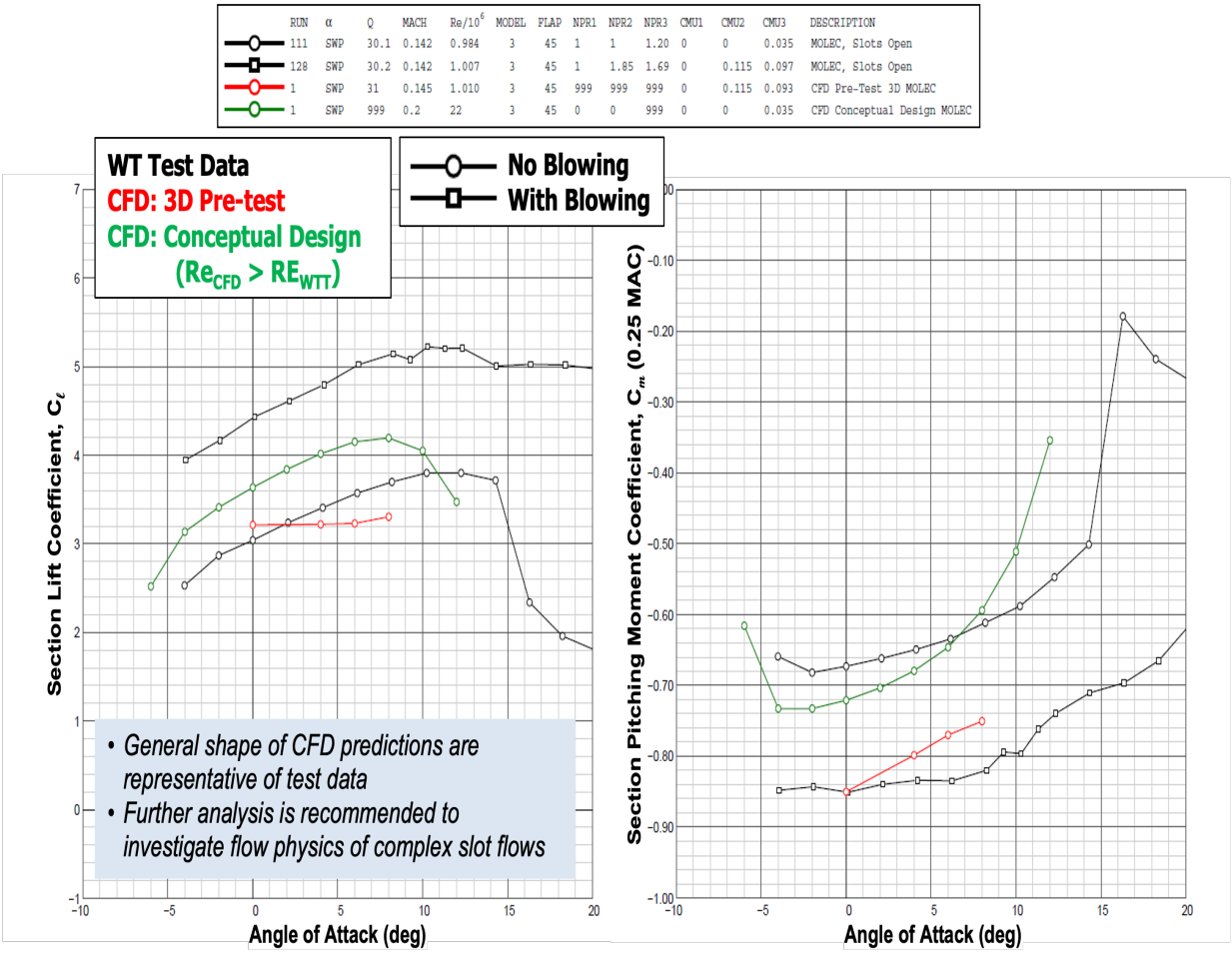


Figure 8-21. Comparison of wind tunnel test data to CFD.

In a final comparison, wind tunnel test data are assessed against CFD predictions for the MOLEC configuration. Figure 8-21 reports these comparisons. The wind tunnel data appear in black, the 3D pretest predictions are shown in red, and the conceptual design (Re = 22M) predictions are shown in green. The general shape of all curves is the same with an underprediction of c_l values in all predicted cases. Further analysis is recommended to investigate flow physics of the complex slot flows, especially on the leading-edge slots.

Task 7 – MOLEC: CFD Comparisons

- Comparison of WT test data to CFD predictions – Cp distribution

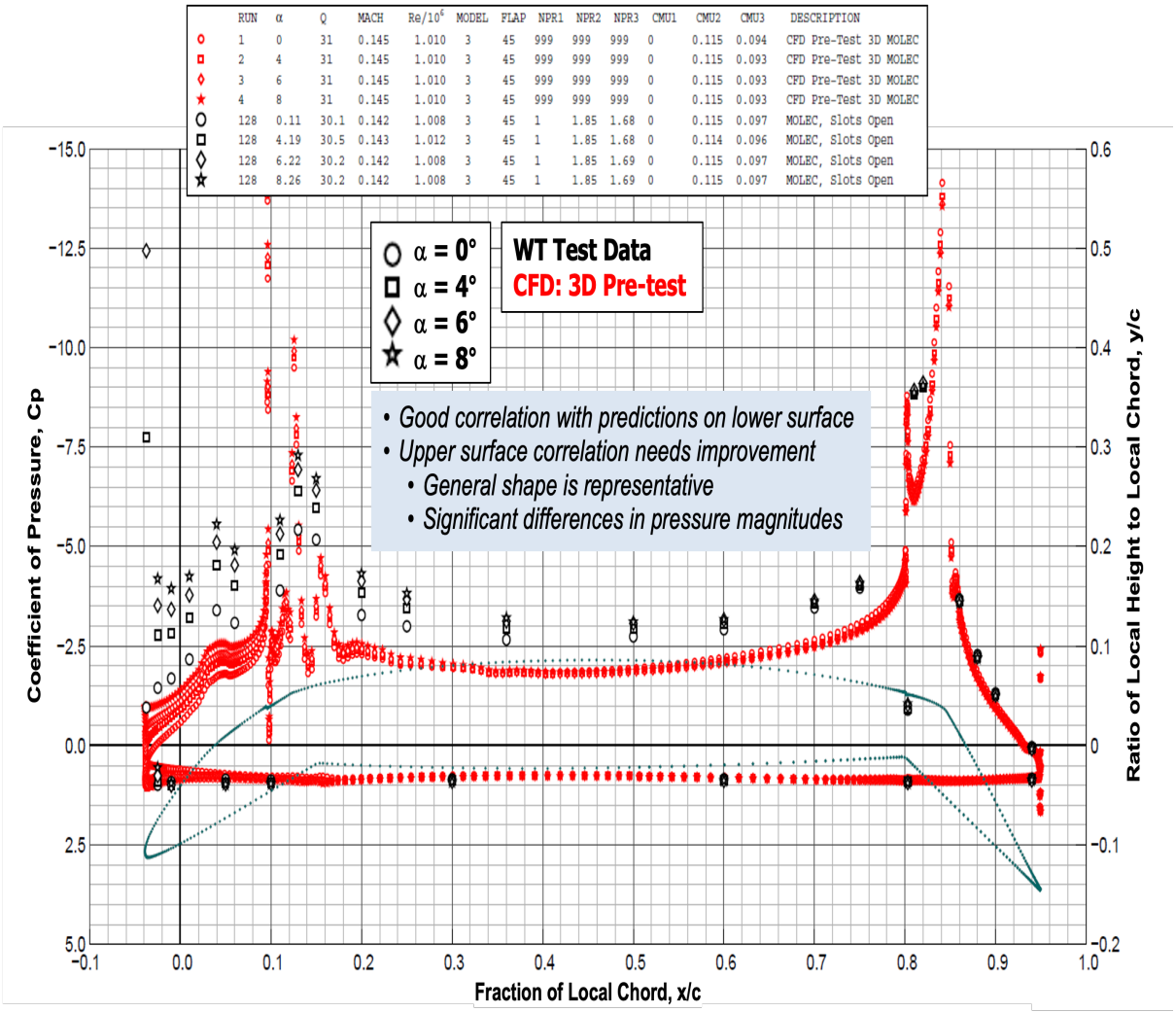


Figure 8-22. C_P distribution comparisons.

The C_P distributions were generated for wind tunnel test data versus CFD pretest predictions. These predictions show good correlation on the MOLEC model for the lower surface. The upper surface predictions for all angles of attack show significant differences in pressure magnitudes but consistent behavior in general shapes. This is definitely attributed to the complexity of the flows at that leading-edge slot.

Figure 8-23 examines some additional data through the use of a boundary layer rake fixed to the OML of the MOLEC configuration. The rake was positioned at 13% and 55% chord to examine

the separation and reattachment behavior in and above the boundary layer. A sample NPR sweep at 13% chord is shown for zero degrees alpha. These data show that it is feasible to measure boundary layer properties in future efforts and may provide better insight into flow physics of high-lift concepts.

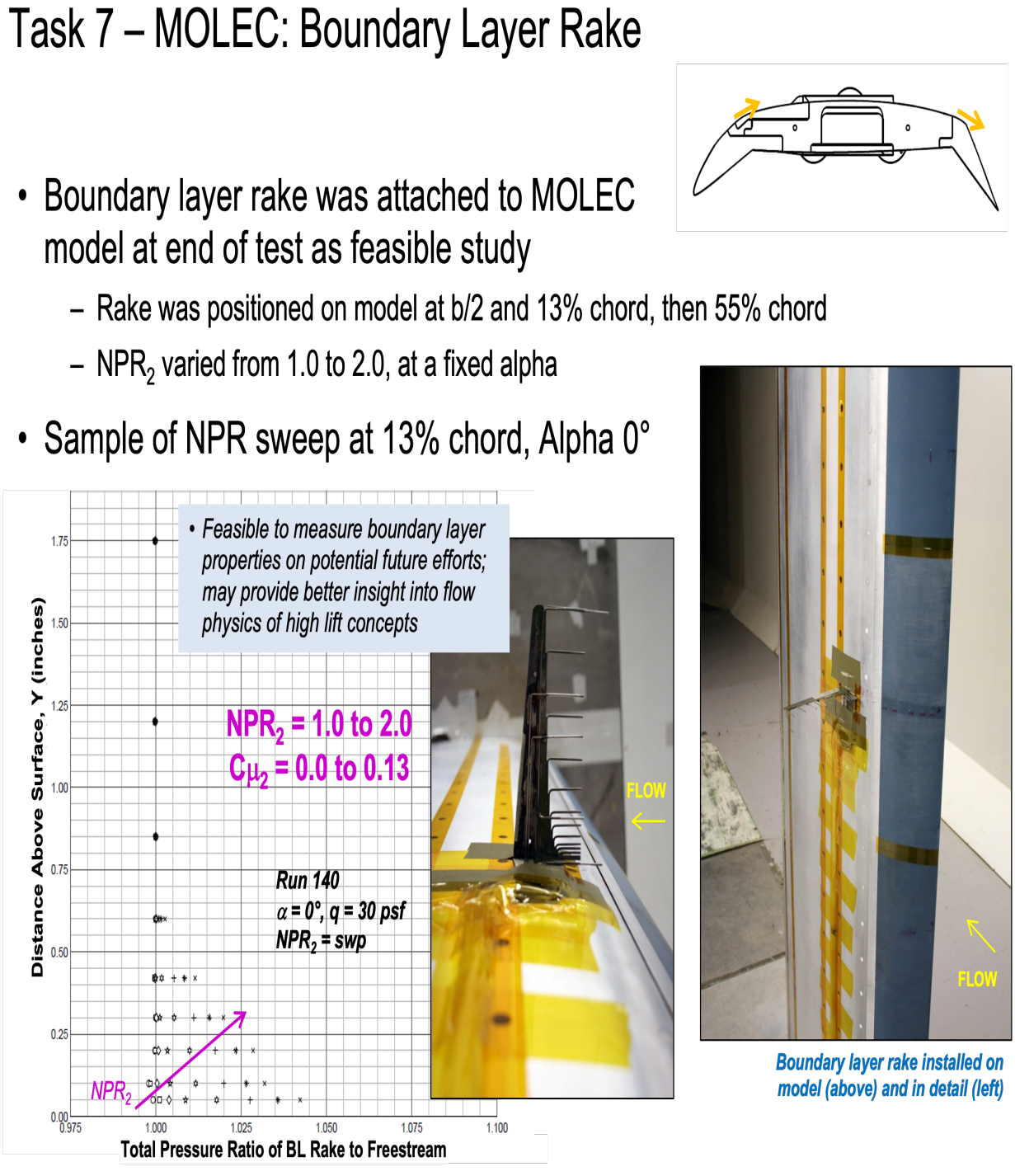


Figure 8-23. Boundary layer rake data.

RUN	α	Q	MACH	$Re/10^6$	MODEL	FLAP	NPR1	NPR2	NPR3	CMU1	CMU2	CMU3	DESCRIPTION
24	SWP	29.7	0.141	0.953	1	45	1	1	1	0	0	0	Baseline, Slots Taped
17	SWP	SWP	0.142	0.975	1	0	1	1	1	0	0	0	Baseline, Slots Taped
57	SWP	30.0	0.142	0.973	1	45	1	1	1.20	0	0	0.035	Baseline, Slots Taped
104	SWP	29.8	0.142	0.988	2	45	1.40	1.86	1.20	0.059	0.132	0.036	LAVLET, Slots Open
111	SWP	30.1	0.142	0.984	3	45	1	1	1.20	0	0	0.035	MOLEC, Slots Open
126	SWP	29.5	0.140	0.952	3	45	1	1.79	1.21	0	0.111	0.037	MOLEC, Slots Open

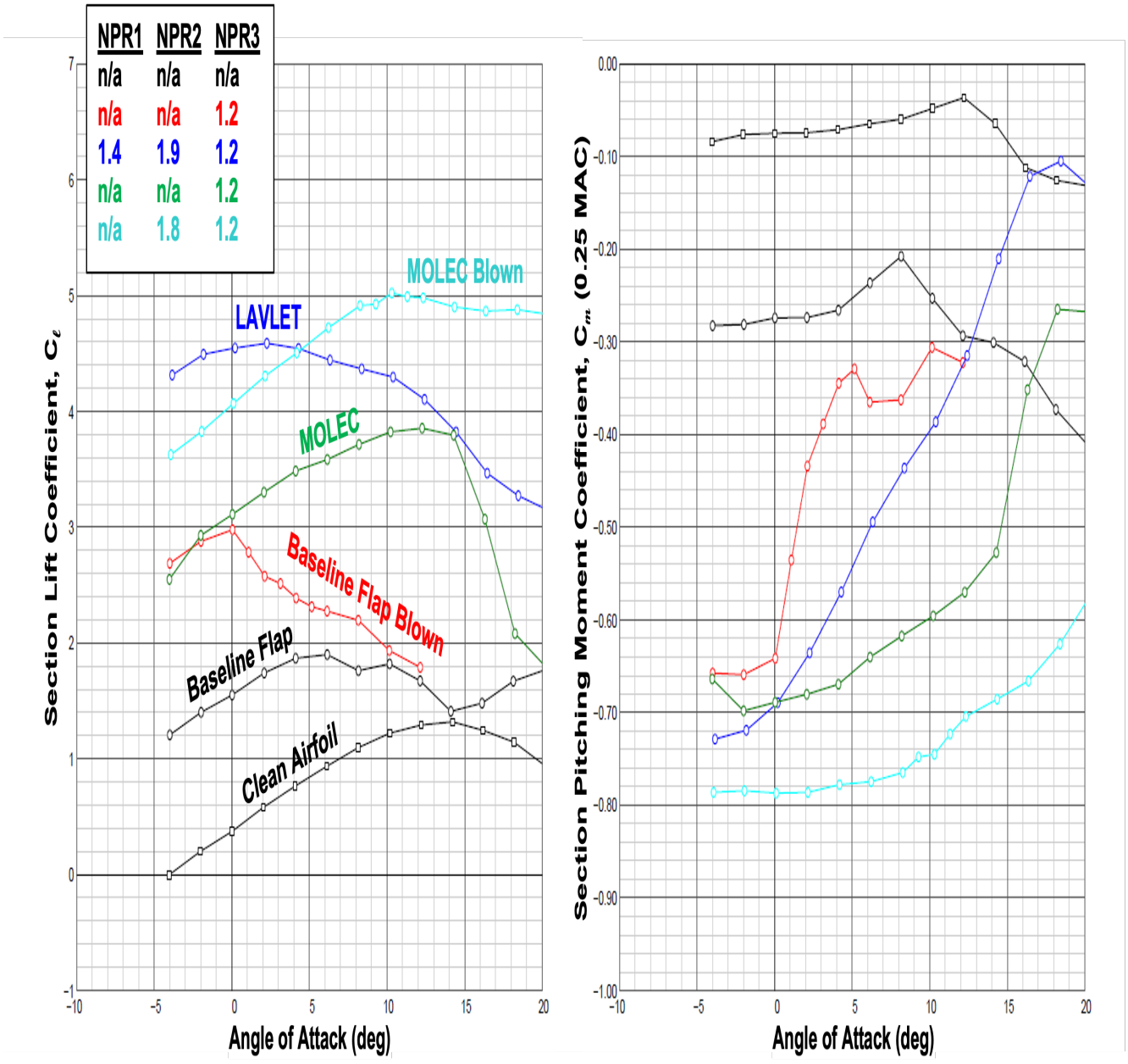


Figure 8-24. High-lift results for all AHLLE configurations.

The final two data analysis plots show the high-lift comparisons all on a single plot. Figure 8-24 reports the lift and moment vs. alpha curves for all the AHLLE configurations studied. Figure 8-25 assesses all the AHLLE configurations regarding integrated C_P distributions.

Task 7 – High-Lift Configuration Comparisons

- Comparison of high-lift configurations tested on AHLLE

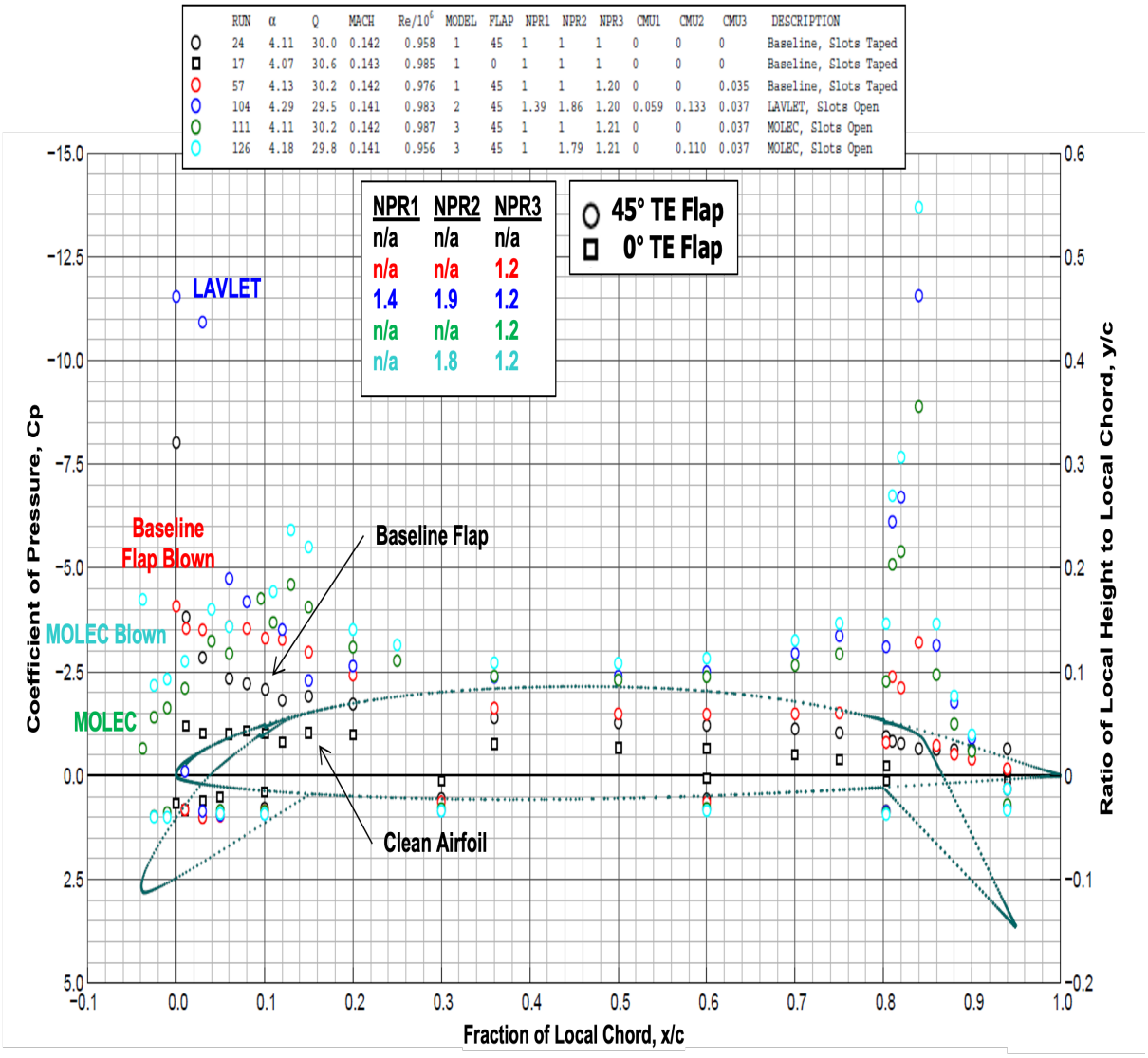


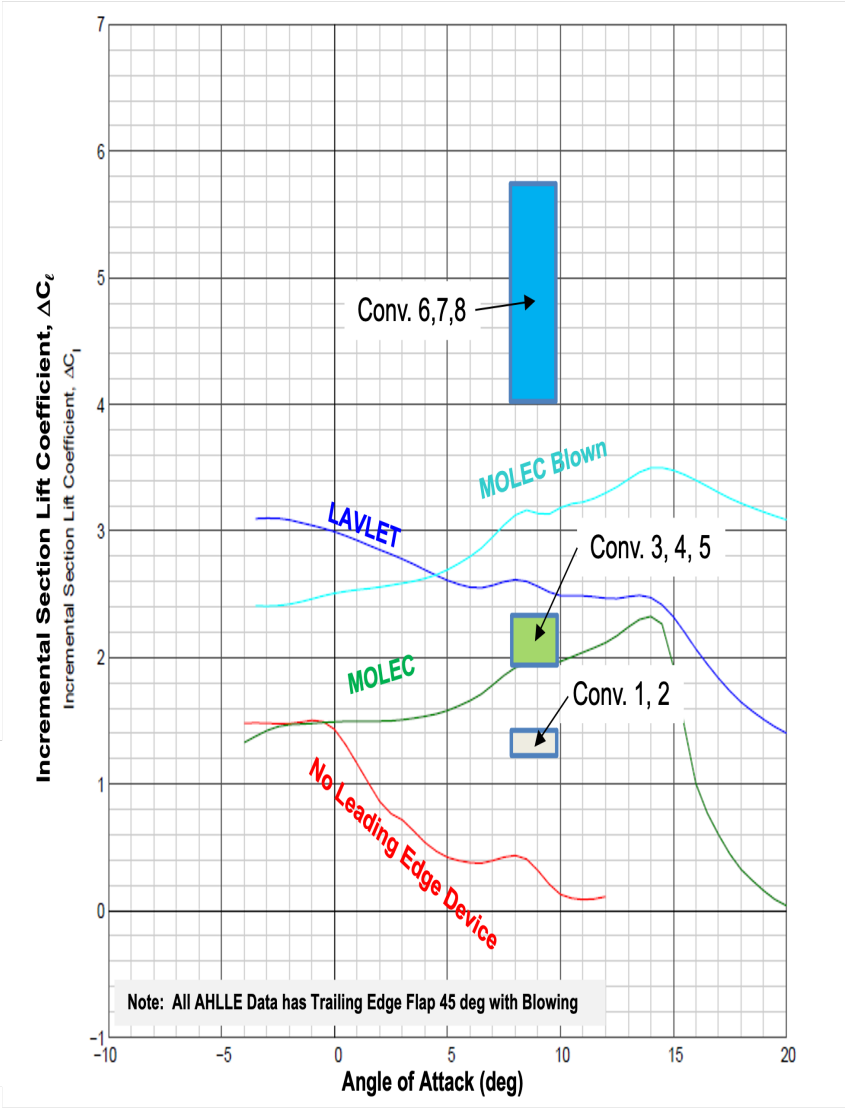
Figure 8-25. C_P distributions for all AHLLE configurations.

9. Summary

The AHLLE program examined several high-lift leading-edge concepts that are compatible with laminar flow in the cruise configuration. The program examined a minimum of three configurations in a conceptual design process that included aerodynamic analysis (CFD) and structural design assessment. The configurations were assessed during a downselection process that included QFD analysis to determine two final candidates for wind tunnel testing. The QFD analysis included weighting factors such as high-lift capability, laminar flow compatibility, weight, structural design, complexity, acoustics, power, maintainability, and TRL level. The resulting candidates for ground testing were a blown leading-edge configuration that created a virtual slat through two leading-edge slots. A second configuration was a multiobjective leading-edge configuration that included a spanwise slot at 12% chord. All models had a common blown flap deflected to 45 degrees. The summary results of the wind tunnel test compared to other traditional high-lift configurations are shown in figure 9-1.

Summary Comparison of AHLLE and High Lift Concepts

- The LAVLET configuration achieved a section CL = 4.6 (LE Cμ = 0. 19)
- The MOLEC configuration achieved a section CL = 4.0 (LE Cμ = 0)
- The blown MOLEC achieved a section CL = 5.3 (LE Cμ = 0.11)



Un-Powered High Lift (NACA 64A010)
Conv. 1 – LE Slat + TE Split Flap
Conv. 2 – LE Flap + TE Split Flap
Conv. 3 – LE Slat + TE Dbl Slotted Flap
Conv. 4 – LE Flap + TE DBL Slotted Flap
Powered Lift Concepts
Conv. 5 – Vectored Thrust
Conv. 6 – Externally Blown Flap
Conv. 7 – Upper Surface Blown Flap
Conv. 8 – Internally Blown Flap

Figure 9-1. Lift summary of AHLLE configurations.

Traditionally, a conventional Krueger flap typically achieves a $\Delta c_L = 1.5$. On LAVLET a high-lift increment of $\Delta c_L = 3.1$ was achieved over the baseline laminar airfoil configuration. The AHLLE MOLEC configuration achieved a $\Delta c_L = 2.4$ over the baseline airfoil. The blown MOLEC configuration achieved a $\Delta c_L = 3.5$. Compared to conventional unpowered high-lift configurations, these AHLLE concepts achieved a remarkable $c_L = 4.6$ on LAVLET, $c_L = 4.0$ on MOLEC, and $c_L = 5.3$ on blown MOLEC.

In the Phase I Northrop Grumman N+3 study, an additional $\Delta C_L = 0.65$ equated to approximately 1000 ft in runway length. The target 2D section lift for this ground test was $c_l = 4.0$. In this study, a section lift of 5.3 was achieved.

In conclusion, all deliverables and review activities were successfully completed on schedule. The wind tunnel test was completed three weeks behind schedule due to a high-pressure supply line failure. However, the duration of the test and completion of the test fell within the originally scheduled two-month window. All model design, fabrication and delivery of the model to the wind tunnel tasks were completed on schedule. Two AHLLE configurations were successfully wind tunnel tested to TRL 4. Incremental lift of $\Delta C_L = 3.5$ or $\Delta C_L = 3.1$ were achieved on the two laminar compatible airfoil configurations (at cruise). Maximum lift was achieved in the MOLEC configuration with blown slot.

As a result of this program approach, a successful demonstration of high-lift leading-edge technology was reached, and the target goals for improved lift were exceeded by 32.5% with a maximum section $C_L = 5.3$. Our high-lift design yielded a massive 94% lift improvement over conventional high-lift configurations while allowing laminar flow capability on the cruise configuration.

Our execution of the NASA AHLLE program statement of work has yielded some game changing results. Emerging high-lift technology, LAVLET and MOLEC concepts, were wind tunnel tested at the 7×1 ft LSWT at Northrop Grumman. During representative Mach and Reynolds number conditions for take-off and landing, both methodologies exceeded prediction of lift vs. alpha. High-lift $C_{lmax} = 4.8$ was achieved using the LAVLET configuration and showed a 73% improvement over the baseline laminar airfoil configuration in the absence of slats. The MOLEC and blown MOLEC configurations also exceeded prediction for lift vs. alpha, stalling at 12 degrees in the drooped configuration and 14 degrees in the blown and drooped configuration. The addition of a blown spanwise slot at the 12% chord location achieved a stall benefit and improved lift behavior by 32.5%. Unidirectional blowing has been proven for significant lift benefit on a laminar airfoil for high-lift applications. These data now establishe a baseline for further expansion of these high-lift concepts to swept wing laminar airfoils.

- The Northrop Grumman team would like to sincerely thank Dr. John Lin, technical POC, the NASA Subsonic Fixed Wing Program and Ms. Kim Pham for their support



Figure 9-2. The AHLLE team.

10. References

[1] Wang, D., Bartley-Cho, J., Kjerstad, K., Kwon, H., Rahrig, K., Schein, D., Ho, B., and Speer, S., "Multi-Objective Leading-Edge Concepts (MOLEC)," NASA Contractor Report, June 30, 2009.

[2] Bright, M., Korntheuer, A., Komadina, S., and Lin, J., "Development of Advanced High Lift Leading Edge Technology for Laminar Flow Wings," AIAA Paper 2013-0211, 51st AIAA Aerospace Sciences Meeting, Grapevine, TX, January 7-10, 2013.

[3] Collins, S. W., Westra, B. W., Lin, J. C., Jones, G. S., and Zeune, C. H., "Wind Tunnel Testing of A Powered Lift All-Wing STOL Model," The Aeronautical Journal, v. 113, no. 1140, February 2009, pp. 129-137.

[4] Lin, J. C., Jones, G. S., Allan, B. G., Westra, B. W., Collins, S. W., and Zeune, C. H., "Flow-Field Measurements of a Hybrid Wing Body Model with Blown Flaps," AIAA 2008-6718, 26th Applied Aerodynamics Conference, Honolulu, HI, August 2008.

[5] Su, W., and Cesnik, C., "Nonlinear Aeroelasticity of a Very Flexible Blended-Wing-Body Aircraft," AIAA 2009-2402, 50th AIAA/ASME/ASCE/AHS/ASC Structures, Structural Dynamics, and Materials Conference, Palm Springs, CA, May 2009.

REPORT DOCUMENTATION PAGE

Form Approved
OMB No. 0704-0188

Public reporting burden for this collection of information is estimated to average 1 hour per response, including the time for reviewing instructions, searching existing data sources, gathering and maintaining the data needed, and completing and reviewing this collection of information. Send comments regarding this burden estimate or any other aspect of this collection of information, including suggestions for reducing this burden to Department of Defense, Washington Headquarters Services, Directorate for Information Operations and Reports (0704-0188), 1215 Jefferson Davis Highway, Suite 1204, Arlington, VA 22202-4302. Respondents should be aware that notwithstanding any other provision of law, no person shall be subject to any penalty for failing to comply with a collection of information if it does not display a currently valid OMB control number. **PLEASE DO NOT RETURN YOUR FORM TO THE ABOVE ADDRESS.**

1. REPORT DATE *(DD-MM-YYYY)*	**2. REPORT TYPE**	**3. DATES COVERED** *(From - To)*
04-30-2012	Final Technical Report	April 2011- April 2012

4. TITLE AND SUBTITLE
Advanced High-Lift Leading-Edge (AHLLE) Technologies for Laminar Wings

5a. CONTRACT NUMBER
NNL10AA07B

5b. GRANT NUMBER
●

5c. PROGRAM ELEMENT NUMBER

6. AUTHOR(S)
Bright, Michelle M.;
Korntheuer, Andrea
Komadina, Steve
Tehrani, Kian

5d. PROJECT NUMBER

5e. TASK NUMBER
NNL11AB27T

5f. WORK UNIT NUMBER

7. PERFORMING ORGANIZATION NAME(S) AND ADDRESS(ES)

Advanced Programs & Technology
Northrop Grumman Systems Corporation
One Hornet Way
El Segundo, CA 90245-2804

8. PERFORMING ORGANIZATION REPORT NUMBER

9. SPONSORING / MONITORING AGENCY NAME(S) AND ADDRESS(ES)
NASA Langley Research Center
9B Langley Blvd., Bldg. 1195B
M/S 126
Hampton VA 23681-2199

10. SPONSOR/MONITOR'S ACRONYM(S)
NASA LaRC

11. SPONSOR/MONITOR'S REPORT NUMBER(S)

12. DISTRIBUTION / AVAILABILITY STATEMENT

Government Purpose rights

13. SUPPLEMENTARY NOTES

14. ABSTRACT

Northrop Grumman conducted conceptual aerodynamic CFD analysis and QFD analysis to downselect two leading-edge concepts for high-lift. Wind tunnel model design created a 7-foot span model of the complex AHLLE configuration. A wind tunnel test plan, which included baseline, deflected trailing-edge, blown deflected trailing-edge, blown leading-edge, morphed leading-edge and blown/morphed leading-edge airfoil configurations was developed. As a result of this program approach, a successful demonstration of high-lift leading-edge technology was reached, and the target goals for improved lift were exceeded by 30% with a maximum section $c_l = 5.2$. Incremental lift of $\Delta C_L = 3.5$ and $\Delta C_L = 3.1$ was achieved on the two laminar compatible airfoil configurations (at cruise). Our high-lift design yielded a massive 94% lift improvement over conventional high-lift Krueger flap configurations while providing laminar flow capability on the cruise configuration.

15. SUBJECT TERMS
National Aeronautics and Space Administration (NASA), Northrop Grumman Corporation (NGC), high lift, flow control, laminar flow, blown leading edge, morphed leading edge, low speed wind tunnel experiment

16. SECURITY CLASSIFICATION OF:			**17. LIMITATION OF ABSTRACT**	**18. NUMBER OF PAGES**	**19a. NAME OF RESPONSIBLE PERSON**
a. REPORT	**b. ABSTRACT**	**c. THIS PAGE**			Dr. Michelle Bright
U	U	U	UU	98	**19b. TELEPHONE NUMBER** *(include area code)* (858) 618-6370

INSTRUCTIONS FOR COMPLETING SF 298

1. REPORT DATE. Full publication date, including day, month, if available. Must cite at least the year and be Year 2000 compliant, e.g. 30-06-1998; xx-06-1998-, xx-xx-1998.

2. REPORT TYPE. State the type of report, such as final, technical, interim, memorandum, master's thesis, progress, quarterly, research, special, group study, etc.

3. DATES COVERED. Indicate the time during which the work was performed and the report was written, e.g., Jun 1997 - Jun 1998; 1-10 Jun 1996; May - Nov 1998; Nov 1998.

4. TITLE. Enter title and subtitle with volume number and part number, if applicable. On classified documents, enter the title classification in parentheses.

5a. CONTRACT NUMBER. Enter all contract numbers as they appear in the report, e.g. F33615-86-C-5169.

5b. GRANT NUMBER. Enter all grant numbers as they appear in the report, e.g. AFOSR-82-1234.

5c. PROGRAM ELEMENT NUMBER. Enter all program element numbers as they appear in the report, e.g. 61101A.

5d. PROJECT NUMBER. Enter all project nurnbers as they appear in the report, e.g. 1F665702D1257; ILIR.

5e. TASK NUMBER. Enter all task numbers as they appear in the report, e.g. 05; RF0330201; T4112.

5f. WORK UNIT NUMBER. Enter all work unit numbers as they appear in the report, e.g. 001; AFAPL30480105.

6. AUTHOR(S). Enter name(s) of person(s) responsible for writing the report, performing the research, or credited with the content of the report. The form of entry is the last name, first name, middle initial, and additional qualifiers separated by commas, e.g. Smith, Richard, J, Jr.

7. PERFORMING ORGANIZATION NAME(S) AND ADDRESS(ES). Self-explanatory.

8. PERFORMING ORGANIZATION REPORT NUMBER. Enter all unique alphanumeric report numbers assigned by the performing organization, e.g. BRL-1234; AFWL-TR-85-4017-Vol-21-PT-2.

9. SPONSORING/MONITORING AGENCY NAME(S) AND ADDRESS(ES). Enter the name and address of the organization(s) financially responsible for and monitoring the work.

10. SPONSOR/MONITOR'S ACRONYM(S). Enter, if available, e.g. BRL, ARDEC, NADC.

11. SPONSOR/MONITOR'S REPORT NUMBER(S). Enter report number as assigned by the sponsoring/ monitoring agency, if available, e.g. BRL-TR-829; -21 5.

12. DISTRIBUTION/AVAILABILITY STATEMENT. Use agency-mandated availability statements to indicate the public availability or distribution limitations of the report. If additional limitations/ restrictions or special markings are indicated, follow agency authorization procedures, e.g. RD/FRD, PROPIN, ITAR, etc. Include copyright information.

13. SUPPLEMENTARY NOTES. Enter information not included elsewhere such as: prepared in cooperation with; translation of; report supersedes; old edition number, etc.

14. ABSTRACT. A brief (approximately 200 words) factual summary of the most significant information.

15. SUBJECT TERMS. Key words or phrases identifying major concepts in the report.

16. SECURITY CLASSIFICATION. Enter security classification in accordance with security classification regulations, e.g. U, C, S, etc. If this form contains classified information, stamp classification level on the top and bottom of this page.

17. LIMITATION OF ABSTRACT. This block must be completed to assign a distribution limitation to the abstract. Enter UU (Unclassified Unlimited) or SAR (Same as Report). An entry in this block is necessary if the abstract is to be limited.